UNIVERSITY of GREENWICH

Greenwich Academic Literature Archive (GALA)
– the University of Greenwich open access repository
http://gala.gre.ac.uk

Contact: gala@gre.ac.uk

1   LOW TEMPERATURE, AUTHIGENIC ILLITE AND CARBONATES IN A MIXED

2   DOLOMITE-CLASTIC LAGOONAL AND PEDOGENIC SETTING, SPANISH

3   CENTRAL SYSTEM, SPAIN

4

5

6   Jennifer Huggett[a,b], Javier Cuadros[b], Andrew S. Gale[c], David Wray[d] and Jacob

7   Adetunji[e]

8

9

10   [a] Petroclays Ltd, Sandy Cross, Heathfield, E Sussex, TN21 8QP, UK

11   [b] The Natural History Museum, London, SW7 5BD, UK

12   [c] Department of Earth Sciences, The University of Portsmouth, PO1 3QL, UK

13   [d] School of Science, University of Greenwich, ME4 4TB, UK

14   [e] Department of Natural Science, University of Derby, DE22 1GB, UK

15

16

17   E-mail of corresponding author (Jennifer Huggett): info@petroclays.com

18

19   ABSTRACT

20

21   The aim of this study was to further our understanding of the pedogenic and

22   lacustrine modification of clay minerals. Some of these modifications are of

23   special interest because they constitute reverse weathering reactions, rare in

24   surface environments, and because there is not yet an accurate assessment of

25   their global relevance in mineralogical and geochemical cycles. For this study,

26   two sections from the Central System in Spain were selected. Both are sections

27   through the Uppper Cenomanian-Turonian mixed clastic and carbonate

28   succession, containing both calcite and dolomite, in the Sierra de Guadarrama.

29   Mid-Turonian sea level fall resulted in the formation of a coastal plain

30   environment in which extensive pedogenesis occurred around saline lagoons.

31   The mineralogical changes that have occurred as a result of sedimentation in

32   saline lagoons and as a consequence of pedogenesis are described. Textural

33   relationships indicate that the dolomite cement pre-dates the calcite. Silicate

34   minerals are represented by quartz, kaolinite, illite-smectite, illite, minor

35   plagioclase and alkali feldspar, and trace chlorite and palygorskite. There is a

36   positive correlation between the intensity of pedogenesis and the proportion of

37   illite in the clay assemblage in one of the sections, indicating pedogenic

38   illitisation. In this section, the intensity of the illitisation process increases up,

39   reaching a maximum where pedogenesis is most intense in the middle part, and

40   then decreases as marine influence increases towards the top of the Alcorlo

41   Formation and the overlying marine Tranquera Formation. The clay assemblages

42 are consistent with a slow transformation process from kaolinite to illite by way of

43 illite-smectite, taking place under surface conditions. The illitisation process has

44 resulted in a less Fe-rich, more Mg-, and Al-rich illite than the majority of

45 previously documented cases in the near surface. Formation of Al-rich illite is not

46 therefore restricted to the deep subsurface.

47 The mechanism for low temperature illitisation involves enhanced layer charge

48 resulting from Mg^{2+} substitution for Al^{3+} (or Fe^{3+}) and Fe^{3+} to Fe^{2+} reduction. Mg^{2+}

49 enrichment may have occurred principally in saline lagoons or lakes, while Fe^{3+}

50 to Fe^{2+} reduction occurred as a result of wetting and drying in a pedogenic

51 environment. So far as it has been possible to establish, this dual mechanism

52 has not previously been documented. This study indicates clearly that the

53 dolomite and calcite are authigenic cements that precipitated in a clastic

54 sediment, probably soon after deposition. Dolomitisation and Mg enrichment of

55 the clay may have occurred at the same time. Seawater is the most probable

56 source of Mg.

57

58 Keywords: Dolomite, Illitisation, Kaolinite, Lagoonal, Pedogenesis, Smectite

59

60 **1. Introduction**

61

62   This study was initiated with the intention of improving our understanding

63 of modification of clay minerals in pedogenic and lacustrine environments. Clay

64 assemblages in chemical equilibrium with the surface sediments in which they

65 form, or are modified, are important palaeoenvironmental and palaeoclimatic

66 indicators. Most clays formed at the Earth's surface are predominantly a result of

67 weathering, and clay mineralogy is considered to reflect the intensity and

68 duration of weathering conditions. Hence, most illite in sediments is the result of

69 high latitude weathering of rocks (e.g., Nesteroff et al., 1964; Chamley, 1989 and

70 references therein), where cold and dry conditions prevail. In low-latitude, non-

71 arid climates illite is expected to degrade into smectite and kaolinite (e.g.,

72 Chamley et al., 1983; Griffin et al., 1968), depending of the specific conditions.

73 Illitisation, however, also takes place in specific surface environments in warm

74 climates (see below); for accurate palaeoenvironmental reconstruction it is

75 necessary to identify such environments. The present investigation, in quartz and

76 dolomite-rich sediments, complements previous studies (Huggett et al., 2001;

77 Huggett and Cuadros, 2005, 2010) of pedogenic modification of clay minerals,

78 including ilitisation, in calcite- and quartz-rich sediments.

79   Pedogenic illitisation of smectite is fairly well documented in the literature

80 (e.g., Watts, 1980; Robinson and Wright, 1987; Huggett et al., 2001; Huggett and

81 Cuadros, 2005, 2010; Gilg et al., 2003; Stanjek and Marchel, 2008), as is

82 lacustrine illitisation (e.g., Gabis, 1963; Singer and Stoffers, 1980; Jones and

83 Weir, 1983; Norrish and Pickering, 1983; Deconinck et al., 1988). Low

84 temperature illitisation in soils and lakes has been linked to Fe uptake and

85 microbial reduction (Stucki et al., 1984; Siyuan and Stucki, 1994; Stucki, 1997;

86 Huggett et al., 2001; Huggett and Cuadros, 2005, 2010). Others (e.g., Keller,

87 1958; Gabis, 1963; Gilg et al., 2003) have observed weathering of volcanic rock

88 to form iron-rich illite in soils and lakes. Illitisation driven by Fe uptake and

89 reduction has also been described in mangrove forests (Andrade et al., 2014). All

90 the above processes are of interest not only due to palaeoenvironmental

91 implications but also for geochemical cycles. Illitisation at surface environments

92 may represent continental or coastal K sinks of yet unrecognised importance.

93 Given the connection of some of these illitisation processes to Fe uptake they

94 may also be relevant to the Fe biogeochemical cycles. In this study we report an

95 occurrence of low temperature illitisation that has produced an Fe-poor illite.

96　　　The localities studied here were part of a study of the facies and sequence

97 stratigraphy of a transect running obliquely NE-SW across the boundary between

98 the Hesperian Massif and the Iberian Basin in central Spain (García-Hildalgo et

99 al., 2007). Two sections (Figure 1) were studied in the present work, a roadcut

100 between Torrelaguna and El Berrueco on the M131 road, Calle del las Cercas, 3

101 km north west of Torrelaguna, and a roadcut on the GU1065, 750 m south of

102 Tortuero, some 20 km to the north east of the Torrelaguna section (Figure 2).

103 Samples from Torrelaguna have the prefix A, and those from Tortuero have the

104 prefix T.

105　　　The lithostratigraphical terminology applied to this succession (Fig. 2 in

106   García-Hildalgo et al., 2007) is complex, because the strata show extensive

107   interdigitation, and their boundaries have not been effectively defined at the

108   localities studied here. Furthermore, the detailed sequence stratigraphy

109   described by García-Hildalgo et al. (2007) did not apply lithostratigraphical

110   nomenclature, but rather used four named sequences (their Fig. 3, successively,

111   Atienza, Patones, El Molar and the youngest, Somolinos), which are not precisely

112   related to the formations. Our study involved the Alcorlo Formation (dolomitic

113   sands, marls and clays) and the basal part of the overlying Tranquera Formation

114   (thinly to medium bedded dolostones and marls), which are interpreted to fall in

115   the upper El Molar and lower Somolinos sequences of García-Hildalgo et al.

116   (2007).

117   The Upper Cenomanian-Turonian succession in the Sierra de

118   Guadarrama region of central Spain (Fig. 1), is composed of mixed clastic and

119   carbonate sediments deposited in a variety of coastal and marine shelf

120   environments: alluvial plain–estuarine, lagoon, shoreface, offshore hemipelagic,

121   and carbonate ramp (García-Hidalgo et al., 2007). Transgression onto Hercynian

122   basement of the Hesperian Massif commenced in the Late Cenomanian, and

123   reached its maximum extent in the Late Cenomanian-Early Turonian. During the

124   Mid-Turonian, sea level fell, resulting in the development of lagoonal facies in

125   which extensive soil development took place within lacustrine marls and sands.

126   Finally, marine transgression of Late Turonian age resulted in extensive

127   deposition in a carbonate ramp setting (García-Hildago et al., 2007). The sea

128   level changes probably reflect global eustatic events (Hancock, 1990; Gale,

129 1996). Using data in García-Hildalgo et al. (2007) and Martin-Serrano (1996),

130 maximum burial is estimated to be <1.5 km.

131   The studied interval incorporated two facies groups within the

132 classification of García-Hildalgo et al. (2007): the lagoonal (their facies D) and

133 carbonate ramp (their facies E). The sediments of the upper Alcorlo Formation

134 fall mostly within the lagoonal facies association D3 (silts and sandstones) of

135 García-Hildalgo et al. (2007, p. 1259), which they described from field

136 observations as "thin-bedded muddy silts, and silty fine grained sandstones". A

137 transgression to shallow marine carbonate sedimentation is represented by the

138 Tranquera Formation, at the top of both sections. This formation falls within the

139 Carbonate Ramp (E1) of García-Hildalgo et al. (2007).

140   The lagoonal facies in the Alcorlo Formation shows extensive evidence of

141 pedogenesis, including root traces, soil horizons, cutans, glaebules, peds and

142 variegated iron mineralisation (Retallack, 2001). It has been widely interpreted as

143 representing mudflats developed over shoreface sands, with local stromatolite

144 formation, and local washover fans within tidal channels (García-Hildalgo et al.,

145 2007). The two studied sections (at Torrelaguna and Tortuero) display features

146 that permit a broad correlation to be made; the lower portion of both is rich in

147 quartz sand, the middle comprises clay-rich dolomitic marls, and the upper part

148 (Tranquero Formation) comprises dolostones.

149

150 **2. Materials and methods**

151

152 *2.1. Samples*

153

154   Samples, 31 in total, were taken from every bed over approximately 10 m

155 of exposure at both Tortuero and Torrelaguna (Figures 2-4), with the most

156 samples being taken over the pedogenically modified intervals. Individual

157 samples are described briefly (Table 1). The samples were examined by optical

158 and electron microscopy, detailed clay analysis using X-ray diffraction (XRD),

159 inductively coupled plasma atomic emission spectrometry (ICP-OES/MS), and

160 Mössbauer spectroscopy (only performed on the clay-rich samples). The degree

161 of pedogenic modification was assessed for each sample using a simple

162 numerical system in which 1 point was assigned to each of the following

163 pedogenic features: root traces, peds, and variegated iron mineralisation. Cutans

164 and glaebules do not occur in these soils, and slikensides are excluded as they

165 are lithology dependent, and would not be observed in dolomite-rich, clay-poor

166 soils. The score for each sample is from zero to three, depending of the number

167 of the above features present in the horizon. This score was used for comparison

168 with chemical and mineralogical aspects of the samples.

169

170 *2.2. XRD*

171

172   The untreated, whole-rock samples were analysed by means of random

173 powder XRD to determine their mineral composition. Samples were ground with

174 acetone in a rod mill, dried and gently ground in an agate mortar before being

175   side-packed into sample holders and scanned at a rate of 1 s per 0.02 º2θ step

176   width, using 0.3 mm Soller and detector slits, from 5 to 65 º2θ, in a Philips

177   PW1710 diffractometer (Almelo, The Netherlands) at 45 kV and 40 mA using a

178   Cu anode (X-ray wavelength 1.5418 Å) and a graphite secondary

179   monochromator.

180   For further analysis, calcite was removed with 30% acetic acid (Fisher

181   Scientific, Loughborough, UK) and the insoluble residue washed three times with

182   distilled water. The <2 µm fraction was separated using centrifugation. The

183   sodium dithionite method (Smith, 1994) was used to remove any Fe or Al

184   (oxyhydr)oxide. Oriented mounts for XRD were prepared by allowing a few drops

185   of the clay slurry to dry on a glass slide. Samples were analysed using the

186   equipment described above in the range 2-40 or 2-30 º2θ, with a 0.3 mm Soller

187   slit and a 0.1 mm detector slit. The samples were scanned at 0.015 º2θ step size

188   and 8 s/step. The analyses were carried out in an air-dry state (20-25ºC, 50-60%

189   relative humidity) and after overnight glycolation at 60 ºC in a glycol atmosphere.

190

191   *2.3. XRD quantification and modelling*

192

193   In order to investigate the processes taking place in the silicate phases,

194   the powder XRD traces were used for the relative quantification of the silicate

195   minerals. The following diffraction-peak areas were measured and normalised to

196   their sum: quartz (4.26 Å), feldspar (~3.25 Å), kaolinite (~7 Å), illite (~10 Å) and

197   smectite-rich I-Sm phases (16-17 Å). Peak areas were measured using the

198 software package GRAMS AI (Thermo Galactic, Salem, New Hampshire, USA).

199 The XRD patterns of the glycolated, oriented mounts were modelled with

200 NEWMOD (Reynolds & Reynolds, 1996; Moore & Reynolds, 1997), a program

201 that allows calculation of $00l$ profiles for end-member and mixed-layer

202 phyllosilicates with different interlayer complexes. The NEWMOD calculations

203 included illite-smectite (I-Sm) of different compositions, illite, kaolinite and

204 kaolinite-smectite (Kaol-Sm) with high kaolinite content. The variables used to

205 obtain the best match with the experimental patterns were % layers in the

206 interstratified phases, layer ordering (R) in the interstratified stacking sequence,

207 Fe and K abundance, and size of the coherent scattering domain. The orientation

208 of the particles was set at $\sigma^* = 20^\circ$ or 30° by best match with the experimental

209 patterns, where σ^* is the standard deviation from a 0° angle (layers perfectly

210 parallel to the substrate) in a Gaussian distribution.

211

212 *2.4. ICP-OES/MS*

213

214 ICP-OES analysis was carried out on the bulk rock samples, and on

215 portions of the <2 μm fraction from which carbonates had been removed using

216 30% acetic acid. For the few samples from which sufficient amount of the <2 μm

217 fraction could be extracted, duplicate chemical analyses were carried out on

218 splits from which Fe and Al oxides had been removed using the sodium dithionite

219 method (Mehra and Jackson, 1960; all chemicals were reagent grade from VWR

220 International Ltd, Lutterworth, Leicestershire, UK). Major, trace, and rare-earth

221   element (REE) data were derived from samples after dissolution by lithium

222   metaborate fusion and quantification by a combination of ICP-OES and ICP-MS

223   (Jarvis and Jarvis, 1985). The instruments used were a Thermo iCAP 6500 radial

224   ICP-OES and a Thermo X Series 2 ICP-MS (Thermo Fisher Scientific, Hemel

225   Hempstead, Hertfordshire, UK). Data were acquired with an ISO17025

226   accredited laboratory (testing lab 2180). Calibration was by way of matrix-

227   matched, traceable synthetic standards. QA/QC protocols included the analysis

228   and charting of in-house QC samples and the analysis of a series of geological

229   reference materials at regular intervals through the analytical sequence. Prior to

230   plotting, REE data were normalised to the values derived from analysis of USGS

231   reference material Cody Shale (SCo-1) that is considered to have a chemical

232   composition representative of the average shale. The complete data sets are

233   available from the archival website http://data.nhm.ac.uk/dataset/chemistry-

234   samples-central-system-carbonate-clays. Accuracy was assessed by repeated

235   measurement of USGS Reference Material SCo-1. All values were found to be

236   within ±5% of the mean reference value for major elements and ±10% for trace

237   and REE; precision error as defined by two standard deviations of four separate

238   duplicate measurements of SCo-1 was less than 5% for all elements.

239

240   *2.5. Mössbauer spectroscopy*

241

242   The ^{57}Fe Mössbauer spectroscopy experiment was carried out at the

243   University of Derby, UK. The spectrometer was manufactured by the Centre for

244 Advanced Technologies and Materials, Olomouc, Czech Republic. Each

245 absorber was prepared from ~70 mg of the clay sample, mixed with boron nitride

246 as a binder. The mixture was spread uniformly over an area of ~1.8 cm^2, and

247 pressed into a pellet. The spectrum was recorded at room temperature with a 25

248 mCi ^{57}Co source in a rhodium matrix, mounted on a constant-acceleration

249 transducer operated in a triangular mode in a velocity range of ±6 mm/s. The

250 Doppler energies from the 14.4 keV γ-rays were detected with a YAlO$_3$:Ce

251 scintillation counter. The data were recorded in 1024 channels, which cover twice

252 the Doppler velocity range. Spectra were calibrated against a high purity

253 (99.99%) natural α-Fe foil and all peak positions reported with respect to the

254 centroid shift (CS) of the natural α-Fe. Lorentzian lines of the folded data were

255 fitted, using the least-square RECOIL 1.04 Mössbauer Spectral Analysis

256 Software developed by Lagarec and Rancourt (1998). Reduced χ^2 was used as a

257 parameter to evaluate the statistical best-fit and uncertainties were calculated

258 using a covariant matrix. Errors were estimated at about ±0.018 mm/s and

259 ±0.020 mm/s for centroid shift (CS) and quadrupole splitting (QS), respectively.

260

261 *2.6. Electron microscopy and microprobe analysis*

262

263   Carbon-coated, polished blocks of every whole-rock sample were

264 examined by Back-Scattered Electron Microscopy (BSEM) in a Zeiss EVO 15LS

265 SEM equipped with Energy Dispersive X-ray Spectroscopy (EDS) (Cambridge,

266 UK); qualitative EDS analyses were obtained of the clay matrix and of grains.

267 Quantitative EDS analyses of single particles from the purified <2 µm clay

268 fraction were obtained, from selected samples, to compare with the ICP-OES

269 clay data. The samples were dispersed in distilled water, sonicated for 3 minutes

270 in an ultrasonic bath, and then a droplet was placed on a carbon tab on a stub.

271 Operating conditions were a 2 µA beam current at 15 kV accelerating voltage,

272 and a spot diameter of approximately 2 µm. Detection limits vary according to the

273 analysed elements and the matrix in which they are contained. For these

274 samples detection limits were 0.2% for Mg, Ca and K; 0.4-0.6% for Al, Si, P, Mn,

275 Ti and Fe. Calibration using a cobalt standard was performed prior to analysis,

276 and the beam current was monitored during analysis. The quantitative data were

277 used to calculate structural formulae averaged over ~30 particles per sample.

278 A series of transects across single calcite and dolomite crystals in T14

279 (only this sample and the adjacent T13 have large enough crystals for

280 microprobe analysis) were obtained using wavelength dispersive spectroscopy

281 (WDS) with a Cameca SX100 microprobe equipped with four spectrometers

282 (Gennevilliers, France). The WDS detection limits are 0.02% for S, Mn and Fe;

283 0.03% for Mg, and 0.05% for Ca, Ba and Sr. Accuracy is the same as or slightly

284 less than the detection limit.

285

286 *2.7. Measurement of Total Organic Carbon*

287

288 Portions of the two black clays, samples A10 and A11, in which organic

289 carbon was suspected, were finely ground, weighed into silver boats, de-

290 carbonated by exposure to hydrochloric acid vapour followed by drop-wise

291 addition of HCl, and then dried. Quantification of organic C was achieved using a

292 Thermo Finnigan Flash EA1112 CHN analyser (Ringoes, New Jersey, USA)

293 calibrated against traceable standards.

294

295 **3. Results**

296

297 *3.1. Sedimentology*

298

299   In both successions, the Alcorlo Formation constitutes most of the

300 stratigraphic thickness sampled, and consists of fine-grained dolomitic

301 sandstone, quartz sand-bearing dolomicrites, and silty marls, with thin clay-rich

302 beds that have been variably modified by penecontemporaneous soil formation

303 processes (Table 1). At Tortuero, pedogenically modified clay-rich dolomicrite

304 intervals occur over a 5 m thickness in the middle of the section (Fig. 3); at

305 Torrelaguna the pedogenesis occurs over an interval of similar thickness (Fig. 4)

306 but, from field observations, is much less intense, with no roots present, less

307 intense development of peds, less colour mottling, and less slickensiding (though

308 this last criterion is lithology dependent). Palaeosol features include rootlets, ped

309 fabrics, slikensiding, and blue-green/red/buff mottling of clays. Two thin layers of

310 dark clays are also present towards the top of the Torrelaguna section (samples

311 A10 and A11). Between the pedogenically modified intervals the sediment

312 comprises dolomicrite, quartz-sand-rich dolomite, dolomitic sandstone, and

313 quartzose siltstone. Invertebrate burrows are filled with sand or haematite

314 cement. The Tranquera Formation, at the top of the sections (Figs. 3 and 4),

315 comprises glauconitic blocky dolostone, deposited in a marine environment,

316 inferred to be low energy from the moderate clay content and, in non-dolomitised

317 localities, bioturbation, and infauna (García-Hidalgo, 2007).

318

319 *3.2. Mineralogy*

320

321 Authigenic dolomite and detrital quartz are the principal components

322 overall (Fig. 5), with calcite (authigenic) the most abundant mineral only in T11.

323 Clay is a major component in the marls, with minor silt- and sand-size detrital

324 plagioclase and alkali feldspar present throughout. Total clay varies from trace to

325 around 25% of the sediment, and comprises varying proportions of illite, illite-

326 smectite (I-Sm) of a wide compositional range, kaolinite, plus trace chlorite and

327 palygorskite. In addition, two samples include kaolinite-rich kaolinite-smectite

328 (Kaol-Sm). Palygorskite is only found at Tortuero, and is present there in all

329 analysed samples from T8ii and above (Table 1). Kaolinite has sharper XRD

330 peaks than the other clays. Authigenic haematite is only associated with

331 pedogenically modified intervals and gives the sediment a light to dark pink

332 colour.

333 In order to investigate the detrital or authigenic character of the clay

334 minerals, correlations between the several minerals were studied. The

335 hypotheses being tested were that saline waters and the subsequent soil

336   conditions destabilised kaolinite and feldspars and generated authigenic I-Sm

337   and illite. Such processes would produce negative correlations between mineral

338   phases. For this investigation, the areas of diagnostic XRD peaks representative

339   of each silicate mineral phase were measured in the patterns from random

340   powders (see methods section) and normalised to 100%. These measurements

341   do not represent percent mineral abundance but the relative variation of the

342   silicate mineral phases from sample to sample. Four variables are involved

343   (content variation of quartz, feldspars, kaolinite, and I-Sm), and thus statistically

344   significant correlations found between any two of them should be meaningful.

345   The only apparent correlation is between kaolinite and I-Sm phases, where, for

346   most data points, kaolinite decreases with increasing I-Sm (Fig. 6). Five data

347   points located below a hypothetical straight line connecting 30% kaolinite with

348   60% I-Sm are outside this broad correlation (Fig. 6). These five data points

349   correspond to samples with large quartz contents (52-84% area), well above

350   those found for the other samples (3-43% area). The larger quartz contents

351   (above 50% of the total normalised area measured for the four mineral phases)

352   cause the affected data points to be largely displaced down and towards the left

353   of the plot (Fig. 6), effectively outside the broad pattern generated by the other

354   data points. In other words, the variable quartz content in the samples causes

355   scatter in the correlation between kaolinite and feldspars where quartz content is

356   below a certain limit (50% of total measured areas) but displaces the data points

357   out of the correlation for samples in which quartz is above that limit (>50% of the

358   total measured areas).

359   García-Hidalgo et al. (2007) indicate that feldspar and kaolinite contents

360   are inversely correlated, although they do not show a statistical analysis

361   supporting this conclusion. This relationship is consistent with the results of the

362   present study, although a meaningful correlation was not found between feldspar

363   and kaolinite contents.

364

365   *3.3. Dolomite*

366

367   Dolomite crystals were euhedral, intergrown and with or without slight

368   chemical zonation indicated by X-ray element mapping, although the zonation

369   was not generally apparent from the atomic number contrast in BSEM images

370   (Fig. 7a). In the Tranquera Formation, and T10a and in T1 in the Alcorlo

371   Formation, dolomite crystals had leached cores and/or selective leaching of

372   particular chemical zones (e.g., Fig. 7b). In all other samples the dolomite was

373   apparently chemically homogenous as seen in BSEM images. SEM-EDS

374   analyses indicated low to very low Fe contents in the dolomite. No other trace

375   elements were detected by EDS, but trace Mn, Ba, and Sr were detected in the

376   course of mapping using WDS. The FeO content of dolomite increased from <1%

377   at the base of the section to 1-2% in samples from the top of the Alcorlo

378   Formation and the Tranquera Formation. In the Tranquera Formation the

379   dolomite was chemically zoned with two Fe-enriched zones, including the

380   outermost zone, and two Fe-poor zones, including the core (Fig. 7b). In the

381   Alcorlo Formation dolomicrite beds, dolomite crystallite size varied from 10 to 100

382   μm. Dolomite in the Tranquera Formation comprised coarser rhombs (100-200

383   μm) than the underlying dolomicrite of the Alcorlo Formation. No correlation

384   between dolomite crystallite size and any other lithological or sedimentological

385   feature was observed.

386

387   *3.4. Calcite*

388

389   Coarsely crystalline, poikilotopic calcite had cemented intercrystalline

390   porosity between dolomite rhombs in samples T13 (Fig. 7c) and A6. This infilling

391   texture indicates that the calcite precipitated after the dolomite. The calcite had

392   low Mg and Fe concentrations, with a very slight increase in Mg of ~0.2%

393   towards crystal margins. Fe was higher both at the core and at the rim. As with

394   the dolomite, trace Mn, Ba and Sr were present in the calcite.

395

396   *3.5. Haematite*

397

398   In dolomicrite beds with pedogenic reddening, clusters of octagonal

399   haematite crystals had grown in the clay matrix, between rhombs of dolomite

400   (Fig. 7a). Haematite is also responsible for the reddening of pedogenically

401   modified clay beds. Haematite clusters were typically ~5-10 μm across.

402

403   *3.6. Clay minerals*

404

405   Experimental and simulated patterns of the glycolated, oriented mounts

406   (<2 μm size fraction) provided detailed information on the clays (Fig. 8).

407   Mismatches between calculated and experimental patterns below 9 °2θ are due

408   to a known problem of the simulation program that generates erroneously high

409   intensity values (Plançon, 2002). Some samples contained traces of quartz and

410   feldspars (Fig. 8). The clay assemblage was dominated by illite layers in both

411   sections (Table 2). The most illitic clays were those with a green colour in hand

412   specimen, which implies that it is the illite that is responsible for this colour.

413   Measurements of the *060* reflection (1.499-1.505 Å) were consistent with the clay

414   being illite rather than ferric illite or glauconite. Typically, kaolinite was the second

415   most abundant component and correlated inversely with illite layers (Table 2).

416   The black clay beds at Torrelaguna did not have a different clay assemblage,

417   although one of them, A11, had the highest smectite content of the two sections.

418   All analysed samples were complex mixtures of illite, I-Sm of several

419   compositions and kaolinite phases (Table 2). The stacking order of the layers in I-

420   Sm increased with increasing illite content, although not uniformly. The amount of

421   Fe required for a good fit in the XRD calculations was moderate (0.2-0.3 atoms

422   per $O_{10}[OH]_2$). The large coherent scattering domains of kaolinite (N_{max} and N_{ave}

423   values, Table 2) indicate large stacks of parallel layers of detrital origin (kaolinites

424   developed in soils typically have broad basal diffraction peaks; e.g., Ryan and

425   Huertas, 2009), whereas the corresponding values for illite would indicate more

426   weathered crystals or the existence of low-temperature illite, possibly authigenic.

427   It is not likely that all the illite is detrital (up to 80-90%) because the Iberian

428 Peninsula was located at low latitude during the Cenomanian-Turonian and the

429 tropical climate would have been reflected in kaolinite-rich soils (Weaver, 1989).

430 Around 5% (visual estimate) pellets and fragments of mature glauconite were

431 present in the Tranquera Formation at Tortuero. These particles, being indurated,

432 did not contaminate the clay fraction, and were visible in the >2 μm fraction when

433 examined under a binocular microscope. Minor to trace amounts of palygorskite

434 were present from 6 m above the base of the Tortuero section, to the top of the

435 section, including the Tranquera Formation.

436   Seven samples were analysed using Mössbauer spectroscopy. The

437 spectra displayed two Fe^{3+} octahedral components, as is typical in clay minerals

438 (Dyar et al., 2008), and a much smaller Fe^{2+} octahedral component (Fig. 9). The

439 range of % Fe^{2+}, measured as the relative area of the Fe^{2+} component, was 4-

440 13%, with an average of 9%. Thus, the level of Fe reduction in the samples was

441 limited. All Fe^{2+} is in illite layers because Fe^{2+} is not stable in smectite layers and

442 it oxidises within minutes to hours of exposure to the atmosphere (Neumann et

443 al., 2011).

444   ICP-OES analyses (Table 3) for splits of green clays (<2 μm) are

445 consistent with the XRD data. Samples with the most illite are those with the

446 highest K_2O values (Table 3). TiO_2 may be clay-size authigenic or detrital

447 particles; both are commonly found in palaeosols (Summerfield, 1983). Results

448 from four splits of green clays (<2 μm) from which Fe and Al oxides had been

449 removed were sufficiently similar to those from which Fe and Al oxides had *not*

450 been removed to conclude that Fe and Al oxides were rare or absent. This is

451 surprising but consistent with the observation that haematite aggregates imaged

452 in BS-SEM were 5-10 µm in diameter. In some instances, higher concentrations

453 of Fe and Al oxides were measured in the cleaned split, which suggests that

454 there may be some sample inhomogeneity. Only samples A3 and A8 contained

455 significant haematite associated with the clay. The ICP-OES for the bulk <2 µm

456 clay fraction and EDS data for individual clay particles from the <2 µm fraction

457 yielded compositions within a few % of each other, indicating that the ICP-OES

458 data did not include significant contamination from other components such as

459 clay-size quartz. CaO was more widely present in the clay splits than was

460 detected by EDS; this difference may correspond to differences in detection limit

461 (higher for EDS), as carbonates were effectively removed prior to ICP-OES

462 analysis. A proportion of the CaO was associated with P_2O_5, where the latter is

463 present. The increase in MgO measured by ICP-OES in the upper part of the

464 Tortuero section (sample T8ii and above) reflects the presence of palygorskite in

465 addition to other MgO-bearing clays.

466 EDS data for illitic clay were recalculated to structural formulae (Table 4).

467 Where Mössbauer data were available, the Fe abundance was split into Fe^{3+} and

468 Fe^{2+}. For the remainder of the analyses, it was assumed that Fe^{2+} is ~10% of the

469 total Fe, because the average value from Mössbauer data was 9% (see below).

470 The structural formulae of the particles are compatible with I-Sm of a wide range

471 of illitic content (Table 4). The layer charge ranged from smectitic to illitic and

472 there was a group of them with intermediate values, between 0.5-0.7 per

473 $O_{10}(OH)_2$. The fact that K was the main interlayer cation is compatible with a

474 process of illitisation. The composition was dioctahedral, with Al as the main

475 octahedral cation, with significant amounts of Mg and Fe. Significant tetrahedral

476 substitution of Al for Si had also occurred. From the above it can be concluded

477 that the layer charge was generated by several factors: tetrahedral Al for Si

478 substitution, octahedral Mg for Al substitution, and partial Fe reduction in the

479 octahedral sheet.

480

481 **4. Discussion**

482

483 4.1. Non-clay mineral diagenesis

484

485   The dolomite and calcite are authigenic cements that precipitated in a

486 predominantly clastic sediment. Textural relationships indicate that the dolomite

487 pre-dates the calcite. Precipitation of dolomite direct from solution rarely occurs;

488 in seawater it is inhibited by SO_4 (Baker and Kastner, 1981). In lacustrine or

489 lagoonal sediments such as occur in the Alcorlo Formation, where the SO_4 is

490 diluted by freshwater or absent, it may be possible for dolomite to precipitate

491 directly from solution, penecontemporaneously with sedimentation. Early

492 dolomitisation in a recent lacustrine/lagoonal setting, of either early calcite

493 cement or bioclasts, has been documented by Aqrawi (1995). Bioclasts were not

494 observed in any of our samples but shallow water gastropods and bivalves were

495 reported by García-Hidalgo et al. (2007).

496   Dolomitisation also occurred in the shallow marine sediments of the

497   Tranquera Formation. The larger size of the dolomite crystals in the marine

498   Tranquera Formation, compared with the lagoonal Alcorlo Formation, may reflect

499   the difference in depositional environment. Seawater is the most probable source

500   of Mg for dolomitisation. To the southwest of this region dolomitisation has

501   probably occurred as a result of Mg rich brines from evaporite dissolution in the

502   younger Valle de Tabladillo Formation east of Patones (Benito and Mas, 2007).

503   For this to have occurred in the Sierra de Guadarrama the Mg rich fluid would

504   have had to flow both laterally 1-2 km and down, making it a less likely source of

505   Mg enrichment of pore fluid. The lack of chemical zonation in the majority of the

506   carbonates suggests that fluctuations in the water chemistry during precipitation

507   were minimal. The selective leaching of narrow zones in a few samples may

508   have occurred during pedogenesis. Haematite appears to have replaced

509   dolomite in some instances, implying that the haematite formed after the

510   dolomite. This is entirely consistent with the haematite having formed during

511   pedogenesis. Dolomite also occurs in clay-rich sediment affected by

512   pedogenesis.

513

514   4.2. Clay minerals

515

516   The estimated maximum burial depth (<1.5 km) equates to a maximum

517   burial temperature ~50-60°C for temperature gradients typical of sedimentary

518   basins (Giles, 1997; Palumbo et al., 1999). Such temperatures are too low for

519 significant illitisation to have occurred as a result of diagenesis, which occurs

520 over a temperature range of 50-120°C (Hower and Perry, 1970; Eberl and

521 Hower, 1976) and is most intense at the upper end of the temperature range

522 (e.g., Ehrenbert and Nadeau, 1989; Glassman et al., 1989).

523 Kaolinite may have originated by alteration of feldspars in the rocks of the

524 sediment source area, as suggested by García-Hidalgo et al. (2007), and not

525 diagenetically in the sediment. The sharp basal XRD peaks are consistent with

526 this interpretation. Given the dominance of Hercynian granite in Sierra de

527 Guadarrama (Fig. 1), that granite and gneiss are the main rocks in the sediment

528 source area (García-Hidalgo, 2007), and the important hydrothermal event that

529 affected the emplaced granites during the Late Jurassic (Galindo et al., 1994) the

530 high-temperature alteration interpretation is very likely. Although no correlation

531 between the kaolinite and feldspar minerals was observed in the present study,

532 this origin is plausible and the lack of correlation may be due to (1) the changes

533 produced in the contents of the two minerals during transport from the hinterland

534 and (2) the transformation of kaolinite into I-Sm in situ. This second hypothesis is

535 discussed below.

536 The interpretation of the negative correlation between kaolinite and illite

537 layers (including both illite and I-Sm with a wide range of composition) needs to

538 take into consideration the geochemical environment where a possible kaolinite-

539 to-illite transformation could have taken place. Such an evaluation should be able

540 to firstly determine whether the negative correlation between kaolinite and illite

541 layers was caused by a process taking place in situ rather than by a variation in

542   the composition of the detrital clay, and secondly, indicate the direction in which a

543   potential in situ transformation took place (kaolinisation or illitisation). Based on

544   the observation that pedogenic evidence appeared to be positively correlated

545   with illite content in the clay, a method was devised to investigate such a

546   correlation in more detail. Several pedogenic characteristics were used to create

547   a "score for soil development" (see methods) and this score was plotted vs. illite

548   content from XRD of oriented clay mounts, for all samples (Fig. 10). The illite

549   content was obtained from the normalisation of the proportions of kaolinite, illite,

550   and smectite layers. The result is that the increase in the soil development is

551   accompanied by a stepwise increase of illite content for Tortuero (T samples) but

552   not for Torrelaguna (A samples). Sample T10, with 82% illite and a soil

553   development score of zero, is interpreted to have been reworked from the

554   underlying horizon because this sediment was deposited during the earliest stage

555   of the marine transgression. If such is the case, sample T10 should be located

556   where the arrow indicates (Fig. 10), further supporting the positive correlation

557   between pedogenic character and illite content of the clays in the Tortuero

558   sequence.

559   The correlation in Tortuero militates against the possibility that the different

560   clay composition up the profile was caused by changes in the clay source

561   because it would be an unlikely coincidence that both clay source and soil

562   development in situ changed at the same time, especially unlikely considering

563   that soil development in the profile increased to a maximum in the middle of the

564   section and then decreased towards the top (i.e., from older to younger

565 sediment), rather than following a constant change in one direction. As for the

566 direction of the transformation process, kaolinitisation can be discounted for

567 several reasons. Firstly, because the high one-dimensional crystal order of

568 kaolinite, as indicated by XRD patterns (Table 2; Figs. 5 and 8), is inconsistent

569 with kaolinisation during pedogenesis, as soil kaolinites typically have wide *00l*

570 peaks (e.g., Ryan and Huertas, 2009). Secondly, because the proportion of

571 kaolinite decreases (and illite increases) with increasing pedogenic character,

572 which indicates that the soil development is causing kaolinite illitisation. Thirdly,

573 the high salinity in the lagoonal, soil and shallow marine environments, in which

574 these sediments were deposited, are incompatible with kaolinitisation.

575 The lack of correlation between soil development and the clay

576 transformation process in the Torrelaguna section (Fig. 10) is because this

577 section was closer to the Late Cenomanian-Turonian palaeoshoreline, and

578 subjected to less extreme pedogenesis and less evaporation in the lagoonal

579 environment. The Torrelaguna samples show a negative correlation between

580 kaolinite and I-Sm in the same way as the Tortuero samples (Fig. 6), which

581 suggests that there was also kaolinite illitisation in Torrelaguna. This issue will be

582 further discussed below.

583 Thus, at least for Tortuero, the inverse correlation of kaolinite with I-Sm

584 (Fig. 6), the high degree of one-dimensional crystal order of kaolinite and the

585 complex clay assemblages, with a wide range of I-Sm compositions, are

586 consistent with a slow transformation process from detrital kaolinite (likely derived

587 from hydrothermally altered granite) to illite by way of I-Sm taking place at

588 surface conditions, similar to the illitisation previously described in pedogenic

589 (e.g., Huggett and Cuadros, 2005, 2010), lacustrine (e.g., Jones and Weir, 1983)

590 and mangrove environments (Andrade et al., 2014). Some of the illite in the

591 samples displays a relatively high one-dimensional crystal order (although not as

592 high as that of kaolinite, Table 2), which could indicate the presence of detrital

593 illite or be a result of the length of time available for pedogenic illitisation. The

594 illitisation process would require the reaction of kaolinite with Mg, Fe, K, Na and

595 Ca in aqueous solution, all of which are expected to be present in a saline

596 lagoon or lake. Wetting and drying cycles, together with reducing-oxidising

597 cycles, would enable Fe uptake and reduction (Huggett and Cuadros, 2005,

598 2010). Cation-enriched fluids would foster incorporation of all these cations. Silica

599 input may not be necessary if two kaolinite layers reacted to generate one layer

600 of 2:1 silicates. Net incorporation of Si was possible, however, from dissolving

601 feldspar and from diatoms in the saline lacustrine and shallow marine

602 environments where some of the samples originated. Although no relicts of

603 diatoms were observed in the SEM investigation, diatoms are abundant in both

604 saline and fresh lacustrine environments (Chamley, 1989; Stenger-Kovács, 2014)

605 and their complete dissolution is perfectly plausible, especially if the Si was taken

606 up by the kaolinite illitisation reaction.

607   The plot of % kaolinite versus % illite layers obtained from XRD modelling

608 analysis in the Tortuero section reveals two groups of samples with a strong

609 negative correlation between kaolinite and illite layers (Fig. 11a). This plot was

610 created by normalising the proportions of kaolinite, illite, and smectite layers, i.e.,

611 the total system contains only 3 variables and there is a correlation between two

612 of them. It might be argued that the observed correlation is forced by the

613 normalisation of the 3 variables. The evidence that this correlation is real is

614 based on the following: (1) kaolinite is also observed to correlate negatively with

615 illite plus I-Sm in the whole rock data (Fig. 6); (2) two groups with a high

616 correlation appear in the analysis of the XRD patterns modelling in Tortuero

617 samples (Fig. 11a), whereas an induced correlation would most likely produce a

618 single broader correlation; (3) these two groups in Tortuero (Fig. 11a) correspond

619 exactly with samples from soils (score 1-3 in Fig. 10; full diamonds in Fig. 11a)

620 and from non-soil sediments (score 0 in Fig. 10; open squares in Fig. 11a), with

621 the exception of sample T10 which is not from a soil but is suspected to be

622 reworked from the underlying sediment (T9a). The two groups of samples

623 establish two fairly well defined trends (regression lines).

624   The corresponding regression lines intersect at ~50% illite, ~50% kaolinite.

625 This can be interpreted as the composition of the clay originally deposited in

626 these sediments. According to this interpretation, the composition of the detrital

627 clay deposited in the sediments is assumed to be approximately constant

628 throughout the stratigraphic section: 50% kaolinite and 50% I-Sm with very few

629 smectite layers. After deposition, the transformation of kaolinite generated first

630 smectitic I-Sm that caused a transient increase of smectite layers, and then illite.

631 The two groups of samples identified in Tortuero (Figs. 11a and 11b) then

632 indicate two different environments where illitisation took place at different speed.

633 The group of samples that experienced soil environments (diamond symbols in

634 Fig. 11) reacted faster towards illite than those that developed in marine and

635 lagoonal environments (square symbols in Fig. 11).

636   Comparing % kaolinite and smectite layers (Fig. 11b), also shows two sets

637 of samples defining two clear trends, with sample T1 positioned between the two.

638 This plot should be similar to the kaolinite vs. illite in that the two reaction

639 sequences should meet at about 50% kaolinite but in this plot the two lines do not

640 cross. The dotted line is in good agreement with the kaolinite vs. illite plot,

641 because it meets the vertical axis at ~50% kaolinite, which indicates an original

642 composition ~50% for each kaolinite and illite, and very little smectite. The other

643 line does not, however, reproduce the results from the kaolinite vs. illite plot

644 because the line meets the vertical axis at ~30% kaolinite. The overall trend

645 implies that kaolinite is transformed into I-Sm and illite, in both

646 lacustrine/pedogenic and marine (or pedogenic/lacustrine sediment flooded

647 during marine transgression) environments, and the composition of the original

648 sediment, as represented by 3 of the 4 lines would be near 50% kaolinite and

649 50% illite (Figs. 11a and 11b). Note that the lines in the kaolinite vs. smectite plot

650 are subjected to greater relative error because the smectite percents are smaller.

651 Thus, it is reasonable to assume that the solid line (Fig. 11b) is displaced or has

652 a distorted slope. The origin of the detrital illite may be "sericitisation" of feldspar

653 in granite and gneiss.

654   The analysis of the data from Torrelaguna is more difficult because there

655 are fewer data points and their distribution does not suggest any specific pattern.

656 As expected from the lack of correlation between soil development and illite

657 content (Fig. 10), no distribution of soil and non-soil samples was found matching

658 linear trends (Fig. 11c and d). The proportions of clay layers in Torrelaguna

659 samples are compatible with kaolinite illitisation but do not allow further analysis.

660 The interpretation that appears most likely to the authors is that kaolinite

661 illitisation took place also in Torrelaguna but that the specific conditions in the soil

662 environments did not produce a transformation that was faster than in lagoonal

663 and marine environments as in Tortuero. The reasons may be that conditions

664 needed for Fe reduction were not as frequently developed.

665 Palygorskite is restricted to the upper half of the Tortuero section. This

666 mineral is associated with arid climates and evaporites (e.g., Millot, 1964; Post,

667 1978; Weaver and Beck, 1977), which is consistent with both the saline waters

668 and wetting and drying cycles suggested by illite formation. Whether the

669 palygorskite is detrital or authigenic is unclear because the clay was only

670 detected by XRD. The palygorskite was most abundant in the most intensely

671 pedogenically modified beds at ~5-6 m above the base of the section, which

672 suggests that it was in-situ pedogenic clay, and was partially reworked into the

673 overlying marine sediment. Conceivably the palygorskite formed in lagoon

674 environments between minor episodes of marine transgression, as indicated by

675 the presence of glauconite in marls beneath the formation boundary.

676

677 *4.3. Major element chemical analysis*

678

679 The chemistry of the clay samples was investigated to identify the chemical

680 changes that accompanied illitisation in I-Sm particles. No clear correlations

681 could be established between any individual chemical element and illite content,

682 corroborating that the illitisation was due to a combination of chemical factors

683 rather than controlled by a single one. Importantly, the existence of the detrital

684 illite (or very illite-rich I-Sm) together with the I-Sm generated by the

685 transformation of kaolinite suggests that there should be two populations of illite-

686 rich I-Sm, the detrital and the authigenic, where the former would probably have

687 lower Mg/Al ratio. No signs were detected of such two populations in the SEM-

688 EDS analyses. It can be speculated that a high degree of mixture between the

689 detrital and authigenic phases precluded their separate observation. Although

690 individual flakes were analyzed, the 2 µm diameter spot of the electron beam at

691 15 kV current can have sufficient penetration to reach other flakes below. One

692 way to investigate the question of mixed detrital and authigenic particles is to

693 study the standard deviations of the EDS data that were obtained to calculate the

694 average compositions in Table 4. All standard deviations of Si and Al were < 5%

695 of the average value, with the highest values (4-4.8%) for samples T9a and T1 in

696 Tortuero and the Torrelaguna samples (A samples). In these samples there was

697 also a higher Mg standard deviation ranging 17-46%, whereas it remained <10%

698 for the rest. Iron followed a similar trend but with lower standard deviations in the

699 high range of 20-27%. The standard deviation for K was also higher in the

700 Torrelaguna samples and T3 and T8 (different from the two samples mentioned

701 above, T9a and T1) in Tortuero, at 20-27% of the average values, and remained

702 2-10% in the rest. These results show the typical level of compositional variability

703 of clay minerals at individual particle level (Bain et al., 1994). Any mixture of

704 phases with different composition must have become nearly homogeneous at

705 such level.

706   It is also possible that the detrital illite underwent partial Mg enrichment in

707 the lagoonal environment and became very similar to the I-Sm derived from

708 kaolinite. The mixture of authigenic I-Sm and detrital illitic I-Sm may be a reason

709 why there are no correlations between individual elements and illite content. In

710 any case, because all our samples have more illite content than the original

711 detrital kaolinite-illite mixture, any chemical trend accompanying illite increase is

712 truly related to the authigenic illitisation process.

713   Two relationships were found between chemical and geological variables,

714 which apply to both the Tortuero and Torrelaguna sequences. A plot of Mg in I-

715 Sm vs. the stratigraphic height above the base of the field exposure (Fig. 12a)

716 revealed the following pattern, both in Tortuero and Torrelaguna. From bottom to

717 top, Mg first decreases, then progressively increases and finally decreases again.

718 This is consistent with increasing evaporation of lake or lagoon water, and hence

719 increased Mg concentration, going up section, followed by a reversal of the trend

720 as sea level rose and marine influence increased towards the top of both

721 sections. The Mg concentration caused by this process would also be consistent

722 with the widespread distribution of early diagenetic or syn-sedimentary dolomite.

723 A plot of Fe^{2+} content in I-Sm versus height in the sequence suggests that Fe^{2+}

724 increases generally with height above the base of the section, both in Tortuero

725 and Torrelaguna (Fig. 12b). This plot was created using only samples for which

726   Fe^{2+} was determined using Mössbauer spectroscopy. Height values in the

727   Torrelaguna and Tortuero successions have no direct geological correlation,

728   however these two plots indicate that not only is it possible to correlate the

729   overall sedimentological sequence of the two localities, but also the chemistry

730   resulting from mineral modification during and soon after deposition.

731   Considering all the above data, the most likely interpretation is that kaolinite

732   illitisation took place both in Tortuero and Torrelaguna. In Tortuero, a single clay

733   source and soil conditions that produced faster illitisation than in lagoonal and

734   marine environments generated two recognisable illitisation trends. In

735   Torrelaguna, variations of the detrital clay composition or in the environmental

736   conditions may have existed and any correlation between soil development and

737   illitisation was weakly developed (Fig. 10, Fig. 11c and d).

738   The Sierra de Guadarrama I-Sm has only 3-6% total Fe_2O_3, a range lower

739   than that of the non-marine, syn-sedimentary glauconite reported by Huggett and

740   Cuadros (2010) or ferric illite (e.g. Keller, 1958; Gabis, 1963; Deconinck et al,

741   1988; Baker, 1997; Eggleton and Fitz Gerald, 2011). This fact may be partly or

742   completely due to the mixture of authigenic I-Sm and detrital illite, so that the

743   detrital illite is more Al-rich and the authigenic I-Sm more Fe-rich. In the

744   authigenic illitisation process, in order for K^+ to be fixed in the interlayer site,

745   there has to be an increase in the layer charge of the 2:1 clay mineral. In Fe-rich

746   illite and glauconite this is normally achieved through reduction of octahedral Fe^{3+}

747   to Fe^{2+}, with substitution of Al^{3+} for Si^{4+} in the tetrahedral sheet increasing with

748   burial (Ireland et al., 1983; Kazerouni et al., 2013). In the Fe-poor, Mg-rich

749 dolomitic lacustrine environment of the Alcorlo Formation, a significant proportion

750 of the layer charge increase may have occurred through substitution of Mg^{2+} for

751 trivalent cations in the octahedral sheet. The MgO content of the Alcorlo

752 Formation illite is of the order of 3-4% which is at the upper end of the range for

753 published non-marine neoformed Fe-rich illite (Keller, 1958; Gabis, 1963;

754 Deconinck et al., 1988; Baker, 1997; Eggleton and Fitz Gerald, 2011), and is high

755 compared with 1-2% in the lacustrine glauconite reported by Huggett and

756 Cuadros (2010). It is therefore concluded that Mg substitution for Al (or Fe^{3+}) was

757 more important in low-temperature illitisation of the Alcorlo Formation clay than

758 reduction of Fe^{3+} to Fe^{2+}. The Al for Si substitution in the tetrahedral sheet was

759 also important in creating layer charge (Table 4), perhaps also due to the

760 presence of the detrital illite in the original sediment.

761   In Tortuero, the intensity of the illitisation process increased up through the

762 section, reaching a maximum where pedogenesis is most intense in the middle

763 section, and then decreased as marine influence increased towards the top of the

764 Alcorlo Formation and the marine Tranquera Formation. The proportion of Mg in

765 the Tranquera Formation illitic clay is lower than that in the Alcorlo Formation.

766 This may be due to inhibition of Mg fixation in the marine setting. Illitisation

767 through Mg replacement of trivalent cations has only rarely been previously

768 reported. Chamley (1989) hypothesised that Mg enrichment of smectite and illite

769 may occur in saline lakes with 30-90 g/kg salt concentration. Hover and Ashley

770 (2003) reported neoformation of Mg-rich celadonite (Mg content of 0.35-0.63 per

771 $O_{10}[OH]_2$), in the volcaniclastic Plio-Pleistocene sediments of Lake Olduvai in

772 Tanzania, while Deocampo (2004) found that illite in the <0.1 μm fractions of

773 Olduvai sediments showed systematic stratigraphic Mg variations correlating

774 positively with lake regression indicators. Deocampo et al. (2009) also found Mg

775 enrichement of smectite and I-Sm to correlate with low water levels in the Olduvai

776 palaeolake, but no such correlation existed with K or illite proportion. From this it

777 was concluded by Deocampo et al. (2009) that Mg uptake and K fixation took

778 place at different stages of lake salinity. This is consistent with the fact that high

779 saline concentration triggering Mg uptake implies low K/Na ratios that do not

780 favour interlayer K fixation. Jones and Weir (1983) reported Mg-rich illite

781 (composition not determined) in the alkaline Lake Abert, in which the Mg illite

782 replaced a stevensite-like Mg-rich smectite. Again, this process differs from the

783 Sierra de Guadarrama illitisation, in the starting material. Neither volcanic

784 sediment nor Mg-rich smectite are present in the Alcorlo formation, with the

785 exception of the distinctive thin black clay beds at Torrelaguna.

786 Qualitative EDS analysis of the black clays at Torrelaguna indicated that

787 they are Mg-rich smectite. The relatively high smectite content, and very fine

788 grain-size of the black clays (samples A10 and A11) suggest that they include

789 volcanic ash; however, the REE data indicates that this is unlikely to be the case.

790 The lack of lateral continuity of these strata is also consistent with the black clays

791 not being primary ash-falls. Total organic C data for these samples indicate very

792 low C content (0.25% for A10, 0.29% for A11), hence the colour is not due to the

793 presence of organic matters. At present the origin of these beds remains

794 enigmatic.

795   The presence of glaucony pellets in the Tranquera Formation is consistent

796   with this being a transgressive marine sediment (Amorosi, 1995). Maturation of

797   clay-rich faecal pellets to glauconitic clay in marine environments has been

798   widely described as a process that may be summarised as Fe enrichment (e.g.,

799   Odin and Matter, 1981; Odin and Fullager, 1988), Fe partial reduction, increased

800   layer charge, and interlayer K fixation.

801

802   4.4. Rare Earth Element analysis

803

804   For both sections the whole-sample REE data reflect the interplay of signals

805   from carbonate- and clay-dominated end members (Figs. 3-4; Table 5). The

806   carbonate-dominated end member is best typified by REE profiles T1 and A2,

807   with a similar trend to those reported by Tlig and M'Rabet (1985). The T1 and A2

808   REE profiles are enriched in the middle REE and have a slight negative shale-

809   normalised Eu anomaly. The clay profile end member is best typified by profile T4

810   and shows depletion in the middle REE with a moderate negative Eu anomaly.

811   REE profiles, which are noticeably irregular such as those of samples A6 and A7,

812   are likely to reflect modification by pedogenic processes. Previous work by Wray

813   (e.g., Wray, 1999; Wray and Jeans, 2014) has used the presence of a negative

814   shale-normalised Eu anomaly to indicate that sediment was of volcanogenic

815   origin, most probably a bentonite. In the sections currently under study this

816   interpretation is unlikely; more probably the clay REE profile is controlled by the

817   composition of the proximal granitic hinterland from which the clay fraction of the

818   sediment is believed to be derived. Both granite and pedogenic processes in soil

819   overlying granite contribute to a negative Eu anomaly in the weathered material

820   (Aubert et al., 2001). The clay-rich beds A10 and A11 have comparable REE

821   profiles to the other clay-rich beds in the succession, best typified by bed A1, and

822   the REE data show no evidence that beds A10 and A11 have a difference

823   provenance to the remainder of the succession.

824

825   **5. Conclusions**

826

827   1) Mid Turonian sea level fall (reflecting a global eustatic signal) in the studied

828   localities resulted in the formation of a coastal plain environment in which

829   extensive pedogenesis occurred around lagoons (Alcorlo Formation).

830

831   2) Detrital clay sediments consisting of kaolinite and illite were deposited and

832   transformed in the soil/lagoon environment. The existence of detrital illite creates

833   uncertainty about the specific range of chemical changes that took place in the

834   soil/lagoon environment but the trends are reliable. These trends indicate that

835   low-temperature illitisation of kaolinite via smectite and I-Sm took place through

836   enhanced layer charge resulting from Mg substitution for Al (or Fe^{3+}), Al for Si

837   substitution and Fe^{3+} to Fe^{2+} reduction. This may be the first documented

838   occurrence of illitisation by this dual mechanism.

839

840 3) Mg enrichment of the clay may have occurred principally in saline lagoons or

841 lakes, while Fe^{3+} to Fe^{2+} reduction occurred as a result of wetting and drying in a

842 pedogenic environment. Iron reduction may have continued with the deposition of

843 the Tranquera Formation, but in a marine environment. The MgO content of the

844 clay in the marine sediments, towards the top of the sampled intervals, is ~4%,

845 implying that enrichment continued in the marine environment, although to a

846 lesser extent than in the lagoonal-pedogenic environments represented by lower

847 horizons.

848

849 4) The intensity of the illitisation process increased up through the Tortuero

850 section, reaching a maximum where pedogenesis was most intense in the middle

851 section, and then decreased as marine influence increased towards the top of the

852 Alcorlo Formation and the marine Tranquera Formation. No clear pattern is

853 apparent linking soil development and illitisation in the Torrelaguna section.

854

855 5) The illitisation process, influenced by the existence of detrital illite in the

856 original sediment, has resulted in a less Fe-rich, more Mg- and Al-rich illite than

857 the majority of previously documented cases.

858

859 6) From the above conclusions, the range of environments and processes (both

860 geological and geochemical) by which surface illitisation takes place is wider than

861 described previously, and these processes can act in combination, making this

862 reaction more relevant globally.

863

864 7) The trace amounts of palygorskite found towards the top of the Tortuero

865 section are probably produced in the same Mg-enriching diagenetic process(es)

866 promoting illitisation and dolomitisation.

867

868 8) Dolomitisation of pre-existing carbonates, either bioclasts or cement, occurred

869 in coastal (Alcorlo Formation) and shallow marine (Tranquera Formation)

870 sediments. By analogy with recent saline lacustrine sediments in Iraq (Aqrawi,

871 1995), this probably happened soon after deposition.

872

873 9) Dolomitisation and Mg enrichment of the clay may have occurred at the same

874 time. Seawater is the most probable source of Mg, though it is conceivable that it

875 was also derived through dissolution of evaporites in the younger Valle de

876 Tabladillo Formation.

877

878 10) Dessication of lake or lagoonal sediment was accompanied by formation of

879 haematite in both clay and dolomite-rich samples.

880

885 did not receive any specific grant from funding agencies in the public,

886 commercial, or not-for-profit sectors.

887

References

888 Amorosi, A., 1995. Glaucony and sequence stratigraphy: a conceptual framework

891 of distribution in siliciclastic sequences. J. Sediment. Res. 65, 419-425.

892 DOI: 10.1306/D4268275-2B26-11D7-8648000102C1865D

893 Andrade, G., de Azevedo, A., Cuadros, J., Souza, V., Correia- Furquim, S.A.,

894 Kiyohara, P., Vidal-Torrado, P., 2014. Transformation of kaolinite into

895 smectite and iron-illite in Brazilian mangrove soils. Soil Sci. Soc. Am. J. 78,

896 655-672.

897 Aqrawi, A.A.M., 1995. Brackish-water and evaporitic Ca-Mg carbonates in the

898 Holocene lacustrine/deltaic deposits of southern Mesopotamia. J. Geol.

899 Soc. London 152, 259-268.

900 Aubert, D., Stille, P., Probst, A., 2001. REE fractionation during granite

901 weathering and removal by waters and suspended loads: Sr and Nd

902 isotopic evidence. Geochim. Cosmochim. Acta 65, 387-406.

903 Bain, D.C., McHardy, W.J., Lachowski, E.E., 1994. X-ray fluorescence

904 spectroscopy and microanalysis. In: Wilson, M.J. (Ed.) Clay Mineralogy:

905 Spectroscopic and Chemical Determinative Methods. Chapman and Hall,

906 London, pp. 260-299 (Chapter 7).

907 Baker, J.C., 1997. Green ferric clay in non-marine sandstones of the Rewan

908 Group, southern Bowen Basin, Eastern Australia. Clay Miner. 32, 499-506.

909 Baker, P.A., Kastner, M., 1981. Constraints on the formation of sedimentary

910 dolomite. Science 213, 214-216.

911   Benito, M.I. and Mas, R. 2007. Origin of Late Cretaceous dolomites at the

912   southern margin of the Central System, Madrid Province, Spain. J. Iber.

913   Geol. 33, 41-54.

914   Chamley, H., 1989. Clay Sedimentology. Springer-Verlag, Berlin.

915   Chamley, H., Debrabant, P., Candillier, A.-M., Foulon, J., 1983. Clay mineralogy

916   and inorganic geochemical stratigraphy of Blake-Bahama Basin since the

917   Callovian, site 534, Deep Sea Drilling Project leg 76. Initial Reports DSDP

918   76, 437-451.

919   Deconinck, J.F., Strasser, A., Debrabant, P., 1988. Formation of illitic minerals at

920   surface temeratures in Purbeckian sediments (lower Berriasian, Swiss and

921   French Jura). Clay Miner. 23, 91-103.

922   Deocampo, D.M., 2004. Authigenic clays in East Africa: Regional trends and

923   paleolimnology at the Plio-Pleistocene boundary, Olduvai Gorge,

924   Tanzania. J. Paleolimnol. 31, 1-9.

925   Deocampo, D.M., Cuadros, J., Wing-Dudek, T., Olives, J., Amouric, M., 2009.

926   Saline lake diagenesis as revealed by coupled mineralogy and

927   geochemistry of multiple ultrafine clay phases: Pliocene Olduvai Gorge,

928   Tanzania. Am. J. Sci. 309, 834-868.

929   Dyar, M.D., Schaefer, M.W., Sklute, E.C., Bishop, J.L., 2008. Mössbauer

930   spectroscopy of phyllosilicates: effects of fitting models on recoil-free

931   fractions and redox ratios. Clay Miner. 43, 3-33.

932   Eberl, D. and Hower, J. 1976. Kinetics of illite formation. Geol. Soc. Amer. Bull.

933   87, 1326-1330.

934

935 Ehrenberg, S.N. and Nadeau, P.H., 1989. Formation of diagenetic illite in

936   sandstones of the Garn Formation Haltenbanken Area, Mid-Norwegian

937   Continetnal Shelf. Clay Miner. 24, 233-253.

938 Eggleton, R.A., Fitz Gerald, J., 2011. Illite from Muloorina, South Australia. Clays

939   Clay Miner. 59, 608-612.

940 Gabis, V., 1963. Etude minéralogique et géochimique de la série sedimentaire

941   Oligocène du Velay. Bull. Soc. Fr. Minéral. Crist. 86, 315-354.

942 Gale, A.S., 1996. Turonian correlation and sequence stratigraphy of the Chalk in

943   southern England. Sequence stratigraphy in the United Kingdom. In:

944   Hesselbo, S.P., Parkinson, D.N. (Eds.) Sequence Stratigraphy in British

945   Geology. Geological Society of London Special Publication 103, London,

946   pp. 177-195.

947 Galindo, C., Tornos, F., Darbyshire, D.P.F., Casquet, C., 1994. The age and

948   origin of the barite–fluorite (Pb–Zn) veins of the Sierra del Guadarrama

949   (Spanish Central System, Spain): a radiogenic (Nd, Sr) and stable isotope

950   study. Chem. Geol. 112, 351–364.

951 García-Hildalgo, J.F., Gil, J., Segura, M., Dominguez, C., 2007. Internal anatomy

952   of a mixed siliciclastic–carbonate platform: the Late Cenomanian–Mid

953   Turonian at the southern margin of the Spanish Central System.

954   Sedimentology 54, 1245–1271.

955 Giles, M.R., 1997. Diagenesis: A Quantitative Perspective. Kluwer Academic

956   Publishers, Dordrecht.

957   Gilg, A., Weber, B., Kasbohm, J., Frei, R., 2003. Isotope geochemistry and orgin

958   of illite-smectite and kaolinite from the Seelitz and Kemmlitz kaolin

959   deposits, Saxony, Germany. Clay Miner. 38, 95-112.

960   Glasmann, J.R., Lundgard, P.D., Clark, R.A., Penny, B.K. and Collins, I.D., 1989.

961   Geochemical evidence of the history of diagenesis and fluid migration:

962   Brent Sandstone, Heather Field, North Sea. Clay Miner. 24, 255-284.

963   Griffin, J.J., Windom, H. Goldberg, E.D., 1968. Distribution of clay minerals in the

964   world ocean. Deep-Sea Res. 15, 433-461.

965   Hancock, J.M., 1990. Sea level changes in the British region during the Late

966   Cretaceous. P. Geologist. Assoc. 100, 565-594.

967   Hover, V.C., Ashley, G.M., 2003. Geochemical signatures of paleodepositional

968   and diagenetic environments: a STEM/AEM study of authigenic clay

969   minerals from an arid rift basin. Olduvai Gorge, Tanzania. Clays Clay

970   Miner. 51, 231-251.

971   Huggett, J.M., Cuadros, J., 2005. Low-temperature illitization of smectite in the

972   late Eocene and early Oligocene of the Isle of Wight (Hampshire basin),

973   UK. Am. Mineral. 90, 1192-1202.

974   Huggett, J. M., Cuadros, J., 2010. Glauconite formation in lacustrine/palaeosol

975   sediments, Isle of Wight (Hampshire basin), UK. Clay Miner. 45, 35-50.

976   Huggett, J.M., Gale, A.S., Clauer, N., 2001. The nature and origin of non-

977   marine 10 Å green clays from the late Eocene and Oligocene of the Isle

978   of Wight (Hampshire basin), UK. Clay Miner. 36, 447-464.

979   Ireland, B.J., Curtis, C.D. and Whiteman, J.A. 1983. Compositional variation

45

980   within some glauconites and illites and implications for their stability and

981   origins. Sedim. 30, 769–786.

982   Jarvis, I., Jarvis, K.E., 1985. Rare-earth element geochemistry of standard

983   sediments: a study using inductively coupled plasma spectrometry. Chem.

984   Geol. 53, 335-344.

985   Jones, B.F., Weir, A.H., 1983. Clay minerals of Lake Abert, an alkaline saline

986   lake. Clays Clay Miner. 31, 161-172.

987   Keller, W.D., 1958. Glauconitic mica in the Morrison Formation in Colorado.

988   Clays Clay Miner. 5, 120-128.

989   Kazerouni, A.M., Poulsen, M.K., Friis, H., Svendsen, J.B., Hansent, J.P.V., 2013.

990   Illite/smectite transformation in detrital glaucony during burial diagenesis of

991   sandstone: A study from Siri Canyon – Danish North Sea. Sedimentology

992   60, 679–692.

993   Lagarec, K., Rancourt, G.K., 1998. Mössbauer Spectral Analysis Software.

994   Mössbauer Group Physics Department, University of Ottawa, Canada.

995   Martin-Serrano, A., Santisteban, J.L. and Mediavilla, D.R., 1996. Tertiary of

996   Central System basins. In: Friend, P.F. and Dabrio, C.J. (Eds.) Tertiary

997   Basins of Spain. Cambridge University Press, pp. 255-260.

998   McLennan, S.M.,1989. Rare earth elements in sedimentary rocks: influence of

999   provenance and sedimentary processes. In: Lipin, B.R., McKay, G.A.

1000   (Eds.) Geochemistry and Mineralogy of the Rare Earth Elements,

1001   Mineralogical Society of America, Reviews in Mineralogy 21, Chantillly,

1002   Virginia, pp. 169-200 (Chapter 7).

1003 Mehra, O.P., Jackson, M.L., 1960. Iron oxide removal from soils and clays by

1004   dithionite-citrate system buffered with sodium bicarbonate. Clays Clay

1005   Miner. 7, 317-327.

1006 Millot, G., 1964. Géologie des Argiles. Masson, Paris.

1007 Moore, D.M., Reynolds, R.C., 1997. X-ray Diffraction and the Identification and

1008   Analysis of Clay Minerals. Oxford University Press, Oxford.

1009 Nesteroff, W.D., Sabatier, G., Heezen, B.C., 1964. Les minéraux argileux, le

1010   quartz et le calcaire dans quelques sédiments de l'océan Arctique. C.R.

1011   Acad. Sci. 258, 991-993.

1012 Neumann, A., Petit, S., Hofstetter, T., 2011. Evaluation of redox-active iron sites

1013   in smectites using middle and near infrared spectroscopy. Geochim.

1014   Cosmochim. Acta 75, 2336-2355.

1015 Norrish, K., Pickering, J.G., 1983. Clay Minerals. In: Soils, an Australian

1016   Viewpoint. CSIRO, Melbourne, and Academic Press, London, pp. 281-

1017   308.

1018 Odin, G.S., Fullager, P.D., 1988. Geological significance of the glaucony facies.

1019   In: Green marine clays (Odin, G.S., Ed.). Elsevier, Developments in

1020   Sedimentology, Volume 45, Amsterdam, pp. 295-332 (Chapter C4).

1021 Odin, G.S., Matter, A., 1981. De glauconiarum origine. Sedimentology 28, 611-

1022   641.

1023 Palumbo, F. Main, I.G. and Zito, G., 1999. The thermal evolution of sedimentary

1024   basins and its effect on the maturation of hydrocarbons. Geophys. J. Int.

1025   139, 248–260.

1026   Perry, E. and Hower, J. 1970. Burial diagenesis in Gulf Coast pelitic sediments.

1027   Clays Clay Miner. 18, 165-178.

1028   Plançon, A., 2002. New modeling of X-ray diffraction by disordered lamellar

1029   structures, such as phyllosilicates. Am. Mineral. 87, 1672-1677.

1030   Post, J.L., 1978. Sepiolite deposits of the Las Vegas, Nevada area. Clays Clay

1031   Miner. 26, 58-64.

1032   Retallack, G.J., 2001. Soils of the past. 2nd Edition, Blackwell Science, Oxford.

1033   Reynolds, R.C. Jr., Reynolds, R.C. III, 1996. NEWMOD: The Calculation of One-

1034   Dimensional X-ray Diffraction Patterns of Mixed-Layered Clay Minerals.

1035   Computer Program. 8 Brook Road, Hanover, New Hampshire, USA.

1036   Robinson, D., Wright, V.P., 1987. Ordered illite-smectite and kaolinite-smectite:

1037   pedogenic minerals in a lower Carboniferous paleosol sequence, South

1038   Wales? Clay Miner. 22, 109-118.

1039   Ryan, P.C., Huertas, F.J., 2009. The temporal evolution of pedogenic Fe-

1040   smectite to Fe-kaolin via interstratified kaolin-smectite in a moist tropical

1041   soil chronosequence. Geoderma 151, 1-15.

1042   Singer, A., Stoffers, P.,1980. Clay mineral diagenesis in two East African lake

1043   sediments. Clay Miner. 15, 291-307.

1044   Siyuan, S., Stucki, J., 1994. Effects of iron oxidation state on the fate and

1045   behaviour of potassium in soils. In: Havlin, J.L, Jacobson, J., Fixen, P.,

1046   Herbert, G. (Eds) Soil Testing: Prospects for improving nutrient

1047   recommendations. Soil Sci. Soc. Am. Special Publication 40, Madison, pp.

1048   173-185.

1049 Smith B., 1994. Characterization of poorly ordered minerals by selective chemical

1050   methods. In: Wilson, M.J. (Ed) Clay Mineralogy: Spectroscopic and

1051   Chemical Determinative Methods. Chapman & Hall, London, pp. 333-357

1052   (Chapter 9).

1053 Stanjek, H., Marchel, C., 2008. Linking the redox cycles of Fe oxides and Fe-rich

1054   clay minerals: an example from a palaeosol of the Upper Freshwater

1055   Molasse. Clay Miner. 43, 69-82.

1056 Stenger-Kovács,C., Lengyel, E., Buczkó, K., Tóth, F.M., Crossetti, L.O.,

1057   Pellinger, A., Doma, Z.Z., Padisák, J., 2014. Vanishing world: alkaline,

1058   saline lakes in Central Europe and their diatom assemblages. Inland

1059   Waters 4, 383-396.

1060 Stucki, J.W., 1997. Redox processes in smectite: soil environmental signifiance.

1061   Adv. GeoEcol. 30, 395-406.

1062 Stucki, J.W., Low, P.F., Roth, C.B., Golden, D.C., 1984. Effects of iron oxidation

1063   state on clay swelling. Clays Clay Miner. 32, 357-362.

1064 Summerfield, M.A., 1983. Petrography and diagenesis of silcrete from the

1065   Kalahari basin and Cape Coastal zone, southern Africa. J. Sediment.

1066   Petrol. 53, 895-909.

1067 Tlig, S., M'rabet, A., 1985. A Comparative-Study of the Rare-Earth Element

1068   (REE) Distributions within the Lower Cretaceous Dolomites and

1069   Limestones of Central Tunisia. Sedimentology 32, 897-907.

1070 Watts, N.L., 1980. Quaternary pedogenic calcretes from the Kalahari (southern

1071   Africa): mineralogy, genesis and diagenesis. Sedimentology 27, 661-686.

1072   Weaver, C.E., 1989. Clays, Muds, and Shales. Developments in Sedimentology,

1073   Volumen 44. Elsevier, Amsterdam.

1074   Weaver, C.E., Beck, K.C., 1977. Miocene of the S.E. United States: a model for

1075   chemical sedimentation in a peri-marine environment. Sediment. Geol. 17,

1076   1- 234.

1077   Wray, D.S., 1999. Identification and long-range correlation of bentonites in

1078   Turonian - Coniacian (Upper Cretaceous) chalks of northwest Europe.

1079   Geol. Mag. 136, 361-371.

1080   Wray, D.S., Jeans, C.V., 2014. Chemostratigraphy and provenance of clays and

1081   other non-carbonate minerals in chalks of Campanian age (Upper

1082   Cretaceous) from Sussex, southern England. Clay Miner. 49, 327-340.

1083   Figures

1084

1085   Figure 1. Map of Spain with the location of Sierra de Guadarrama and geological

1086   map of the investigated sites. The sampled sites, Tortuero (T) and Torrelaguna

1087   (A), are shown.

1088

1089   Figure 2. Roadside section through the sampled interval at Tortuero, in 2011.

1090   Numbers refer to the sample numbers as shown in Figure 3.

1091

1092   Figure 3. Sedimentological log for the Tortuero section with clay assemblage, X-

1093   ray diffraction data shown as a bar chart for clay-bearing samples, and whole

1094   sample REE element plots for all samples. Vertical scale is in meters above the

1095   base of the measured section. Illite and smectite are present in illite-smectite

1096   mixed-layer; here the percent of each layer is represented. Sample labels are left

1097   of the clay-proportion bars, at the corresponding sampling height. Some samples

1098   do not have detailed clay composition.Vertical distance is shown in m at the left

1099   of the diagram. Grain size (clay, silt, very fine and fine sand) is indicated at the

1100   base of the log.

1101

1102   Figure 4. Sedimentological log for the Torrelaguna section, caption as in Figure

1103   3.

1104

1105   Figure 5. Powder XRD diagrams of two samples from Tortuero (T3) and

1106   Torrelaguna (A10), with different contents of carbonate and silicate phases.

1107   Values are d-values in Å. I-Sm is illite-smectite, Kaol is kaolinite, Qz is quartz,

1108   and Dol is dolomite. The 3.34 Å peak in A10 is truncated.

1109

1110

1111   Figure 6. Plot of the relative areas of XRD peaks corresponding to illite-smectite

1112   (I-Sm) phases (range 17-10 Å) and kaolinite (~7 Å), in Tortuero (T) and

1113   Torrelaguna (A). The areas were normalised to the sum of the areas of selected

1114   peaks for all the silicate phases (see Methods section). The data indicate an

1115   inverse correlation between the abundance of kaolinite and I-Sm phases (see

1116   text).

1117

1118 Figure 7. BSEM images: (a) Haematite infilling fractures in dolomite. In this

1119 sample (T8a) the clay appears homogenous. (b) Clay-rich dolomite from the

1120 Tranquera Formation (sample T14). Dolomite is faintly zoned; in some crystals

1121 the core has been leached out (D1), while in others one or two chemical zones

1122 have been leached out (D2). Sand-size quartz is widespread and a selection of

1123 grains are indicated with an arrow. Note that contrast is similar to dolomite, but

1124 the two minerals may be distinguished by their different shapes, i.e. quartz is

1125 sub-rounded, dolomite is rhombic. Glt = glauconite. (c) Part of a calcite-cemented

1126 fracture in dolomite (sample A6).

1127

1128 Figure 8. Experimental and calculated XRD patterns of the oriented mounts of

1129 samples from Tortuero and Torrelaguna with different clay contents. Pal indicates

1130 palygorskite and Fsp is feldspar. Only illite-smectite (I-Sm) and kaolinite (Kaol)

1131 are included in the model.

1132

1133 Figure 9. Mössbauer spectra of two samples (dots), with the corresponding

1134 calculated components and fit to the experimental data (lines). Two octahedral

1135 Fe^{3+} components (small quadrupole splitting) and one octahedral Fe^{2+}

1136 component (large quadrupole splitting) occur in each spectrum.

1137

1138 Figure 10. Percent illite in the clay fraction as calculated from XRD data (oriented

1139 mounts) plotted vs. a soil development score, calculated from the number of

1140 pedogenic characteristics present (colour mottling, rootlets and peds). T and A

1141 indicate samples from Tortuero and Torrelaguna sections, respectively. The

1142 arrow indicates that clay from horizon T10, with no soil development, is

1143 suspected to be reworked from the underlying horizon, T9a, which has a soil

1144 score of 3, and the position that sample T10 would have in the plot.

1145

1146 Figure 11. Plots of layer type percent from modelling of the XRD patterns of

1147 oriented and glycolated mounts. The data from Tortuero define two groups of

1148 samples with established trends (see text). The smaller number of data points

1149 from Torrelaguna do not define clear trends. The labels of the samples are

1150 included in a and c.

1151

1152 Figure 12. Octahedral Mg and Fe^{2+} content of illite-smectite versus stratigraphic

1153 height at Tortuero and Torrelaguna. Heights are meaningful only within each

1154 sequence, as there is no geological correspondence between height values at

1155 Tortuero and Torrelaguna. Chemical values are from averaged SEM-EDS

1156 analyses and recalculated to the structural formula ($O_{10}[OH]_2$, i.e., atoms per half

1157 formula unit: a.p.h.f.u.). The b plot has data only from samples analysed with

1158 Mössbauer spectroscopy.

1159

1   LOW TEMPERATURE, AUTHIGENIC ILLITE AND CARBONATES IN A MIXED

2   DOLOMITE-CLASTIC LAGOONAL AND PEDOGENIC SETTING, SPANISH

3   CENTRAL SYSTEM, SPAIN

4

5

6   Jennifer Huggett[a,b], Javier Cuadros[b], Andrew S. Gale[c], David Wray[d] and Jacob

7   Adetunji[e]

8

9

10   [a] Petroclays Ltd, Sandy Cross, Heathfield, E Sussex, TN21 8QP, UK

11   [b] The Natural History Museum, London, SW7 5BD, UK

12   [c] Department of Earth Sciences, The University of Portsmouth, PO1 3QL, UK

13   [d] School of Science, University of Greenwich, ME4 4TB, UK

14   [e] Department of Natural Science, University of Derby, DE22 1GB, UK

15

16

17   E-mail of corresponding author (Jennifer Huggett): info@petroclays.com

18

19 ABSTRACT

20

21 The aim of this study was to further our understanding of the pedogenic and

22 lacustrine modification of clay minerals. Some of these modifications are of

23 special interest because they constitute reverse weathering reactions, rare in

24 surface environments, and because there is not yet an accurate assessment of

25 their global relevance in mineralogical and geochemical cycles. For this study,

26 two sections from the Central System in Spain were selected. Both are sections

27 through the Uppper Cenomanian-Turonian mixed clastic and carbonate

28 succession, containing both calcite and dolomite, in the Sierra de Guadarrama.

29 Mid-Turonian sea level fall resulted in the formation of a coastal plain

30 environment in which extensive pedogenesis occurred around saline lagoons.

31 The mineralogical changes that have occurred as a result of sedimentation in

32 saline lagoons and as a consequence of pedogenesis are described. Textural

33 relationships indicate that the dolomite cement pre-dates the calcite. Silicate

34 minerals are represented by quartz, kaolinite, illite-smectite, illite, minor

35 plagioclase and alkali feldspar, and trace chlorite and palygorskite. There is a

36 positive correlation between the intensity of pedogenesis and the proportion of

37 illite in the clay assemblage in one of the sections, indicating pedogenic

38 illitisation. In this section, the intensity of the illitisation process increases up,

39 reaching a maximum where pedogenesis is most intense in the middle part, and

40 then decreases as marine influence increases towards the top of the Alcorlo

41 Formation and the overlying marine Tranquera Formation. The clay assemblages

42 are consistent with a slow transformation process from kaolinite to illite by way of

43 illite-smectite, taking place under surface conditions. The illitisation process has

44 resulted in a less Fe-rich, more Mg-, and Al-rich illite than the majority of

45 previously documented cases in the near surface. Formation of Al-rich illite is not

46 therefore restricted to the deep subsurface.

47 The mechanism for low temperature illitisation involves enhanced layer charge

48 resulting from Mg^{2+} substitution for Al^{3+} (or Fe^{3+}) and Fe^{3+} to Fe^{2+} reduction. Mg^{2+}

49 enrichment may have occurred principally in saline lagoons or lakes, while Fe^{3+}

50 to Fe^{2+} reduction occurred as a result of wetting and drying in a pedogenic

51 environment. So far as it has been possible to establish, this dual mechanism

52 has not previously been documented. This study indicates clearly that the

53 dolomite and calcite are authigenic cements that precipitated in a clastic

54 sediment, probably soon after deposition. Dolomitisation and Mg enrichment of

55 the clay may have occurred at the same time. Seawater is the most probable

56 source of Mg.

57

59

1. Introduction

This study was initiated with the intention of improving our understanding of modification of clay minerals in pedogenic and lacustrine environments. Clay assemblages in chemical equilibrium with the surface sediments in which they form, or are modified, are important palaeoenvironmental and palaeoclimatic indicators. Most clays formed at the Earth's surface are predominantly a result of weathering, and clay mineralogy is considered to reflect the intensity and duration of weathering conditions. Hence, most illite in sediments is the result of high latitude weathering of rocks (e.g., Nesteroff et al., 1964; Chamley, 1989 and references therein), where cold and dry conditions prevail. In low-latitude, non-arid climates illite is expected to degrade into smectite and kaolinite (e.g., Chamley et al., 1983; Griffin et al., 1968), depending of the specific conditions. Illitisation, however, also takes place in specific surface environments in warm climates (see below); for accurate palaeoenvironmental reconstruction it is necessary to identify such environments. The present investigation, in quartz and dolomite-rich sediments, complements previous studies (Huggett et al., 2001; Huggett and Cuadros, 2005, 2010) of pedogenic modification of clay minerals, including ilitisation, in calcite- and quartz-rich sediments.

Pedogenic illitisation of smectite is fairly well documented in the literature (e.g., Watts, 1980; Robinson and Wright, 1987; Huggett et al., 2001; Huggett and Cuadros, 2005, 2010; Gilg et al., 2003; Stanjek and Marchel, 2008), as is lacustrine illitisation (e.g., Gabis, 1963; Singer and Stoffers, 1980; Jones and

83 Weir, 1983; Norrish and Pickering, 1983; Deconinck et al., 1988). Low

84 temperature illitisation in soils and lakes has been linked to Fe uptake and

85 microbial reduction (Stucki et al., 1984; Siyuan and Stucki, 1994; Stucki, 1997;

86 Huggett et al., 2001; Huggett and Cuadros, 2005, 2010). Others (e.g., Keller,

87 1958; Gabis, 1963; Gilg et al., 2003) have observed weathering of volcanic rock

88 to form iron-rich illite in soils and lakes. Illitisation driven by Fe uptake and

89 reduction has also been described in mangrove forests (Andrade et al., 2014). All

90 the above processes are of interest not only due to palaeoenvironmental

91 implications but also for geochemical cycles. Illitisation at surface environments

92 may represent continental or coastal K sinks of yet unrecognised importance.

93 Given the connection of some of these illitisation processes to Fe uptake they

94 may also be relevant to the Fe biogeochemical cycles. In this study we report an

95 occurrence of low temperature illitisation that has produced an Fe-poor illite.

96   The localities studied here were part of a study of the facies and sequence

97 stratigraphy of a transect running obliquely NE-SW across the boundary between

98 the Hesperian Massif and the Iberian Basin in central Spain (García-Hildalgo et

99 al., 2007). Two sections (Figure 1) were studied in the present work, a roadcut

100 between Torrelaguna and El Berrueco on the M131 road, Calle del las Cercas, 3

101 km north west of Torrelaguna, and a roadcut on the GU1065, 750 m south of

102 Tortuero, some 20 km to the north east of the Torrelaguna section (Figure 2).

103 Samples from Torrelaguna have the prefix A, and those from Tortuero have the

104 prefix T.

105   The lithostratigraphical terminology applied to this succession (Fig. 2 in

106 García-Hildalgo et al., 2007) is complex, because the strata show extensive

107 interdigitation, and their boundaries have not been effectively defined at the

108 localities studied here. Furthermore, the detailed sequence stratigraphy

109 described by García-Hildalgo et al. (2007) did not apply lithostratigraphical

110 nomenclature, but rather used four named sequences (their Fig. 3, successively,

111 Atienza, Patones, El Molar and the youngest, Somolinos), which are not precisely

112 related to the formations. Our study involved the Alcorlo Formation (dolomitic

113 sands, marls and clays) and the basal part of the overlying Tranquera Formation

114 (thinly to medium bedded dolostones and marls), which are interpreted to fall in

115 the upper El Molar and lower Somolinos sequences of García-Hildalgo et al.

116 (2007).

117   The Upper Cenomanian-Turonian succession in the Sierra de

118 Guadarrama region of central Spain (Fig. 1), is composed of mixed clastic and

119 carbonate sediments deposited in a variety of coastal and marine shelf

120 environments: alluvial plain–estuarine, lagoon, shoreface, offshore hemipelagic,

121 and carbonate ramp (García-Hidalgo et al., 2007). Transgression onto Hercynian

122 basement of the Hesperian Massif commenced in the Late Cenomanian, and

123 reached its maximum extent in the Late Cenomanian-Early Turonian. During the

124 Mid-Turonian, sea level fell, resulting in the development of lagoonal facies in

125 which extensive soil development took place within lacustrine marls and sands.

126 Finally, marine transgression of Late Turonian age resulted in extensive

127 deposition in a carbonate ramp setting (García-Hildago et al., 2007). The sea

128 level changes probably reflect global eustatic events (Hancock, 1990; Gale,

129   1996). Using data in García-Hildalgo et al. (2007) and Martin-Serrano (1996),

130   maximum burial is estimated to be <1.5 km.

131   The studied interval incorporated two facies groups within the

132   classification of García-Hildalgo et al. (2007): the lagoonal (their facies D) and

133   carbonate ramp (their facies E). The sediments of the upper Alcorlo Formation

134   fall mostly within the lagoonal facies association D3 (silts and sandstones) of

135   García-Hildalgo et al. (2007, p. 1259), which they described from field

136   observations as "thin-bedded muddy silts, and silty fine grained sandstones". A

137   transgression to shallow marine carbonate sedimentation is represented by the

138   Tranquera Formation, at the top of both sections. This formation falls within the

139   Carbonate Ramp (E1) of García-Hildalgo et al. (2007).

140   The lagoonal facies in the Alcorlo Formation shows extensive evidence of

141   pedogenesis, including root traces, soil horizons, cutans, glaebules, peds and

142   variegated iron mineralisation (Retallack, 2001). It has been widely interpreted as

143   representing mudflats developed over shoreface sands, with local stromatolite

144   formation, and local washover fans within tidal channels (García-Hildalgo et al.,

145   2007). The two studied sections (at Torrelaguna and Tortuero) display features

146   that permit a broad correlation to be made; the lower portion of both is rich in

147   quartz sand, the middle comprises clay-rich dolomitic marls, and the upper part

148   (Tranquero Formation) comprises dolostones.

149

150   **2. Materials and methods**

151

152 *2.1. Samples*

153

154   Samples, 31 in total, were taken from every bed over approximately 10 m

155 of exposure at both Tortuero and Torrelaguna (Figures 2-4), with the most

156 samples being taken over the pedogenically modified intervals. Individual

157 samples are described briefly (Table 1). The samples were examined by optical

158 and electron microscopy, detailed clay analysis using X-ray diffraction (XRD),

159 inductively coupled plasma atomic emission spectrometry (ICP-OES/MS), and

160 Mössbauer spectroscopy (only performed on the clay-rich samples). The degree

161 of pedogenic modification was assessed for each sample using a simple

162 numerical system in which 1 point was assigned to each of the following

163 pedogenic features: root traces, peds, and variegated iron mineralisation. Cutans

164 and glaebules do not occur in these soils, and slikensides are excluded as they

165 are lithology dependent, and would not be observed in dolomite-rich, clay-poor

166 soils. The score for each sample is from zero to three, depending of the number

167 of the above features present in the horizon. This score was used for comparison

168 with chemical and mineralogical aspects of the samples.

169

170 *2.2. XRD*

171

172   The untreated, whole-rock samples were analysed by means of random

173 powder XRD to determine their mineral composition. Samples were ground with

174 acetone in a rod mill, dried and gently ground in an agate mortar before being

175　side-packed into sample holders and scanned at a rate of 1 s per 0.02 º2θ step

176　width, using 0.3 mm Soller and detector slits, from 5 to 65 º2θ, in a Philips

177　PW1710 diffractometer (Almelo, The Netherlands) at 45 kV and 40 mA using a

178　Cu anode (X-ray wavelength 1.5418 Å) and a graphite secondary

179　monochromator.

180　　　For further analysis, calcite was removed with 30% acetic acid (Fisher

181　Scientific, Loughborough, UK) and the insoluble residue washed three times with

182　distilled water. The <2 µm fraction was separated using centrifugation. The

183　sodium dithionite method (Smith, 1994) was used to remove any Fe or Al

184　(oxyhydr)oxide. Oriented mounts for XRD were prepared by allowing a few drops

185　of the clay slurry to dry on a glass slide. Samples were analysed using the

186　equipment described above in the range 2-40 or 2-30 º2θ, with a 0.3 mm Soller

187　slit and a 0.1 mm detector slit. The samples were scanned at 0.015 º2θ step size

188　and 8 s/step. The analyses were carried out in an air-dry state (20-25ºC, 50-60%

189　relative humidity) and after overnight glycolation at 60 ºC in a glycol atmosphere.

190

191　*2.3. XRD quantification and modelling*

192

193　　　In order to investigate the processes taking place in the silicate phases,

194　the powder XRD traces were used for the relative quantification of the silicate

195　minerals. The following diffraction-peak areas were measured and normalised to

196　their sum: quartz (4.26 Å), feldspar (~3.25 Å), kaolinite (~7 Å), illite (~10 Å) and

197　smectite-rich I-Sm phases (16-17 Å). Peak areas were measured using the

198   software package GRAMS AI (Thermo Galactic, Salem, New Hampshire, USA).

199   The XRD patterns of the glycolated, oriented mounts were modelled with

200   NEWMOD (Reynolds & Reynolds, 1996; Moore & Reynolds, 1997), a program

201   that allows calculation of *00l* profiles for end-member and mixed-layer

202   phyllosilicates with different interlayer complexes. The NEWMOD calculations

203   included illite-smectite (I-Sm) of different compositions, illite, kaolinite and

204   kaolinite-smectite (Kaol-Sm) with high kaolinite content. The variables used to

205   obtain the best match with the experimental patterns were % layers in the

206   interstratified phases, layer ordering (R) in the interstratified stacking sequence,

207   Fe and K abundance, and size of the coherent scattering domain. The orientation

208   of the particles was set at $\sigma^* = 20^\circ$ or 30° by best match with the experimental

209   patterns, where σ^* is the standard deviation from a 0° angle (layers perfectly

210   parallel to the substrate) in a Gaussian distribution.

211

212   *2.4. ICP-OES/MS*

213

214   ICP-OES analysis was carried out on the bulk rock samples, and on

215   portions of the <2 µm fraction from which carbonates had been removed using

216   30% acetic acid. For the few samples from which sufficient amount of the <2 µm

217   fraction could be extracted, duplicate chemical analyses were carried out on

218   splits from which Fe and Al oxides had been removed using the sodium dithionite

219   method (Mehra and Jackson, 1960; all chemicals were reagent grade from VWR

220   International Ltd, Lutterworth, Leicestershire, UK). Major, trace, and rare-earth

221 element (REE) data were derived from samples after dissolution by lithium

222 metaborate fusion and quantification by a combination of ICP-OES and ICP-MS

223 (Jarvis and Jarvis, 1985). The instruments used were a Thermo iCAP 6500 radial

224 ICP-OES and a Thermo X Series 2 ICP-MS (Thermo Fisher Scientific, Hemel

225 Hempstead, Hertfordshire, UK). Data were acquired with an ISO17025

226 accredited laboratory (testing lab 2180). Calibration was by way of matrix-

227 matched, traceable synthetic standards. QA/QC protocols included the analysis

228 and charting of in-house QC samples and the analysis of a series of geological

229 reference materials at regular intervals through the analytical sequence. Prior to

230 plotting, REE data were normalised to the values derived from analysis of USGS

231 reference material Cody Shale (SCo-1) that is considered to have a chemical

232 composition representative of the average shale. The complete data sets are

233 available from the archival website http://data.nhm.ac.uk/dataset/chemistry-

234 samples-central-system-carbonate-clays. Accuracy was assessed by repeated

235 measurement of USGS Reference Material SCo-1. All values were found to be

236 within ±5% of the mean reference value for major elements and ±10% for trace

237 and REE; precision error as defined by two standard deviations of four separate

238 duplicate measurements of SCo-1 was less than 5% for all elements.

239

240 *2.5. Mössbauer spectroscopy*

241

242   The ^{57}Fe Mössbauer spectroscopy experiment was carried out at the

243 University of Derby, UK. The spectrometer was manufactured by the Centre for

244 Advanced Technologies and Materials, Olomouc, Czech Republic. Each

245 absorber was prepared from ~70 mg of the clay sample, mixed with boron nitride

246 as a binder. The mixture was spread uniformly over an area of ~1.8 cm^2, and

247 pressed into a pellet. The spectrum was recorded at room temperature with a 25

248 mCi ^{57}Co source in a rhodium matrix, mounted on a constant-acceleration

249 transducer operated in a triangular mode in a velocity range of $\pm$6 mm/s. The

250 Doppler energies from the 14.4 keV γ-rays were detected with a YAlO$_3$:Ce

251 scintillation counter. The data were recorded in 1024 channels, which cover twice

252 the Doppler velocity range. Spectra were calibrated against a high purity

253 (99.99%) natural α-Fe foil and all peak positions reported with respect to the

254 centroid shift (CS) of the natural α-Fe. Lorentzian lines of the folded data were

255 fitted, using the least-square RECOIL 1.04 Mössbauer Spectral Analysis

256 Software developed by Lagarec and Rancourt (1998). Reduced χ^2 was used as a

257 parameter to evaluate the statistical best-fit and uncertainties were calculated

258 using a covariant matrix. Errors were estimated at about ±0.018 mm/s and

259 ±0.020 mm/s for centroid shift (CS) and quadrupole splitting (QS), respectively.

260

261 *2.6. Electron microscopy and microprobe analysis*

262

263 Carbon-coated, polished blocks of every whole-rock sample were

264 examined by Back-Scattered Electron Microscopy (BSEM) in a Zeiss EVO 15LS

265 SEM equipped with Energy Dispersive X-ray Spectroscopy (EDS) (Cambridge,

266 UK); qualitative EDS analyses were obtained of the clay matrix and of grains.

267 Quantitative EDS analyses of single particles from the purified <2 µm clay

268 fraction were obtained, from selected samples, to compare with the ICP-OES

269 clay data. The samples were dispersed in distilled water, sonicated for 3 minutes

270 in an ultrasonic bath, and then a droplet was placed on a carbon tab on a stub.

271 Operating conditions were a 2 µA beam current at 15 kV accelerating voltage,

272 and a spot diameter of approximately 2 µm. Detection limits vary according to the

273 analysed elements and the matrix in which they are contained. For these

274 samples detection limits were 0.2% for Mg, Ca and K; 0.4-0.6% for Al, Si, P, Mn,

275 Ti and Fe. Calibration using a cobalt standard was performed prior to analysis,

276 and the beam current was monitored during analysis. The quantitative data were

277 used to calculate structural formulae averaged over ~30 particles per sample.

278   A series of transects across single calcite and dolomite crystals in T14

279 (only this sample and the adjacent T13 have large enough crystals for

280 microprobe analysis) were obtained using wavelength dispersive spectroscopy

281 (WDS) with a Cameca SX100 microprobe equipped with four spectrometers

282 (Gennevilliers, France). The WDS detection limits are 0.02% for S, Mn and Fe;

283 0.03% for Mg, and 0.05% for Ca, Ba and Sr. Accuracy is the same as or slightly

284 less than the detection limit.

285

286 *2.7. Measurement of Total Organic Carbon*

287

288   Portions of the two black clays, samples A10 and A11, in which organic

289 carbon was suspected, were finely ground, weighed into silver boats, de-

290   carbonated by exposure to hydrochloric acid vapour followed by drop-wise

291   addition of HCl, and then dried. Quantification of organic C was achieved using a

292   Thermo Finnigan Flash EA1112 CHN analyser (Ringoes, New Jersey, USA)

293   calibrated against traceable standards.

294

295   **3. Results**

296

297   *3.1. Sedimentology*

298

299   In both successions, the Alcorlo Formation constitutes most of the

300   stratigraphic thickness sampled, and consists of fine-grained dolomitic

301   sandstone, quartz sand-bearing dolomicrites, and silty marls, with thin clay-rich

302   beds that have been variably modified by penecontemporaneous soil formation

303   processes (Table 1). At Tortuero, pedogenically modified clay-rich dolomicrite

304   intervals occur over a 5 m thickness in the middle of the section (Fig. 3); at

305   Torrelaguna the pedogenesis occurs over an interval of similar thickness (Fig. 4)

306   but, from field observations, is much less intense, with no roots present, less

307   intense development of peds, less colour mottling, and less slickensiding (though

308   this last criterion is lithology dependent). Palaeosol features include rootlets, ped

309   fabrics, slikensiding, and blue-green/red/buff mottling of clays. Two thin layers of

310   dark clays are also present towards the top of the Torrelaguna section (samples

311   A10 and A11). Between the pedogenically modified intervals the sediment

312   comprises dolomicrite, quartz-sand-rich dolomite, dolomitic sandstone, and

313   quartzose siltstone. Invertebrate burrows are filled with sand or haematite

314   cement. The Tranquera Formation, at the top of the sections (Figs. 3 and 4),

315   comprises glauconitic blocky dolostone, deposited in a marine environment,

316   inferred to be low energy from the moderate clay content and, in non-dolomitised

317   localities, bioturbation, and infauna (García-Hidalgo, 2007).

318

319   *3.2. Mineralogy*

320

321   Authigenic dolomite and detrital quartz are the principal components

322   overall (Fig. 5), with calcite (authigenic) the most abundant mineral only in T11.

323   Clay is a major component in the marls, with minor silt- and sand-size detrital

324   plagioclase and alkali feldspar present throughout. Total clay varies from trace to

325   around 25% of the sediment, and comprises varying proportions of illite, illite-

326   smectite (I-Sm) of a wide compositional range, kaolinite, plus trace chlorite and

327   palygorskite. In addition, two samples include kaolinite-rich kaolinite-smectite

328   (Kaol-Sm). Palygorskite is only found at Tortuero, and is present there in all

329   analysed samples from T8ii and above (Table 1). Kaolinite has sharper XRD

330   peaks than the other clays. Authigenic haematite is only associated with

331   pedogenically modified intervals and gives the sediment a light to dark pink

332   colour.

333   In order to investigate the detrital or authigenic character of the clay

334   minerals, correlations between the several minerals were studied. The

335   hypotheses being tested were that saline waters and the subsequent soil

336   conditions destabilised kaolinite and feldspars and generated authigenic I-Sm

337   and illite. Such processes would produce negative correlations between mineral

338   phases. For this investigation, the areas of diagnostic XRD peaks representative

339   of each silicate mineral phase were measured in the patterns from random

340   powders (see methods section) and normalised to 100%. These measurements

341   do not represent percent mineral abundance but the relative variation of the

342   silicate mineral phases from sample to sample. Four variables are involved

343   (content variation of quartz, feldspars, kaolinite, and I-Sm), and thus statistically

344   significant correlations found between any two of them should be meaningful.

345   The only apparent correlation is between kaolinite and I-Sm phases, where, for

346   most data points, kaolinite decreases with increasing I-Sm (Fig. 6). Five data

347   points located below a hypothetical straight line connecting 30% kaolinite with

348   60% I-Sm are outside this broad correlation (Fig. 6). These five data points

349   correspond to samples with large quartz contents (52-84% area), well above

350   those found for the other samples (3-43% area). The larger quartz contents

351   (above 50% of the total normalised area measured for the four mineral phases)

352   cause the affected data points to be largely displaced down and towards the left

353   of the plot (Fig. 6), effectively outside the broad pattern generated by the other

354   data points. In other words, the variable quartz content in the samples causes

355   scatter in the correlation between kaolinite and feldspars where quartz content is

356   below a certain limit (50% of total measured areas) but displaces the data points

357   out of the correlation for samples in which quartz is above that limit (>50% of the

358   total measured areas).

359   García-Hidalgo et al. (2007) indicate that feldspar and kaolinite contents

360 are inversely correlated, although they do not show a statistical analysis

361 supporting this conclusion. This relationship is consistent with the results of the

362 present study, although a meaningful correlation was not found between feldspar

363 and kaolinite contents.

364

365 *3.3. Dolomite*

366

367   Dolomite crystals were euhedral, intergrown and with or without slight

368 chemical zonation indicated by X-ray element mapping, although the zonation

369 was not generally apparent from the atomic number contrast in BSEM images

370 (Fig. 7a). In the Tranquera Formation, and T10a and in T1 in the Alcorlo

371 Formation, dolomite crystals had leached cores and/or selective leaching of

372 particular chemical zones (e.g., Fig. 7b). In all other samples the dolomite was

373 apparently chemically homogenous as seen in BSEM images. SEM-EDS

374 analyses indicated low to very low Fe contents in the dolomite. No other trace

375 elements were detected by EDS, but trace Mn, Ba, and Sr were detected in the

376 course of mapping using WDS. The FeO content of dolomite increased from <1%

377 at the base of the section to 1-2% in samples from the top of the Alcorlo

378 Formation and the Tranquera Formation. In the Tranquera Formation the

379 dolomite was chemically zoned with two Fe-enriched zones, including the

380 outermost zone, and two Fe-poor zones, including the core (Fig. 7b). In the

381 Alcorlo Formation dolomicrite beds, dolomite crystallite size varied from 10 to 100

3
4
5
6
7
8
9
10
11
12
13
14
15
16
17
18
19
20
21
22
23
24
25
26
27
28
29
30
31
32
33
34
35
36
37
38
39
40
41
42
43
44
45
46
47
48
49
50
51
52
53
54
55
56
57
58
59
60
61
62
63
64
65

382 µm. Dolomite in the Tranquera Formation comprised coarser rhombs (100-200

383 µm) than the underlying dolomicrite of the Alcorlo Formation. No correlation

384 between dolomite crystallite size and any other lithological or sedimentological

385 feature was observed.

386

387 *3.4. Calcite*

388

389　　　Coarsely crystalline, poikilotopic calcite had cemented intercrystalline

390 porosity between dolomite rhombs in samples T13 (Fig. 7c) and A6. This infilling

391 texture indicates that the calcite precipitated after the dolomite. The calcite had

392 low Mg and Fe concentrations, with a very slight increase in Mg of ~0.2%

393 towards crystal margins. Fe was higher both at the core and at the rim. As with

394 the dolomite, trace Mn, Ba and Sr were present in the calcite.

395

396 *3.5. Haematite*

397

398　　　In dolomicrite beds with pedogenic reddening, clusters of octagonal

399 haematite crystals had grown in the clay matrix, between rhombs of dolomite

400 (Fig. 7a). Haematite is also responsible for the reddening of pedogenically

401 modified clay beds. Haematite clusters were typically ~5-10 µm across.

402

403 *3.6. Clay minerals*

404

405   Experimental and simulated patterns of the glycolated, oriented mounts

406   (<2 µm size fraction) provided detailed information on the clays (Fig. 8).

407   Mismatches between calculated and experimental patterns below 9 °2θ are due

408   to a known problem of the simulation program that generates erroneously high

409   intensity values (Plançon, 2002). Some samples contained traces of quartz and

410   feldspars (Fig. 8). The clay assemblage was dominated by illite layers in both

411   sections (Table 2). The most illitic clays were those with a green colour in hand

412   specimen, which implies that it is the illite that is responsible for this colour.

413   Measurements of the *060* reflection (1.499-1.505 Å) were consistent with the clay

414   being illite rather than ferric illite or glauconite. Typically, kaolinite was the second

415   most abundant component and correlated inversely with illite layers (Table 2).

416   The black clay beds at Torrelaguna did not have a different clay assemblage,

417   although one of them, A11, had the highest smectite content of the two sections.

418   All analysed samples were complex mixtures of illite, I-Sm of several

419   compositions and kaolinite phases (Table 2). The stacking order of the layers in I-

420   Sm increased with increasing illite content, although not uniformly. The amount of

421   Fe required for a good fit in the XRD calculations was moderate (0.2-0.3 atoms

422   per $O_{10}[OH]_2$). The large coherent scattering domains of kaolinite (N_{max} and N_{ave}

423   values, Table 2) indicate large stacks of parallel layers of detrital origin (kaolinites

424   developed in soils typically have broad basal diffraction peaks; e.g., Ryan and

425   Huertas, 2009), whereas the corresponding values for illite would indicate more

426   weathered crystals or the existence of low-temperature illite, possibly authigenic.

427   It is not likely that all the illite is detrital (up to 80-90%) because the Iberian

428 Peninsula was located at low latitude during the Cenomanian-Turonian and the

429 tropical climate would have been reflected in kaolinite-rich soils (Weaver, 1989).

430 Around 5% (visual estimate) pellets and fragments of mature glauconite were

431 present in the Tranquera Formation at Tortuero. These particles, being indurated,

432 did not contaminate the clay fraction, and were visible in the >2 μm fraction when

433 examined under a binocular microscope. Minor to trace amounts of palygorskite

434 were present from 6 m above the base of the Tortuero section, to the top of the

435 section, including the Tranquera Formation.

436   Seven samples were analysed using Mössbauer spectroscopy. The

437 spectra displayed two Fe^{3+} octahedral components, as is typical in clay minerals

438 (Dyar et al., 2008), and a much smaller Fe^{2+} octahedral component (Fig. 9). The

439 range of % Fe^{2+}, measured as the relative area of the Fe^{2+} component, was 4-

440 13%, with an average of 9%. Thus, the level of Fe reduction in the samples was

441 limited. All Fe^{2+} is in illite layers because Fe^{2+} is not stable in smectite layers and

442 it oxidises within minutes to hours of exposure to the atmosphere (Neumann et

443 al., 2011).

444   ICP-OES analyses (Table 3) for splits of green clays (<2 μm) are

445 consistent with the XRD data. Samples with the most illite are those with the

446 highest K_2O values (Table 3). TiO_2 may be clay-size authigenic or detrital

447 particles; both are commonly found in palaeosols (Summerfield, 1983). Results

448 from four splits of green clays (<2 μm) from which Fe and Al oxides had been

449 removed were sufficiently similar to those from which Fe and Al oxides had *not*

450 been removed to conclude that Fe and Al oxides were rare or absent. This is

451 surprising but consistent with the observation that haematite aggregates imaged

452 in BS-SEM were 5-10 µm in diameter. In some instances, higher concentrations

453 of Fe and Al oxides were measured in the cleaned split, which suggests that

454 there may be some sample inhomogeneity. Only samples A3 and A8 contained

455 significant haematite associated with the clay. The ICP-OES for the bulk <2 µm

456 clay fraction and EDS data for individual clay particles from the <2 µm fraction

457 yielded compositions within a few % of each other, indicating that the ICP-OES

458 data did not include significant contamination from other components such as

459 clay-size quartz. CaO was more widely present in the clay splits than was

460 detected by EDS; this difference may correspond to differences in detection limit

461 (higher for EDS), as carbonates were effectively removed prior to ICP-OES

462 analysis. A proportion of the CaO was associated with P_2O_5, where the latter is

463 present. The increase in MgO measured by ICP-OES in the upper part of the

464 Tortuero section (sample T8ii and above) reflects the presence of palygorskite in

465 addition to other MgO-bearing clays.

466   EDS data for illitic clay were recalculated to structural formulae (Table 4).

467 Where Mössbauer data were available, the Fe abundance was split into Fe^{3+} and

468 Fe^{2+}. For the remainder of the analyses, it was assumed that Fe^{2+} is ~10% of the

469 total Fe, because the average value from Mössbauer data was 9% (see below).

470 The structural formulae of the particles are compatible with I-Sm of a wide range

471 of illitic content (Table 4). The layer charge ranged from smectitic to illitic and

472 there was a group of them with intermediate values, between 0.5-0.7 per

473 $O_{10}(OH)_2$. The fact that K was the main interlayer cation is compatible with a

474   process of illitisation. The composition was dioctahedral, with Al as the main

475   octahedral cation, with significant amounts of Mg and Fe. Significant tetrahedral

476   substitution of Al for Si had also occurred. From the above it can be concluded

477   that the layer charge was generated by several factors: tetrahedral Al for Si

478   substitution, octahedral Mg for Al substitution, and partial Fe reduction in the

479   octahedral sheet.

480

481   **4. Discussion**

482

483   4.1. Non-clay mineral diagenesis

484

485   The dolomite and calcite are authigenic cements that precipitated in a

486   predominantly clastic sediment. Textural relationships indicate that the dolomite

487   pre-dates the calcite. Precipitation of dolomite direct from solution rarely occurs;

488   in seawater it is inhibited by SO_4 (Baker and Kastner, 1981). In lacustrine or

489   lagoonal sediments such as occur in the Alcorlo Formation, where the SO_4 is

490   diluted by freshwater or absent, it may be possible for dolomite to precipitate

491   directly from solution, penecontemporaneously with sedimentation. Early

492   dolomitisation in a recent lacustrine/lagoonal setting, of either early calcite

493   cement or bioclasts, has been documented by Aqrawi (1995). Bioclasts were not

494   observed in any of our samples but shallow water gastropods and bivalves were

495   reported by García-Hidalgo et al. (2007).

496   Dolomitisation also occurred in the shallow marine sediments of the

497   Tranquera Formation. The larger size of the dolomite crystals in the marine

498   Tranquera Formation, compared with the lagoonal Alcorlo Formation, may reflect

499   the difference in depositional environment. Seawater is the most probable source

500   of Mg for dolomitisation. To the southwest of this region dolomitisation has

501   probably occurred as a result of Mg rich brines from evaporite dissolution in the

502   younger Valle de Tabladillo Formation east of Patones (Benito and Mas, 2007).

503   For this to have occurred in the Sierra de Guadarrama the Mg rich fluid would

504   have had to flow both laterally 1-2 km and down, making it a less likely source of

505   Mg enrichment of pore fluid. The lack of chemical zonation in the majority of the

506   carbonates suggests that fluctuations in the water chemistry during precipitation

507   were minimal. The selective leaching of narrow zones in a few samples may

508   have occurred during pedogenesis. Haematite appears to have replaced

509   dolomite in some instances, implying that the haematite formed after the

510   dolomite. This is entirely consistent with the haematite having formed during

511   pedogenesis. Dolomite also occurs in clay-rich sediment affected by

512   pedogenesis.

513

514   4.2. Clay minerals

515

516   The estimated maximum burial depth (<1.5 km) equates to a maximum

517   burial temperature ~50-60°C for temperature gradients typical of sedimentary

518   basins (Giles, 1997; Palumbo et al., 1999). Such temperatures are too low for

519   significant illitisation to have occurred as a result of diagenesis, which occurs

520   over a temperature range of 50-120°C (Perry and Hower, 1970; Eberl and

521   Hower, 1976) and is most intense at the upper end of the temperature range

522   (e.g., Ehrenbert and Nadeau, 1989; Glassman et al., 1989).

523   Kaolinite may have originated by alteration of feldspars in the rocks of the

524   sediment source area, as suggested by García-Hidalgo et al. (2007), and not

525   diagenetically in the sediment. The sharp basal XRD peaks are consistent with

526   this interpretation. Given the dominance of Hercynian granite in Sierra de

527   Guadarrama (Fig. 1), that granite and gneiss are the main rocks in the sediment

528   source area (García-Hidalgo, 2007), and the important hydrothermal event that

529   affected the emplaced granites during the Late Jurassic (Galindo et al., 1994) the

530   high-temperature alteration interpretation is very likely. Although no correlation

531   between the kaolinite and feldspar minerals was observed in the present study,

532   this origin is plausible and the lack of correlation may be due to (1) the changes

533   produced in the contents of the two minerals during transport from the hinterland

534   and (2) the transformation of kaolinite into I-Sm in situ. This second hypothesis is

535   discussed below.

536   The interpretation of the negative correlation between kaolinite and illite

537   layers (including both illite and I-Sm with a wide range of composition) needs to

538   take into consideration the geochemical environment where a possible kaolinite-

539   to-illite transformation could have taken place. Such an evaluation should be able

540   to firstly determine whether the negative correlation between kaolinite and illite

541   layers was caused by a process taking place in situ rather than by a variation in

542   the composition of the detrital clay, and secondly, indicate the direction in which a

543   potential in situ transformation took place (kaolinisation or illitisation). Based on

544   the observation that pedogenic evidence appeared to be positively correlated

545   with illite content in the clay, a method was devised to investigate such a

546   correlation in more detail. Several pedogenic characteristics were used to create

547   a "score for soil development" (see methods) and this score was plotted vs. illite

548   content from XRD of oriented clay mounts, for all samples (Fig. 10). The illite

549   content was obtained from the normalisation of the proportions of kaolinite, illite,

550   and smectite layers. The result is that the increase in the soil development is

551   accompanied by a stepwise increase of illite content for Tortuero (T samples) but

552   not for Torrelaguna (A samples). Sample T10, with 82% illite and a soil

553   development score of zero, is interpreted to have been reworked from the

554   underlying horizon because this sediment was deposited during the earliest stage

555   of the marine transgression. If such is the case, sample T10 should be located

556   where the arrow indicates (Fig. 10), further supporting the positive correlation

557   between pedogenic character and illite content of the clays in the Tortuero

558   sequence.

559   The correlation in Tortuero militates against the possibility that the different

560   clay composition up the profile was caused by changes in the clay source

561   because it would be an unlikely coincidence that both clay source and soil

562   development in situ changed at the same time, especially unlikely considering

563   that soil development in the profile increased to a maximum in the middle of the

564   section and then decreased towards the top (i.e., from older to younger

1
2
3
4
5
6
7
8
9
10
11
12
13
14
15
16
17
18
19
20
21
22
23
24
25
26
27
28
29
30
31
32
33
34
35
36
37
38
39
40
41
42
43
44
45
46
47
48
49
50
51
52
53
54
55
56
57
58
59
60
61
62
63
64
65

26

565   sediment), rather than following a constant change in one direction. As for the

566   direction of the transformation process, kaolinitisation can be discounted for

567   several reasons. Firstly, because the high one-dimensional crystal order of

568   kaolinite, as indicated by XRD patterns (Table 2; Figs. 5 and 8), is inconsistent

569   with kaolinisation during pedogenesis, as soil kaolinites typically have wide *00l*

570   peaks (e.g., Ryan and Huertas, 2009). Secondly, because the proportion of

571   kaolinite decreases (and illite increases) with increasing pedogenic character,

572   which indicates that the soil development is causing kaolinite illitisation. Thirdly,

573   the high salinity in the lagoonal, soil and shallow marine environments, in which

574   these sediments were deposited, are incompatible with kaolinitisation.

575   The lack of correlation between soil development and the clay

576   transformation process in the Torrelaguna section (Fig. 10) is because this

577   section was closer to the Late Cenomanian-Turonian palaeoshoreline, and

578   subjected to less extreme pedogenesis and less evaporation in the lagoonal

579   environment. The Torrelaguna samples show a negative correlation between

580   kaolinite and I-Sm in the same way as the Tortuero samples (Fig. 6), which

581   suggests that there was also kaolinite illitisation in Torrelaguna. This issue will be

582   further discussed below.

583   Thus, at least for Tortuero, the inverse correlation of kaolinite with I-Sm

584   (Fig. 6), the high degree of one-dimensional crystal order of kaolinite and the

585   complex clay assemblages, with a wide range of I-Sm compositions, are

586   consistent with a slow transformation process from detrital kaolinite (likely derived

587   from hydrothermally altered granite) to illite by way of I-Sm taking place at

588   surface conditions, similar to the illitisation previously described in pedogenic

589   (e.g., Huggett and Cuadros, 2005, 2010), lacustrine (e.g., Jones and Weir, 1983)

590   and mangrove environments (Andrade et al., 2014). Some of the illite in the

591   samples displays a relatively high one-dimensional crystal order (although not as

592   high as that of kaolinite, Table 2), which could indicate the presence of detrital

593   illite or be a result of the length of time available for pedogenic illitisation. The

594   illitisation process would require the reaction of kaolinite with Mg, Fe, K, Na and

595   Ca in aqueous solution, all of which are expected to be present in a saline

596   lagoon or lake. Wetting and drying cycles, together with reducing-oxidising

597   cycles, would enable Fe uptake and reduction (Huggett and Cuadros, 2005,

598   2010). Cation-enriched fluids would foster incorporation of all these cations. Silica

599   input may not be necessary if two kaolinite layers reacted to generate one layer

600   of 2:1 silicates. Net incorporation of Si was possible, however, from dissolving

601   feldspar and from diatoms in the saline lacustrine and shallow marine

602   environments where some of the samples originated. Although no relicts of

603   diatoms were observed in the SEM investigation, diatoms are abundant in both

604   saline and fresh lacustrine environments (Chamley, 1989; Stenger-Kovács, 2014)

605   and their complete dissolution is perfectly plausible, especially if the Si was taken

606   up by the kaolinite illitisation reaction.

607   The plot of % kaolinite versus % illite layers obtained from XRD modelling

608   analysis in the Tortuero section reveals two groups of samples with a strong

609   negative correlation between kaolinite and illite layers (Fig. 11a). This plot was

610   created by normalising the proportions of kaolinite, illite, and smectite layers, i.e.,

611   the total system contains only 3 variables and there is a correlation between two

612   of them. It might be argued that the observed correlation is forced by the

613   normalisation of the 3 variables. The evidence that this correlation is real is

614   based on the following: (1) kaolinite is also observed to correlate negatively with

615   illite plus I-Sm in the whole rock data (Fig. 6); (2) two groups with a high

616   correlation appear in the analysis of the XRD patterns modelling in Tortuero

617   samples (Fig. 11a), whereas an induced correlation would most likely produce a

618   single broader correlation; (3) these two groups in Tortuero (Fig. 11a) correspond

619   exactly with samples from soils (score 1-3 in Fig. 10; full diamonds in Fig. 11a)

620   and from non-soil sediments (score 0 in Fig. 10; open squares in Fig. 11a), with

621   the exception of sample T10 which is not from a soil but is suspected to be

622   reworked from the underlying sediment (T9a). The two groups of samples

623   establish two fairly well defined trends (regression lines).

624   The corresponding regression lines intersect at ~50% illite, ~50% kaolinite.

625   This can be interpreted as the composition of the clay originally deposited in

626   these sediments. According to this interpretation, the composition of the detrital

627   clay deposited in the sediments is assumed to be approximately constant

628   throughout the stratigraphic section: 50% kaolinite and 50% I-Sm with very few

629   smectite layers. After deposition, the transformation of kaolinite generated first

630   smectitic I-Sm that caused a transient increase of smectite layers, and then illite.

631   The two groups of samples identified in Tortuero (Figs. 11a and 11b) then

632   indicate two different environments where illitisation took place at different speed.

633   The group of samples that experienced soil environments (diamond symbols in

634   Fig. 11) reacted faster towards illite than those that developed in marine and

635   lagoonal environments (square symbols in Fig. 11).

636   Comparing % kaolinite and smectite layers (Fig. 11b), also shows two sets

637   of samples defining two clear trends, with sample T1 positioned between the two.

638   This plot should be similar to the kaolinite vs. illite in that the two reaction

639   sequences should meet at about 50% kaolinite but in this plot the two lines do not

640   cross. The dotted line is in good agreement with the kaolinite vs. illite plot,

641   because it meets the vertical axis at ~50% kaolinite, which indicates an original

642   composition ~50% for each kaolinite and illite, and very little smectite. The other

643   line does not, however, reproduce the results from the kaolinite vs. illite plot

644   because the line meets the vertical axis at ~30% kaolinite. The overall trend

645   implies that kaolinite is transformed into I-Sm and illite, in both

646   lacustrine/pedogenic and marine (or pedogenic/lacustrine sediment flooded

647   during marine transgression) environments, and the composition of the original

648   sediment, as represented by 3 of the 4 lines would be near 50% kaolinite and

649   50% illite (Figs. 11a and 11b). Note that the lines in the kaolinite vs. smectite plot

650   are subjected to greater relative error because the smectite percents are smaller.

651   Thus, it is reasonable to assume that the solid line (Fig. 11b) is displaced or has

652   a distorted slope. The origin of the detrital illite may be "sericitisation" of feldspar

653   in granite and gneiss.

654   The analysis of the data from Torrelaguna is more difficult because there

655   are fewer data points and their distribution does not suggest any specific pattern.

656   As expected from the lack of correlation between soil development and illite

657 content (Fig. 10), no distribution of soil and non-soil samples was found matching

658 linear trends (Fig. 11c and d). The proportions of clay layers in Torrelaguna

659 samples are compatible with kaolinite illitisation but do not allow further analysis.

660 The interpretation that appears most likely to the authors is that kaolinite

661 illitisation took place also in Torrelaguna but that the specific conditions in the soil

662 environments did not produce a transformation that was faster than in lagoonal

663 and marine environments as in Tortuero. The reasons may be that conditions

664 needed for Fe reduction were not as frequently developed.

665 Palygorskite is restricted to the upper half of the Tortuero section. This

666 mineral is associated with arid climates and evaporites (e.g., Millot, 1964; Post,

667 1978; Weaver and Beck, 1977), which is consistent with both the saline waters

668 and wetting and drying cycles suggested by illite formation. Whether the

669 palygorskite is detrital or authigenic is unclear because the clay was only

670 detected by XRD. The palygorskite was most abundant in the most intensely

671 pedogenically modified beds at ~5-6 m above the base of the section, which

672 suggests that it was in-situ pedogenic clay, and was partially reworked into the

673 overlying marine sediment. Conceivably the palygorskite formed in lagoon

674 environments between minor episodes of marine transgression, as indicated by

675 the presence of glauconite in marls beneath the formation boundary.

676

677 *4.3. Major element chemical analysis*

678

679 The chemistry of the clay samples was investigated to identify the chemical

680 changes that accompanied illitisation in I-Sm particles. No clear correlations

681 could be established between any individual chemical element and illite content,

682 corroborating that the illitisation was due to a combination of chemical factors

683 rather than controlled by a single one. Importantly, the existence of the detrital

684 illite (or very illite-rich I-Sm) together with the I-Sm generated by the

685 transformation of kaolinite suggests that there should be two populations of illite-

686 rich I-Sm, the detrital and the authigenic, where the former would probably have

687 lower Mg/Al ratio. No signs were detected of such two populations in the SEM-

688 EDS analyses. It can be speculated that a high degree of mixture between the

689 detrital and authigenic phases precluded their separate observation. Although

690 individual flakes were analyzed, the 2 µm diameter spot of the electron beam at

691 15 kV current can have sufficient penetration to reach other flakes below. One

692 way to investigate the question of mixed detrital and authigenic particles is to

693 study the standard deviations of the EDS data that were obtained to calculate the

694 average compositions in Table 4. All standard deviations of Si and Al were < 5%

695 of the average value, with the highest values (4-4.8%) for samples T9a and T1 in

696 Tortuero and the Torrelaguna samples (A samples). In these samples there was

697 also a higher Mg standard deviation ranging 17-46%, whereas it remained <10%

698 for the rest. Iron followed a similar trend but with lower standard deviations in the

699 high range of 20-27%. The standard deviation for K was also higher in the

700 Torrelaguna samples and T3 and T8 (different from the two samples mentioned

701 above, T9a and T1) in Tortuero, at 20-27% of the average values, and remained

702 2-10% in the rest. These results show the typical level of compositional variability

703 of clay minerals at individual particle level (Bain et al., 1994). Any mixture of

704 phases with different composition must have become nearly homogeneous at

705 such level.

706   It is also possible that the detrital illite underwent partial Mg enrichment in

707 the lagoonal environment and became very similar to the I-Sm derived from

708 kaolinite. The mixture of authigenic I-Sm and detrital illitic I-Sm may be a reason

709 why there are no correlations between individual elements and illite content. In

710 any case, because all our samples have more illite content than the original

711 detrital kaolinite-illite mixture, any chemical trend accompanying illite increase is

712 truly related to the authigenic illitisation process.

713   Two relationships were found between chemical and geological variables,

714 which apply to both the Tortuero and Torrelaguna sequences. A plot of Mg in I-

715 Sm vs. the stratigraphic height above the base of the field exposure (Fig. 12a)

716 revealed the following pattern, both in Tortuero and Torrelaguna. From bottom to

717 top, Mg first decreases, then progressively increases and finally decreases again.

718 This is consistent with increasing evaporation of lake or lagoon water, and hence

719 increased Mg concentration, going up section, followed by a reversal of the trend

720 as sea level rose and marine influence increased towards the top of both

721 sections. The Mg concentration caused by this process would also be consistent

722 with the widespread distribution of early diagenetic or syn-sedimentary dolomite.

723 A plot of Fe^{2+} content in I-Sm versus height in the sequence suggests that Fe^{2+}

724 increases generally with height above the base of the section, both in Tortuero

725 and Torrelaguna (Fig. 12b). This plot was created using only samples for which

726 Fe^{2+} was determined using Mössbauer spectroscopy. Height values in the

727 Torrelaguna and Tortuero successions have no direct geological correlation,

728 however these two plots indicate that not only is it possible to correlate the

729 overall sedimentological sequence of the two localities, but also the chemistry

730 resulting from mineral modification during and soon after deposition.

731   Considering all the above data, the most likely interpretation is that kaolinite

732 illitisation took place both in Tortuero and Torrelaguna. In Tortuero, a single clay

733 source and soil conditions that produced faster illitisation than in lagoonal and

734 marine environments generated two recognisable illitisation trends. In

735 Torrelaguna, variations of the detrital clay composition or in the environmental

736 conditions may have existed and any correlation between soil development and

737 illitisation was weakly developed (Fig. 10, Fig. 11c and d).

738   The Sierra de Guadarrama I-Sm has only 3-6% total Fe_2O_3, a range lower

739 than that of the non-marine, syn-sedimentary glauconite reported by Huggett and

740 Cuadros (2010) or ferric illite (e.g. Keller, 1958; Gabis, 1963; Deconinck et al,

741 1988; Baker, 1997; Eggleton and Fitz Gerald, 2011). This fact may be partly or

742 completely due to the mixture of authigenic I-Sm and detrital illite, so that the

743 detrital illite is more Al-rich and the authigenic I-Sm more Fe-rich. In the

744 authigenic illitisation process, in order for K^+ to be fixed in the interlayer site,

745 there has to be an increase in the layer charge of the 2:1 clay mineral. In Fe-rich

746 illite and glauconite this is normally achieved through reduction of octahedral Fe^{3+}

747 to Fe^{2+}, with substitution of Al^{3+} for Si^{4+} in the tetrahedral sheet increasing with

748 burial (Ireland et al., 1983; Kazerouni et al., 2013). In the Fe-poor, Mg-rich

749   dolomitic lacustrine environment of the Alcorlo Formation, a significant proportion

750   of the layer charge increase may have occurred through substitution of Mg^{2+} for

751   trivalent cations in the octahedral sheet. The MgO content of the Alcorlo

752   Formation illite is of the order of 3-4% which is at the upper end of the range for

753   published non-marine neoformed Fe-rich illite (Keller, 1958; Gabis, 1963;

754   Deconinck et al., 1988; Baker, 1997; Eggleton and Fitz Gerald, 2011), and is high

755   compared with 1-2% in the lacustrine glauconite reported by Huggett and

756   Cuadros (2010). It is therefore concluded that Mg substitution for Al (or Fe^{3+}) was

757   more important in low-temperature illitisation of the Alcorlo Formation clay than

758   reduction of Fe^{3+} to Fe^{2+}. The Al for Si substitution in the tetrahedral sheet was

759   also important in creating layer charge (Table 4), perhaps also due to the

760   presence of the detrital illite in the original sediment.

761   In Tortuero, the intensity of the illitisation process increased up through the

762   section, reaching a maximum where pedogenesis is most intense in the middle

763   section, and then decreased as marine influence increased towards the top of the

764   Alcorlo Formation and the marine Tranquera Formation. The proportion of Mg in

765   the Tranquera Formation illitic clay is lower than that in the Alcorlo Formation.

766   This may be due to inhibition of Mg fixation in the marine setting. Illitisation

767   through Mg replacement of trivalent cations has only rarely been previously

768   reported. Chamley (1989) hypothesised that Mg enrichment of smectite and illite

769   may occur in saline lakes with 30-90 g/kg salt concentration. Hover and Ashley

770   (2003) reported neoformation of Mg-rich celadonite (Mg content of 0.35-0.63 per

771    $O_{10}[OH]_2$), in the volcaniclastic Plio-Pleistocene sediments of Lake Olduvai in

772 Tanzania, while Deocampo (2004) found that illite in the <0.1 μm fractions of

773 Olduvai sediments showed systematic stratigraphic Mg variations correlating

774 positively with lake regression indicators. Deocampo et al. (2009) also found Mg

775 enrichement of smectite and I-Sm to correlate with low water levels in the Olduvai

776 palaeolake, but no such correlation existed with K or illite proportion. From this it

777 was concluded by Deocampo et al. (2009) that Mg uptake and K fixation took

778 place at different stages of lake salinity. This is consistent with the fact that high

779 saline concentration triggering Mg uptake implies low K/Na ratios that do not

780 favour interlayer K fixation. Jones and Weir (1983) reported Mg-rich illite

781 (composition not determined) in the alkaline Lake Abert, in which the Mg illite

782 replaced a stevensite-like Mg-rich smectite. Again, this process differs from the

783 Sierra de Guadarrama illitisation, in the starting material. Neither volcanic

784 sediment nor Mg-rich smectite are present in the Alcorlo formation, with the

785 exception of the distinctive thin black clay beds at Torrelaguna.

786   Qualitative EDS analysis of the black clays at Torrelaguna indicated that

787 they are Mg-rich smectite. The relatively high smectite content, and very fine

788 grain-size of the black clays (samples A10 and A11) suggest that they include

789 volcanic ash; however, the REE data indicates that this is unlikely to be the case.

790 The lack of lateral continuity of these strata is also consistent with the black clays

791 not being primary ash-falls. Total organic C data for these samples indicate very

792 low C content (0.25% for A10, 0.29% for A11), hence the colour is not due to the

793 presence of organic matters. At present the origin of these beds remains

794 enigmatic.

795   The presence of glaucony pellets in the Tranquera Formation is consistent

796 with this being a transgressive marine sediment (Amorosi, 1995). Maturation of

797 clay-rich faecal pellets to glauconitic clay in marine environments has been

798 widely described as a process that may be summarised as Fe enrichment (e.g.,

799 Odin and Matter, 1981; Odin and Fullager, 1988), Fe partial reduction, increased

800 layer charge, and interlayer K fixation.

801

802 4.4. Rare Earth Element analysis

803

804   For both sections the whole-sample REE data reflect the interplay of signals

805 from carbonate- and clay-dominated end members (Figs. 3-4; Table 5). The

806 carbonate-dominated end member is best typified by REE profiles T1 and A2,

807 with a similar trend to those reported by Tlig and M'Rabet (1985). The T1 and A2

808 REE profiles are enriched in the middle REE and have a slight negative shale-

809 normalised Eu anomaly. The clay profile end member is best typified by profile T4

810 and shows depletion in the middle REE with a moderate negative Eu anomaly.

811 REE profiles, which are noticeably irregular such as those of samples A6 and A7,

812 are likely to reflect modification by pedogenic processes. Previous work by Wray

813 (e.g., Wray, 1999; Wray and Jeans, 2014) has used the presence of a negative

814 shale-normalised Eu anomaly to indicate that sediment was of volcanogenic

815 origin, most probably a bentonite. In the sections currently under study this

816 interpretation is unlikely; more probably the clay REE profile is controlled by the

817 composition of the proximal granitic hinterland from which the clay fraction of the

818 sediment is believed to be derived. Both granite and pedogenic processes in soil

819 overlying granite contribute to a negative Eu anomaly in the weathered material

820 (Aubert et al., 2001). The clay-rich beds A10 and A11 have comparable REE

821 profiles to the other clay-rich beds in the succession, best typified by bed A1, and

822 the REE data show no evidence that beds A10 and A11 have a difference

823 provenance to the remainder of the succession.

824

825 **5. Conclusions**

826

827 1) Mid Turonian sea level fall (reflecting a global eustatic signal) in the studied

828 localities resulted in the formation of a coastal plain environment in which

829 extensive pedogenesis occurred around lagoons (Alcorlo Formation).

830

831 2) Detrital clay sediments consisting of kaolinite and illite were deposited and

832 transformed in the soil/lagoon environment. The existence of detrital illite creates

833 uncertainty about the specific range of chemical changes that took place in the

834 soil/lagoon environment but the trends are reliable. These trends indicate that

835 low-temperature illitisation of kaolinite via smectite and I-Sm took place through

836 enhanced layer charge resulting from Mg substitution for Al (or Fe^{3+}), Al for Si

837 substitution and Fe^{3+} to Fe^{2+} reduction. This may be the first documented

838 occurrence of illitisation by this dual mechanism.

839

840   3) Mg enrichment of the clay may have occurred principally in saline lagoons or

841   lakes, while Fe^{3+} to Fe^{2+} reduction occurred as a result of wetting and drying in a

842   pedogenic environment. Iron reduction may have continued with the deposition of

843   the Tranquera Formation, but in a marine environment. The MgO content of the

844   clay in the marine sediments, towards the top of the sampled intervals, is ~4%,

845   implying that enrichment continued in the marine environment, although to a

846   lesser extent than in the lagoonal-pedogenic environments represented by lower

847   horizons.

848

849   4) The intensity of the illitisation process increased up through the Tortuero

850   section, reaching a maximum where pedogenesis was most intense in the middle

851   section, and then decreased as marine influence increased towards the top of the

852   Alcorlo Formation and the marine Tranquera Formation. No clear pattern is

853   apparent linking soil development and illitisation in the Torrelaguna section.

854

855   5) The illitisation process, influenced by the existence of detrital illite in the

856   original sediment, has resulted in a less Fe-rich, more Mg- and Al-rich illite than

857   the majority of previously documented cases.

858

859   6) From the above conclusions, the range of environments and processes (both

860   geological and geochemical) by which surface illitisation takes place is wider than

861   described previously, and these processes can act in combination, making this

862   reaction more relevant globally.

863

864   7) The trace amounts of palygorskite found towards the top of the Tortuero

865   section are probably produced in the same Mg-enriching diagenetic process(es)

866   promoting illitisation and dolomitisation.

867

868   8) Dolomitisation of pre-existing carbonates, either bioclasts or cement, occurred

869   in coastal (Alcorlo Formation) and shallow marine (Tranquera Formation)

870   sediments. By analogy with recent saline lacustrine sediments in Iraq (Aqrawi,

871   1995), this probably happened soon after deposition.

872

873   9) Dolomitisation and Mg enrichment of the clay may have occurred at the same

874   time. Seawater is the most probable source of Mg, though it is conceivable that it

875   was also derived through dissolution of evaporites in the younger Valle de

876   Tabladillo Formation.

877

878   10) Dessication of lake or lagoonal sediment was accompanied by formation of

879   haematite in both clay and dolomite-rich samples.

880

885 did not receive any specific grant from funding agencies in the public,

886 commercial, or not-for-profit sectors.

887

888 **References**

889

890 Amorosi, A., 1995. Glaucony and sequence stratigraphy: a conceptual framework

891   of distribution in siliciclastic sequences. J. Sediment. Res. 65, 419-425.

892   DOI: 10.1306/D4268275-2B26-11D7-8648000102C1865D

893 Andrade, G., de Azevedo, A., Cuadros, J., Souza, V., Correia- Furquim, S.A.,

894   Kiyohara, P., Vidal-Torrado, P., 2014. Transformation of kaolinite into

895   smectite and iron-illite in Brazilian mangrove soils. Soil Sci. Soc. Am. J. 78,

896   655-672.

897 Aqrawi, A.A.M., 1995. Brackish-water and evaporitic Ca-Mg carbonates in the

898   Holocene lacustrine/deltaic deposits of southern Mesopotamia. J. Geol.

899   Soc. London 152, 259-268.

900 Aubert, D., Stille, P., Probst, A., 2001. REE fractionation during granite

901   weathering and removal by waters and suspended loads: Sr and Nd

902   isotopic evidence. Geochim. Cosmochim. Acta 65, 387-406.

903 Bain, D.C., McHardy, W.J., Lachowski, E.E., 1994. X-ray fluorescence

904   spectroscopy and microanalysis. In: Wilson, M.J. (Ed.) Clay Mineralogy:

905   Spectroscopic and Chemical Determinative Methods. Chapman and Hall,

906   London, pp. 260-299 (Chapter 7).

907 Baker, J.C., 1997. Green ferric clay in non-marine sandstones of the Rewan

908   Group, southern Bowen Basin, Eastern Australia. Clay Miner. 32, 499-506.

909 Baker, P.A., Kastner, M., 1981. Constraints on the formation of sedimentary

910   dolomite. Science 213, 214-216.

911 Benito, M.I. and Mas, R. 2007. Origin of Late Cretaceous dolomites at the

912   southern margin of the Central System, Madrid Province, Spain. J. Iber.

913   Geol. 33, 41-54.

914 Chamley, H., 1989. Clay Sedimentology. Springer-Verlag, Berlin.

915 Chamley, H., Debrabant, P., Candillier, A.-M., Foulon, J., 1983. Clay mineralogy

916   and inorganic geochemical stratigraphy of Blake-Bahama Basin since the

917   Callovian, site 534, Deep Sea Drilling Project leg 76. Initial Reports DSDP

918   76, 437-451.

919 Deconinck, J.F., Strasser, A., Debrabant, P., 1988. Formation of illitic minerals at

920   surface temeratures in Purbeckian sediments (lower Berriasian, Swiss and

921   French Jura). Clay Miner. 23, 91-103.

922 Deocampo, D.M., 2004. Authigenic clays in East Africa: Regional trends and

923   paleolimnology at the Plio-Pleistocene boundary, Olduvai Gorge,

924   Tanzania. J. Paleolimnol. 31, 1-9.

925 Deocampo, D.M., Cuadros, J., Wing-Dudek, T., Olives, J., Amouric, M., 2009.

926   Saline lake diagenesis as revealed by coupled mineralogy and

927   geochemistry of multiple ultrafine clay phases: Pliocene Olduvai Gorge,

928   Tanzania. Am. J. Sci. 309, 834-868.

929 Dyar, M.D., Schaefer, M.W., Sklute, E.C., Bishop, J.L., 2008. Mössbauer

930   spectroscopy of phyllosilicates: effects of fitting models on recoil-free

931   fractions and redox ratios. Clay Miner. 43, 3-33.

932 Eberl, D. and Hower, J. 1976. Kinetics of illite formation. Geol. Soc. Amer. Bull.

933   87, 1326-1330.

934   Ehrenberg, S.N. and Nadeau, P.H., 1989. Formation of diagenetic illite in

935   sandstones of the Garn Formation Haltenbanken Area, Mid-Norwegian

936   Continetnal Shelf. Clay Miner. 24, 233-253.

937   Eggleton, R.A., Fitz Gerald, J., 2011. Illite from Muloorina, South Australia. Clays

938   Clay Miner. 59, 608-612.

939   Gabis, V., 1963. Etude minéralogique et géochimique de la série sedimentaire

940   Oligocène du Velay. Bull. Soc. Fr. Minéral. Crist. 86, 315-354.

941   Gale, A.S., 1996. Turonian correlation and sequence stratigraphy of the Chalk in

942   southern England. Sequence stratigraphy in the United Kingdom. In:

943   Hesselbo, S.P., Parkinson, D.N. (Eds.) Sequence Stratigraphy in British

944   Geology. Geological Society of London Special Publication 103, London,

945   pp. 177-195.

946   Galindo, C., Tornos, F., Darbyshire, D.P.F., Casquet, C., 1994. The age and

947   origin of the barite–fluorite (Pb–Zn) veins of the Sierra del Guadarrama

948   (Spanish Central System, Spain): a radiogenic (Nd, Sr) and stable isotope

949   study. Chem. Geol. 112, 351–364.

950   García-Hildalgo, J.F., Gil, J., Segura, M., Dominguez, C., 2007. Internal anatomy

951   of a mixed siliciclastic–carbonate platform: the Late Cenomanian–Mid

952   Turonian at the southern margin of the Spanish Central System.

953   Sedimentology 54, 1245–1271.

954   Giles, M.R., 1997. Diagenesis: A Quantitative Perspective. Kluwer Academic

955   Publishers, Dordrecht.

956   Gilg, A., Weber, B., Kasbohm, J., Frei, R., 2003. Isotope geochemistry and orgin

957   of illite-smectite and kaolinite from the Seelitz and Kemmlitz kaolin

958   deposits, Saxony, Germany. Clay Miner. 38, 95-112.

959   Glasmann, J.R., Lundgard, P.D., Clark, R.A., Penny, B.K. and Collins, I.D., 1989.

960   Geochemical evidence of the history of diagenesis and fluid migration:

961   Brent Sandstone, Heather Field, North Sea. Clay Miner. 24, 255-284.

962   Griffin, J.J., Windom, H. Goldberg, E.D., 1968. Distribution of clay minerals in the

963   world ocean. Deep-Sea Res. 15, 433-461.

964   Hancock, J.M., 1990. Sea level changes in the British region during the Late

965   Cretaceous. P. Geologist. Assoc. 100, 565-594.

966   Hover, V.C., Ashley, G.M., 2003. Geochemical signatures of paleodepositional

967   and diagenetic environments: a STEM/AEM study of authigenic clay

968   minerals from an arid rift basin. Olduvai Gorge, Tanzania. Clays Clay

969   Miner. 51, 231-251.

970   Huggett, J.M., Cuadros, J., 2005. Low-temperature illitization of smectite in the

971   late Eocene and early Oligocene of the Isle of Wight (Hampshire basin),

972   UK. Am. Mineral. 90, 1192-1202.

973   Huggett, J. M., Cuadros, J., 2010. Glauconite formation in lacustrine/palaeosol

974   sediments, Isle of Wight (Hampshire basin), UK. Clay Miner. 45, 35-50.

975   Huggett, J.M., Gale, A.S., Clauer, N., 2001. The nature and origin of non-marine

976   10 Å green clays from the late Eocene and Oligocene of the Isle of Wight

977   (Hampshire basin), UK. Clay Miner. 36, 447-464.

978   Ireland, B.J., Curtis, C.D. and Whiteman, J.A. 1983. Compositional variation

979   within some glauconites and illites and implications for their stability and

980   origins. Sedim. 30, 769–786.

981   Jarvis, I., Jarvis, K.E., 1985. Rare-earth element geochemistry of standard

982   sediments: a study using inductively coupled plasma spectrometry. Chem.

983   Geol. 53, 335-344.

984   Jones, B.F., Weir, A.H., 1983. Clay minerals of Lake Abert, an alkaline saline

985   lake. Clays Clay Miner. 31, 161-172.

986   Keller, W.D., 1958. Glauconitic mica in the Morrison Formation in Colorado.

987   Clays Clay Miner. 5, 120-128.

988   Kazerouni, A.M., Poulsen, M.K., Friis, H., Svendsen, J.B., Hansent, J.P.V., 2013.

989   Illite/smectite transformation in detrital glaucony during burial diagenesis of

990   sandstone: A study from Siri Canyon – Danish North Sea. Sedimentology

991   60, 679–692.

992   Lagarec, K., Rancourt, G.K., 1998. Mössbauer Spectral Analysis Software.

993   Mössbauer Group Physics Department, University of Ottawa, Canada.

994   Martin-Serrano, A., Santisteban, J.L. and Mediavilla, D.R., 1996. Tertiary of

995   Central System basins. In: Friend, P.F. and Dabrio, C.J. (Eds.) Tertiary

996   Basins of Spain. Cambridge University Press, pp. 255-260.

997   Mehra, O.P., Jackson, M.L., 1960. Iron oxide removal from soils and clays by

998   dithionite-citrate system buffered with sodium bicarbonate. Clays Clay

999   Miner. 7, 317-327.

1000   Millot, G., 1964. Géologie des Argiles. Masson, Paris.

1001   Moore, D.M., Reynolds, R.C., 1997. X-ray Diffraction and the Identification and

1002   Analysis of Clay Minerals. Oxford University Press, Oxford.

1003   Nesteroff, W.D., Sabatier, G., Heezen, B.C., 1964. Les minéraux argileux, le

1004   quartz et le calcaire dans quelques sédiments de l'océan Arctique. C.R.

1005   Acad. Sci. 258, 991-993.

1006   Neumann, A., Petit, S., Hofstetter, T., 2011. Evaluation of redox-active iron sites

1007   in smectites using middle and near infrared spectroscopy. Geochim.

1008   Cosmochim. Acta 75, 2336-2355.

1009   Norrish, K., Pickering, J.G., 1983. Clay Minerals. In: Soils, an Australian

1010   Viewpoint. CSIRO, Melbourne, and Academic Press, London, pp. 281-

1011   308.

1012   Odin, G.S., Fullager, P.D., 1988. Geological significance of the glaucony facies.

1013   In: Green marine clays (Odin, G.S., Ed.). Elsevier, Developments in

1014   Sedimentology, Volume 45, Amsterdam, pp. 295-332 (Chapter C4).

1015   Odin, G.S., Matter, A., 1981. De glauconiarum origine. Sedimentology 28, 611-

1016   641.

1017   Palumbo, F. Main, I.G. and Zito, G., 1999. The thermal evolution of sedimentary

1018   basins and its effect on the maturation of hydrocarbons. Geophys. J. Int.

1019   139, 248–260.

1020   Perry, E. and Hower, J. 1970. Burial diagenesis in Gulf Coast pelitic sediments.

1021   Clays Clay Miner. 18, 165-178.

1022   Plançon, A., 2002. New modeling of X-ray diffraction by disordered lamellar

1023   structures, such as phyllosilicates. Am. Mineral. 87, 1672-1677.

1024   Post, J.L., 1978. Sepiolite deposits of the Las Vegas, Nevada area. Clays Clay

1025   Miner. 26, 58-64.

1026   Retallack, G.J., 2001. Soils of the past. 2nd Edition, Blackwell Science, Oxford.

1027   Reynolds, R.C. Jr., Reynolds, R.C. III, 1996. NEWMOD: The Calculation of One-

1028   Dimensional X-ray Diffraction Patterns of Mixed-Layered Clay Minerals.

1029   Computer Program. 8 Brook Road, Hanover, New Hampshire, USA.

1030   Robinson, D., Wright, V.P., 1987. Ordered illite-smectite and kaolinite-smectite:

1031   pedogenic minerals in a lower Carboniferous paleosol sequence, South

1032   Wales? Clay Miner. 22, 109-118.

1033   Ryan, P.C., Huertas, F.J., 2009. The temporal evolution of pedogenic Fe-

1034   smectite to Fe-kaolin via interstratified kaolin-smectite in a moist tropical

1035   soil chronosequence. Geoderma 151, 1-15.

1036   Singer, A., Stoffers, P.,1980. Clay mineral diagenesis in two East African lake

1037   sediments. Clay Miner. 15, 291-307.

1038   Siyuan, S., Stucki, J., 1994. Effects of iron oxidation state on the fate and

1039   behaviour of potassium in soils. In: Havlin, J.L, Jacobson, J., Fixen, P.,

1040   Herbert, G. (Eds) Soil Testing: Prospects for improving nutrient

1041   recommendations. Soil Sci. Soc. Am. Special Publication 40, Madison, pp.

1042   173-185.

1043   Smith B., 1994. Characterization of poorly ordered minerals by selective chemical

1044   methods. In: Wilson, M.J. (Ed) Clay Mineralogy: Spectroscopic and

1045   Chemical Determinative Methods. Chapman & Hall, London, pp. 333-357

1046   (Chapter 9).

1047   Stanjek, H., Marchel, C., 2008. Linking the redox cycles of Fe oxides and Fe-rich

1048   clay minerals: an example from a palaeosol of the Upper Freshwater

1049   Molasse. Clay Miner. 43, 69-82.

1050 Stenger-Kovács,C., Lengyel, E., Buczkó, K., Tóth, F.M., Crossetti, L.O.,

1051   Pellinger, A., Doma, Z.Z., Padisák, J., 2014. Vanishing world: alkaline,

1052   saline lakes in Central Europe and their diatom assemblages. Inland

1053   Waters 4, 383-396.

1054 Stucki, J.W., 1997. Redox processes in smectite: soil environmental signifiance.

1055   Adv. GeoEcol. 30, 395-406.

1056 Stucki, J.W., Low, P.F., Roth, C.B., Golden, D.C., 1984. Effects of iron oxidation

1057   state on clay swelling. Clays Clay Miner. 32, 357-362.

1058 Summerfield, M.A., 1983. Petrography and diagenesis of silcrete from the

1059   Kalahari basin and Cape Coastal zone, southern Africa. J. Sediment.

1060   Petrol. 53, 895-909.

1061 Tlig, S., M'rabet, A., 1985. A Comparative-Study of the Rare-Earth Element

1062   (REE) Distributions within the Lower Cretaceous Dolomites and

1063   Limestones of Central Tunisia. Sedimentology 32, 897-907.

1064 Watts, N.L., 1980. Quaternary pedogenic calcretes from the Kalahari (southern

1065   Africa): mineralogy, genesis and diagenesis. Sedimentology 27, 661-686.

1066 Weaver, C.E., 1989. Clays, Muds, and Shales. Developments in Sedimentology,

1067   Volumen 44. Elsevier, Amsterdam.

1068 Weaver, C.E., Beck, K.C., 1977. Miocene of the S.E. United States: a model for

1069   chemical sedimentation in a peri-marine environment. Sediment. Geol. 17,

1070   1- 234.

1071 Wray, D.S., 1999. Identification and long-range correlation of bentonites in

1072   Turonian - Coniacian (Upper Cretaceous) chalks of northwest Europe.

1073   Geol. Mag. 136, 361-371.

1074   Wray, D.S., Jeans, C.V., 2014. Chemostratigraphy and provenance of clays and

1075   other non-carbonate minerals in chalks of Campanian age (Upper

1076   Cretaceous) from Sussex, southern England. Clay Miner. 49, 327-340.

1077   Figures

1078

1079   Figure 1. Map of Spain with the location of Sierra de Guadarrama and geological

1080   map of the investigated sites. The sampled sites, Tortuero (T) and Torrelaguna

1081   (A), are shown.

1082

1083   Figure 2. Roadside section through the sampled interval at Tortuero, in 2011.

1084   Numbers refer to the sample numbers as shown in Figure 3.

1085

1086   Figure 3. Sedimentological log for the Tortuero section with clay assemblage, X-

1087   ray diffraction data shown as a bar chart for clay-bearing samples, and whole

1088   sample REE element plots for all samples. Vertical scale is in meters above the

1089   base of the measured section. Illite and smectite are present in illite-smectite

1090   mixed-layer; here the percent of each layer is represented. Sample labels are left

1091   of the clay-proportion bars, at the corresponding sampling height. Some samples

1092   do not have detailed clay composition.Vertical distance is shown in m at the left

1093   of the diagram. Grain size (clay, silt, very fine and fine sand) is indicated at the

1094   base of the log.

1
2
3
4
5
6
7
8
9
10
11
12
13
14
15
16
17
18
19
20
21
22
23
24
25
26
27
28
29
30
31
32
33
34
35
36
37
38
39
40
41
42
43
44
45
46
47
48
49
50
51
52
53
54
55
56
57
58
59
60
61
62
63
64
65

1095

1096 Figure 4. Sedimentological log for the Torrelaguna section, caption as in Figure

1097 3.

1098

1099 Figure 5. Powder XRD diagrams of two samples from Tortuero (T3) and

1100 Torrelaguna (A10), with different contents of carbonate and silicate phases.

1101 Values are d-values in Å. I-Sm is illite-smectite, Kaol is kaolinite, Qz is quartz,

1102 and Dol is dolomite. The 3.34 Å peak in A10 is truncated.

1103

1104

1105 Figure 6. Plot of the relative areas of XRD peaks corresponding to illite-smectite

1106 (I-Sm) phases (range 17-10 Å) and kaolinite (~7 Å), in Tortuero (T) and

1107 Torrelaguna (A). The areas were normalised to the sum of the areas of selected

1108 peaks for all the silicate phases (see Methods section). The data indicate an

1109 inverse correlation between the abundance of kaolinite and I-Sm phases (see

1110 text).

1111

1112 Figure 7. BSEM images: (a) Haematite infilling fractures in dolomite. In this

1113 sample (T8a) the clay appears homogenous. (b) Clay-rich dolomite from the

1114 Tranquera Formation (sample T14). Dolomite is faintly zoned; in some crystals

1115 the core has been leached out (D1), while in others one or two chemical zones

1116 have been leached out (D2). Sand-size quartz is widespread and a selection of

1117 grains are indicated with an arrow. Note that contrast is similar to dolomite, but

1118   the two minerals may be distinguished by their different shapes, i.e. quartz is

1119   sub-rounded, dolomite is rhombic. Glt = glauconite. (c) Part of a calcite-cemented

1120   fracture in dolomite (sample A6).

1121

1122   Figure 8. Experimental and calculated XRD patterns of the oriented mounts of

1123   samples from Tortuero and Torrelaguna with different clay contents. Pal indicates

1124   palygorskite and Fsp is feldspar. Only illite-smectite (I-Sm) and kaolinite (Kaol)

1125   are included in the model.

1126

1127   Figure 9. Mössbauer spectra of two samples (dots), with the corresponding

1128   calculated components and fit to the experimental data (lines). Two octahedral

1129 Fe^{3+} components (small quadrupole splitting) and one octahedral Fe^{2+}

1130   component (large quadrupole splitting) occur in each spectrum.

1131

1132   Figure 10. Percent illite in the clay fraction as calculated from XRD data (oriented

1133   mounts) plotted vs. a soil development score, calculated from the number of

1134   pedogenic characteristics present (colour mottling, rootlets and peds). T and A

1135   indicate samples from Tortuero and Torrelaguna sections, respectively. The

1136   arrow indicates that clay from horizon T10, with no soil development, is

1137   suspected to be reworked from the underlying horizon, T9a, which has a soil

1138   score of 3, and the position that sample T10 would have in the plot.

1139

1140 Figure 11. Plots of layer type percent from modelling of the XRD patterns of

1141 oriented and glycolated mounts. The data from Tortuero define two groups of

1142 samples with established trends (see text). The smaller number of data points

1143 from Torrelaguna do not define clear trends. The labels of the samples are

1144 included in a and c.

1145

1146 Figure 12. Octahedral Mg and Fe^{2+} content of illite-smectite versus stratigraphic

1147 height at Tortuero and Torrelaguna. Heights are meaningful only within each

1148 sequence, as there is no geological correspondence between height values at

1149 Tortuero and Torrelaguna. Chemical values are from averaged SEM-EDS

1150 analyses and recalculated to the structural formula ($O_{10}[OH]_2$, i.e., atoms per half

1151 formula unit: a.p.h.f.u.). The b plot has data only from samples analysed with

1152 Mössbauer spectroscopy.

1153

Under surface conditions a slow transformation has occurred of kaolinite to illite by way of illite-smectite.

Illitisation is most intense where pedogenesis is most intense.

The mechanism involves enhanced layer charge resulting from Mg^{2+} substitution for Al^{3+} (or Fe^{3+}) and Fe^{3+} to Fe^{2+} reduction.

The neoformed illite is less Fe-rich, more Mg-, and Al-rich illite than the majority of previously documented cases in the near surface.

Dolomite and calcite are authigenic cements that precipitated in a clastic sediment, probably soon after deposition.

Dolomitisation and Mg enrichment of the clay may have occurred at the same time.

Table

Sample	Height above base of section (m)	Description	illitic clay	smectitic clay	kaolinite	paly-gorskite	phosphate minerals	calcite	dolomite	Quartz	Feldspar
Tortuero Section											
T14	10.1	Dolomitic sandstone with glauconite granules	x		x	tr			xxx	xx	x
T13	9.4	Sandy dolomite with glauconite granules	x			minor	tr		xx	xxx	x
T12	9.2	Sandy dolomite	x	x	x	N/A		x	xx	xx	
T11	8.4	Dolomicrite with minor clay, calcite and quartz sand	xx			tr	tr	xx	x	xx	
T10a	7.7	Rooted dolomicrite with minor clay, calcite and quartz sand	xx	xx		tr	tr	xx	x	xx	x
T 10	6.9	Dolomicrite with minor clay, calcite and quartz	x	x		tr		x	xx	xx	x
T 9a	6.7	Mottled red-gree-white palaeosol. More intense slickensiding and ped formation than any other sample. Dolomicrite with minor clay, calcite and quartz.	x			tr		x	xxx	xx	x
T 9	6.5	Same palaeosol as 9a, but with less intense pedogenesis	x			tr			xxx	xx	x
T8ii	5.9	Sandy dolomicrite, trace clay	x			minor			xxx	xx	x
T8a	5.4	Sandy dolomicrite, trace clay, vuggy pores. Slightly zoned dolomite with leached zone.	x							xxxx	x
T8i	4.8	Sandy dolomicrite, trace clay	x		x				xx	xx	x
T 8	4.3	Dolomicrite with minor quartz and trace clay	x	x	x				x	xxx	x
T7	4.1	Sandy dolomite with sand-lined burrows	x						xx	xx	x
T6	3.6	Dolomitised calcrete	x		x				xxx	x	x
T5	3.25	Rooted and burrowed dolomicrite	x		x				xxx	xx	
T4	3.1	Clayey quartzose siltstone	xx		x				x	xxx	x
T 3	2.8	Burrowed dolomicrite, minor clay	x		x			x	xxx	xx	x
T 2	2.3	Sandy, silty clay with minor haematite in secondary pores	xx		x			x	x	xxx	x
T1	1.7	Rooted dolomite, minor clay. Dolomite is not zoned in BSEM images.	x		x			x	xxx	xx	x
Torrelaguna section											
A12	9.2	Burrowed sandy slightly zoned, rounded & etched (?) dolomite			tr					x	x
A11	8.6	Dark claystone	x	xxx	x					xx	tr
A10	8.1	Dark claystone with some sand	xx	xx	x		tr			xx	
A9	7.8	Sandy dolomite	x	x	x				x	xxx	xx
A8	7.4	Bioturbated sandy dolomicrite	x		x					x	
A7	6	Sandy dolomite	x		x					xxx	x
A6	4.95	Dolomite with haematite-cemented rootlets, reworked micrite pebbles & calcite cement							xx	x	
A5	4.3	Dolomite with tightly interlocking zoned crystals & rootlets, cemented by haematite and calcite.							x	x	
A4	3.8	Laminated quartzose siltstone			x					xx	x
A3	3.3	Sandy dolomite with clay	xx		xx					xx	x
A2	2.7	Burrowed sandy slightly zoned, rounded & etched (?) dolomite	x		x				x	x	x
A1	0.5	Sandy clay with some grain-size lamination	xx		xx					xx	xx

Table 2. Results of the modelling of the XRD patterns of oriented and glycolated mounts. The error is the accumulated for the three layer types.

Sample	Phase	% Phase	% Sm layers	R	Fe	N max	N ave	Total % Illite	Total % Sm	Total % Kaol	Error (±%)
T 14	Illite	4	0		0.2	35	20				
	I-S	17	1	3	0.2	20	15				
	I-S	25	15	1	0.2	20	15				
	I-S	3	25	1	0.2	20	15				
	I-S	41	47	0	0.2	20	15				
	I-S	2	60	0	0.2	15	10				
	I-S	6	65	0	0.2	15	10				
	Kaol	2	0		0	50	40	69	29	2	12
T 13	Illite	4	0		0.2	35	20				
	I-S	16	2	3	0.2	20	15				
	I-S	8	10	1	0.2	20	15				
	I-S	25	25	1	0.2	20	15				
	I-S	22	35	0.5	0.2	20	15				
	I-S	12	60	0	0.2	15	10				
	I-S	2	95	0	0.2	10	5				
	Kaol	11	0		0	50	40	65	24	11	11
T 11	Illite	5	0		0.2	35	20				
	I-S	21	2	3	0.2	20	15				
	I-S	11	10	1	0.2	20	15				
	I-S	34	25	1	0.2	20	15				
	I-S	13	60	0	0.2	15	10				
	Kaol	16	0		0	50	40	66	18	16	8
T 10a	Illite	27	0		0.2	35	20				
	I-S	18	1	3	0.2	20	15				
	I-S	28	15	1	0.2	20	15				
	I-S	3	30	1	0.2	20	15				
	I-S	3	40	0.5	0.2	20	10				
	Kaol	21	0		0	50	40	73	6	21	8
T 10	Illite	5	0		0.2	35	20				
	I-S	17	1	3	0.2	20	15				
	I-S	46	10	1	0.2	20	15				
	I-S	15	20	1	0.2	20	15				
	I-S	16	40	0	0.2	20	15				
	Kaol	1	0		0	50	40	82	17	1	8
T 9a	Illite	7	0		0.2	35	20				
	I-S	44	1	3	0.2	20	15				
	I-S	11	10	1	0.2	20	15				
	I-S	11	20	1	0.2	20	15				
	I-S	24	40	0	0.2	20	15				
	Kaol	3	0		0	50	40	84	13	3	8
T 9	Illite	5	0		0.2	35	20				
	I-S	24	1	3	0.2	20	15				
	I-S	23	10	1	0.2	20	15				

	I-S	23	20	1	0.2	20	15			
	I-S	24	40	0	0.2	20	15			
	Kaol	1	0		0	50	40	85	14	1	8
T 8ii	Illite	25	0		0.2	20	15			
	I-S	24	10	1	0.2	20	15			
	I-S	25	20	0	0.2	20	15			
	I-S	24	40	0	0.2	20	15			
	Kaol	2	0		0	50	40	81	17	2	7
T 8	I-S	41	1	3	0.2	20	15			
	I-S	36	15	1	0.2	20	15			
	I-S	10	40	0.5	0.2	20	15			
	Kaol	13	0		0	50	40	77	10	13	6
T 4	Illite	18	0		0.2	35	20			
	I-S	15	1	3	0.2	20	15			
	I-S	36	10	1	0.2	20	15			
	I-S	13	20	1	0.2	20	15			
	I-S	5	40	0.5	0.2	20	15			
	Kaol	13	0		0	50	40	79	8	13	8
T 3	I-S	37	1	3	0.2	20	15			
	I-S	30	10	1	0.2	20	15			
	I-S	8	20	1	0.2	20	15			
	I-S	2	40	1	0.2	20	15			
	Kaol	23	0		0	50	40	71	6	23	7
T 2	I-S	33	2	3	0.2	20	15			
	I-S	25	20	0	0.2	20	15			
	I-S	8	40	0	0.2	20	15			
	I-S	4	60	0	0.2	15	10			
	Kaol	30	0		0	50	40	59	11	30	8
T 1	I-S	34	1	3	0.2	20	15			
	I-S	38	20	0	0.2	20	15			
	I-S	9	40	0	0.2	20	15			
	I-S	3	60	0	0.2	15	10			
	Kaol	16	0		0	50	40	71	13	16	8
A 11	I-S	11	1	1	0.3	20	15			
	I-S	21	15	1	0.3	15	10			
	I-S	6	30	0	0.3	20	15			
	I-S	40	50	0	0.3	15	5			
	I-S	15	80	0	0.3	5	3			
	Kaol	7	0		0	90	15	56	37	7	9
A 10	I-S	15	2	1	0.3	50	10			
	I-S	24	2	0	0.3	10	5			
	I-S	16	15	1	0.3	20	10			
	I-S	13	30	0	0.3	20	6			
	I-S	25	40	0	0.3	15	5			
	Kaol	7	0		0	90	15	76	17	7	9
A 9	I-S	41	3	1	0.3	25	10			
	I-S	18	3	1	0.3	8	5			
	I-S	15	15	1	0.3	20	5			
	I-S	30	30	0	0.3	15	5			

				R		Nmax	Nave				
	K-S	19	2	1	0.3*	90	15	74	7	19	9
A 7	I-S	23	4	1	0.2	40	10				
	I-S	8	20	1	0.2	70	5				
	I-S	15	35	0	0.2	25	10				
	Kaol	54	0		0	90	15	38	8	54	6
A 6	I-S	21	2	1	0.2	40	10				
	I-S	26	10	1	0.2	70	5				
	I-S	28	20	1	0.2	70	5				
	I-S	14	35	1	0.2	20	5				
	Kaol	11	0		0	90	10	75	14	11	7
A 3	I-S	30	4	1	0.12	70	10				
	I-S	17	15	1	0.12	70	5				
	I-S	10	35	0	0.12	50	10				
	Kaol	43	0		0	90	15	50	7	43	6
A 1	I-S	58	2	1	0.2	70	5				
	I-S	15	15	1	0.2	70	5				
	I-S	6	30	1	0.2	15	5				
	K-S	21	2	0	0.2*	40	20	74	6	21	6

d-smectite = 16.9 Å; d-kaolinite = 7.14-7.17 Å; d-illite = 9.96-9.98 Å

σ* = 20-30

R = Layer stacking order

N max , N ave = Maximum and avarage number of layers in the coherent scattering domains

Error = number of phases x estimated error per phase / 2

* Fe in the smectite layers only

Table 3. Chemical data of major elements from ICP-OES.

	SiO_2	Al_2O_3	Fe_2O_3	TiO_2	MnO	CaO	MgO	Na_2O	K_2O	P_2O_5	Total
T14	55.14	20.13	3.79	0.70	<0.06	1.01	4.41	0.00	3.64	0.00	88.82
T14*	54.67	20.55	3.44	0.72	<0.06	0.00	4.14	6.38	3.76	0.00	93.66
T13	44.41	25.65	4.44	0.59	<0.06	1.71	2.13	0.00	5.03	5.11	89.07
T11*	53.34	18.30	3.80	0.95	<0.06	0.00	3.00	0.00	3.82	0.00	83.21
T11	48.44	16.41	4.92	0.75	<0.06	2.30	3.05	0.00	3.30	0.00	79.16
T10A	54.35	21.55	3.22	0.68	<0.06	1.53	3.35	0.00	3.36	0.24	88.28
T10	55.29	22.54	5.99	0.68	<0.06	0.64	3.72	0.00	6.00	0.00	94.85
T9A	48.97	20.60	5.99	0.60	<0.06	2.14	4.37	0.00	5.37	0.00	88.04
T9	53.76	22.09	5.47	0.66	<0.06	1.00	4.01	0.00	5.94	0.00	92.92
T8ii	52.41	19.18	4.19	0.77	<0.06	1.12	3.53	0.00	5.16	0.00	86.35
T8ii*	54.67	22.15	4.53	0.90	<0.06	0.00	3.55	0.00	5.93	0.00	91.74
T8	54.52	22.90	4.85	0.77	<0.06	0.73	3.12	0.00	5.15	0.00	92.03
T3	50.45	24.53	4.72	0.69	<0.06	1.61	2.41	0.00	4.43	0.15	88.98
T2	47.31	22.03	4.57	0.66	<0.06	1.40	2.43	0.00	4.48	0.00	82.86
A9	53.77	25.28	5.95	0.69	<0.06	0.07	3.25	0.06	4.98	<0.12	94.05
A8	51.19	21.91	5.90	0.56	<0.06	0.26	3.31	2.07	5.07	<0.08	90.27
A3	48.27	27.81	3.41	0.65	<0.06	0.13	1.31	2.01	3.28	0.11	86.97
A1	53.20	26.25	6.18	0.57	<0.06	0.07	2.90	0.06	5.22	<0.12	94.45

* indicates samples which have been treated to remove Fe and Al oxides.

Table 4. Structural formulae (per $O_{10}[OH]_2$) from EDS data of illite-smectite particles, averaged from ~30 particles per sample. The Fe^{3+} and Fe^{2+} values in normal case are from Mössbauer data; those in italics are assumed, with Fe^{2+} ~10% of total Fe.

	Si	Al tet	Al oct	Mg oct	Fe III	Fe II	Ti	Ca	Na	K	Sum oct	Int charge
T 14	3.451	0.549	1.611	0.186	0.200	0.029	0.027	0.053	0.046	0.428	2.052	0.580
T 13	3.655	0.345	1.600	0.196	*0.171*	*0.019*	0.026	0.056	0.000	0.391	2.011	0.502
T 12	3.844	0.156	1.468	0.433	*0.134*	*0.015*	0.027	0.000	0.000	0.344	2.077	0.344
T 11	3.871	0.129	1.434	0.354	*0.188*	*0.021*	0.049	0.000	0.000	0.317	2.046	0.317
T 10	3.722	0.278	1.431	0.359	0.206	0.025	0.030	0.000	0.000	0.481	2.051	0.481
T 9a	3.620	0.380	1.296	0.426	0.263	0.020	0.041	0.092	0.000	0.466	2.045	0.649
T 8ii	3.670	0.330	1.421	0.355	*0.206*	*0.023*	0.046	0.000	0.000	0.509	2.051	0.509
T 8	3.719	0.281	1.493	0.316	*0.172*	*0.019*	0.041	0.000	0.000	0.449	2.042	0.449
T 3	3.589	0.411	1.510	0.297	0.232	0.015	0.025	0.000	0.000	0.459	2.080	0.459
T 1	3.584	0.416	1.310	0.398	*0.234*	*0.026*	0.032	0.162	0.000	0.485	2.000	0.809
A 9	3.615	0.385	1.455	0.242	0.278	0.035	0.038	0.005	0.007	0.462	2.048	0.479
A 6	3.601	0.399	1.343	0.486	0.211	0.009	0.044	0.075	0.041	0.382	2.093	0.571
A 4	3.496	0.504	1.576	0.210	0.186	0.016	0.032	0.070	0.036	0.463	2.019	0.640
A 3	3.421	0.579	1.841	0.107	*0.107*	*0.012*	0.011	0.046	0.028	0.334	2.078	0.453
A 1	3.527	0.473	1.579	0.286	*0.183*	*0.020*	0.029	0.005	0.008	0.442	2.097	0.459

Table 5. Chemical data of trace elements from ICP-MS, in mg/kg.

	T14	T14*	T13	T11	T11*	T10A	T10	T9A	T9	T8ii	T8ii*	T8	T3	T2	A9	A8	A3	A1
Ba	196	262	n.d.	321	402	164	196	165	143	378	272	220	338	381	115	100	273	139
Be	3.3	3.3	n.d.	4.2	12.6	5.7	7.8	10.2	7.3	4.9	5.6	6.5	7.3	7.1	9.7	8.5	8.1	10.8
Cr	79	79	n.d.	84	93	97	83	83	82	99	91	90	82	83	73	81	96	84
Cu	22	27	n.d.	157	229	63	23	40	22	25	31	22	139	215	102	17	335	23
Ni	27	21	n.d.	19	13	18	29	31	27	32	20	19	27	31	31	22	37	19
Sc	12.7	12.0	n.d.	10.4	12.4	13.2	13.0	17.5	11.0	9.9	11.8	13.2	13.5	12.2	10.3	13.4	14.6	14.1
V	93	76	n.d.	156	114	174	122	130	103	150	157	118	141	122	167	118	106	82
Zn	21	38	n.d.	145	80	31	19	31	22	32	55	25	76	123	84	56	113	74
59Co	3.8	3.6	5.2	4.9	4.0	3.9	7.8	11.0	7.8	5.0	5.2	6.1	7.6	6.4	7.2	7.6	5.6	8.0
71Ga	29	28	39	26	27	30	31	29	31	27	31	32	33	31	33	35	37	36
85Rb	189	181	265	155	178	296	301	268	279	217	245	253	225	223	247	321	203	290
88Sr	40	35	25427	122	67	835	70	63	70	77	78	83	136	105	54	55	441	41
89Y	8.1	6.1	56.8	9.1	9.5	9.2	8.6	16.8	8.0	10.3	9.8	9.5	10.1	9.1	9.1	9.5	13.8	7.5
90Zr	134	125	77	135	139	116	115	103	110	117	134	149	116	117	92	131	98	95
93Nb	17	16	15	20	24	16	17	15	17	19	21	21	17	16	12	19	16	14
95Mo	1.8	1.1	2.0	7.0	1.2	<1.0	<1.0	<1.0	1.4	2.4	<1.0	1.3	<1.0	<1.0	<1.0	<1.0	3.2	<1.0
118Sn	7.4	7.4	13.0	8.2	8.6	7.5	8.7	8.8	7.6	7.5	8.6	8.1	10.0	9.6	10.6	9.5	21.1	11.5
133Cs	27	26	40	21	23	87	36	33	29	22	25	30	29	28	27	46	35	38
139La	16	12	138	25	21	20	15	25	17	26	25	20	34	25	17	20	58	12
140Ce	22	18	339	29	31	33	24	58	27	34	36	31	45	34	30	29	106	17
141Pr	2.3	1.9	42.4	2.9	3.1	3.9	2.4	6.5	2.6	3.4	3.5	3.0	4.5	3.4	3.8	2.8	11.4	1.6
146Nd	7.6	6.3	168.6	9.4	9.9	13.8	7.9	25.4	8.6	10.5	10.6	9.6	12.6	10.4	14.1	8.6	37.9	5.0
147Sm	1.4	1.2	35.9	1.5	1.6	2.5	1.3	5.2	1.4	1.6	1.5	1.6	1.9	1.6	2.7	1.3	5.3	0.9
151Eu	<0.26	<0.26	6.72	0.29	0.28	0.52	0.26	0.94	0.26	0.30	0.28	0.27	0.32	0.25	0.48	<0.26	0.97	<0.26
157Gd	1.1	0.9	27.3	1.2	1.2	2.0	1.1	4.1	1.1	1.2	1.3	1.3	1.7	1.4	2.2	1.2	3.6	0.8
159Tb	<0.28	<0.28	3.59	<0.28	<0.28	0.28	<0.28	0.58	<0.28	<0.28	<0.28	<0.28	<0.28	<0.28	0.34	<0.28	0.49	<0.28
163Dy	1.4	1.3	16.6	1.6	1.8	2.0	1.7	3.9	1.5	1.8	1.9	1.8	1.9	1.8	1.8	1.6	2.7	1.4
165Ho	0.33	<0.33	2.47	0.33	0.39	0.39	0.36	0.74	0.32	0.38	0.43	0.39	0.40	0.40	0.34	0.34	0.52	<0.33
166Er	1.03	0.96	5.65	1.25	1.27	1.23	1.18	2.13	1.05	1.24	1.35	1.23	1.32	1.24	1.08	1.15	1.59	0.94
169Tm	<0.20	<0.20	0.57	<0.20	0.20	<0.20	<0.20	0.30	<0.20	<0.20	0.22	<0.20	<0.20	0.20	<0.20	<0.20	0.22	<0.20
172Yb	1.2	1.1	3.2	1.1	1.4	1.4	1.4	2.0	1.2	1.4	1.5	1.5	1.4	1.3	1.2	1.3	1.6	1.1
175Lu	<0.19	<0.19	0.38	0.19	0.20	0.19	0.20	0.28	0.20	0.22	0.23	<0.19	0.23	0.21	<0.19	0.20	0.25	<0.19
178Hf	4.0	3.8	2.3	4.0	4.1	3.5	3.2	3.1	3.3	3.5	4.0	4.4	3.6	3.2	3.0	3.9	3.5	2.9
181Ta	1.6	1.5	1.7	1.7	2.3	1.4	1.6	1.4	1.5	1.7	2.0	1.9	1.6	1.5	1.3	1.7	1.7	1.5
182W	4.8	3.9	53.1	69.4	70.5	7.7	6.5	42.8	11.6	43.0	25.4	4.9	68.4	39.8	37.7	3.6	18.8	3.9
205Tl	<0.44	<0.44	0.95	0.45	<0.44	1.14	1.07	1.24	0.93	<0.44	0.63	0.74	0.77	<0.44	0.90	2.30	0.80	0.91
208Pb	8.5	9.5	44.7	18.3	594.9	19.9	24.7	62.3	15.3	14.4	16.6	11.5	14.9	14.4	22.2	14.7	39.4	14.7
232Th	16.7	6.4	42.5	8.2	6.7	15.1	10.8	14.1	7.5	7.0	6.6	13.2	10.4	10.4	9.1	11.0	10.9	7.8
238U	2.3	2.1	4.2	4.4	4.6	2.5	2.2	2.8	2.3	2.7	2.9	2.2	1.8	1.9	1.8	2.0	2.0	1.6

* indicates samples which have been treated to remove Fe and Al oxides.

Fig. 5
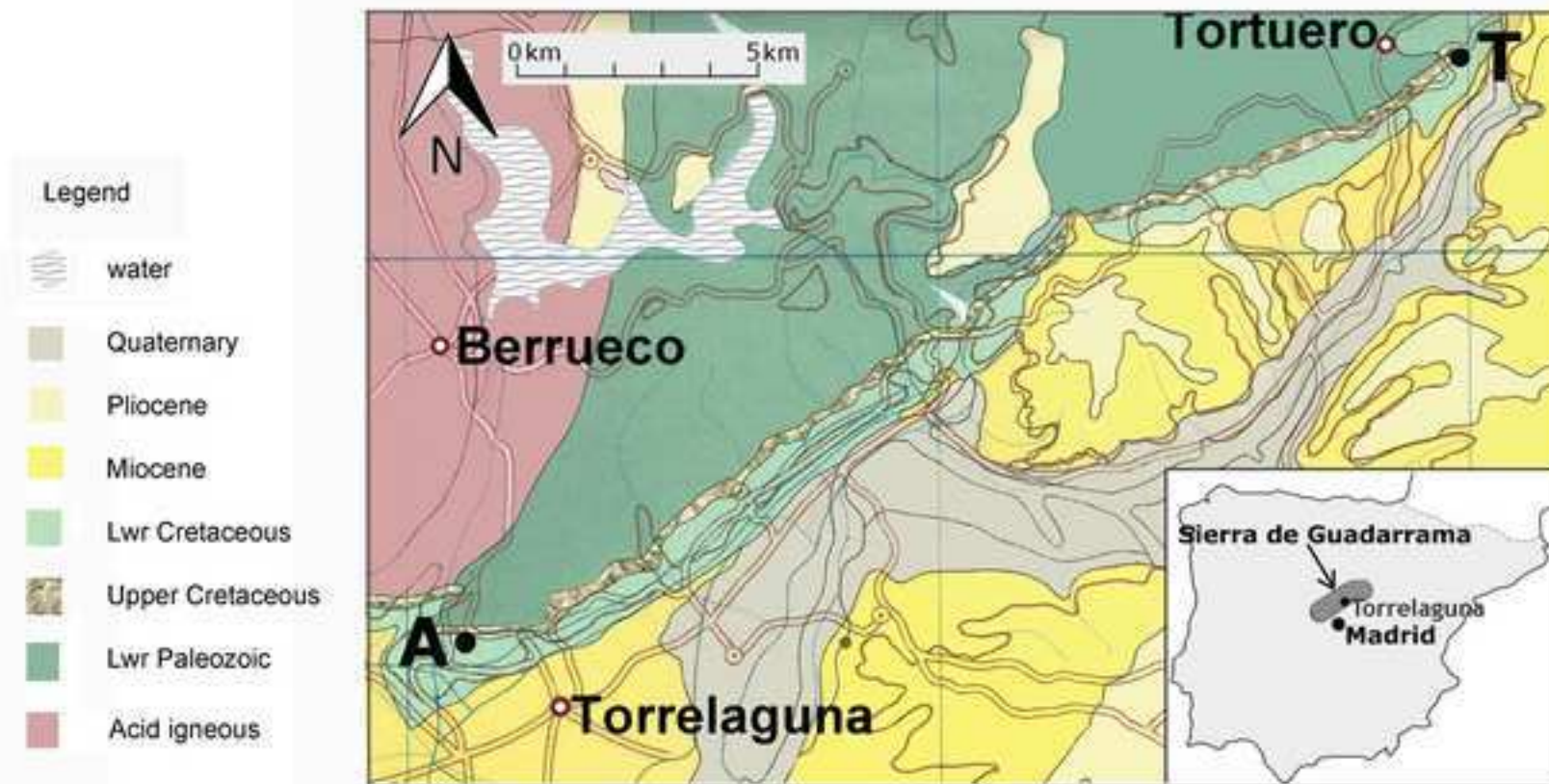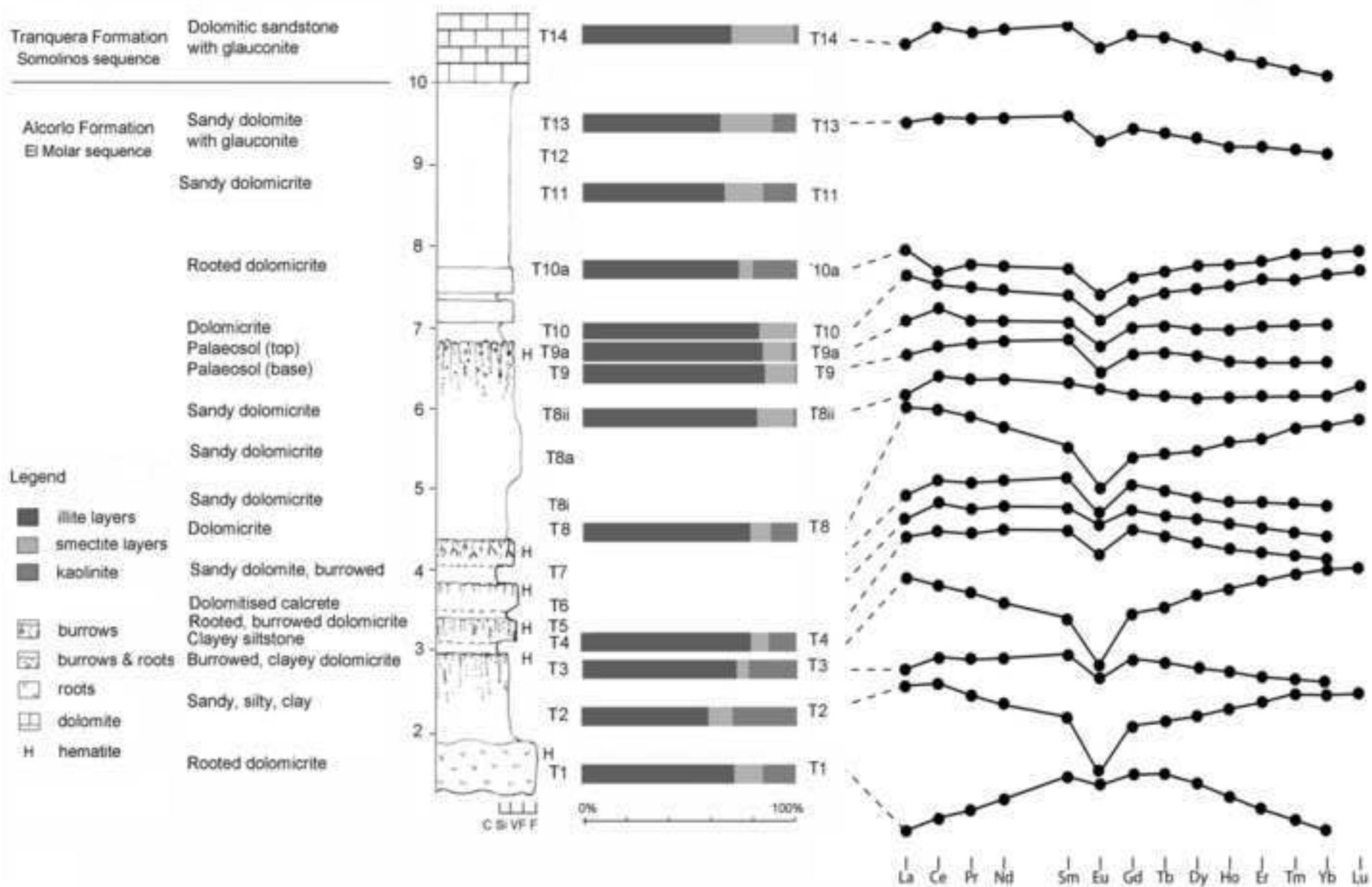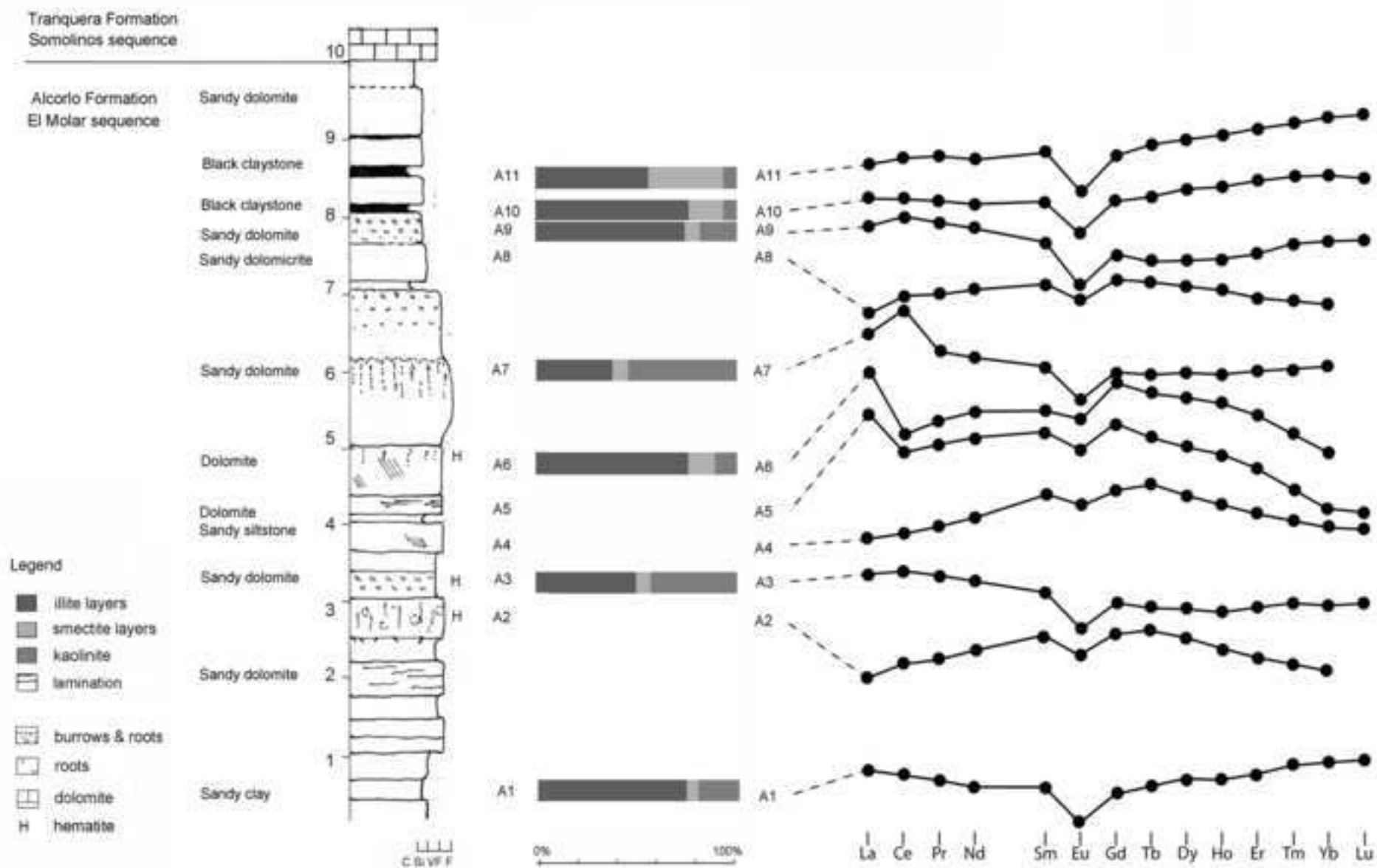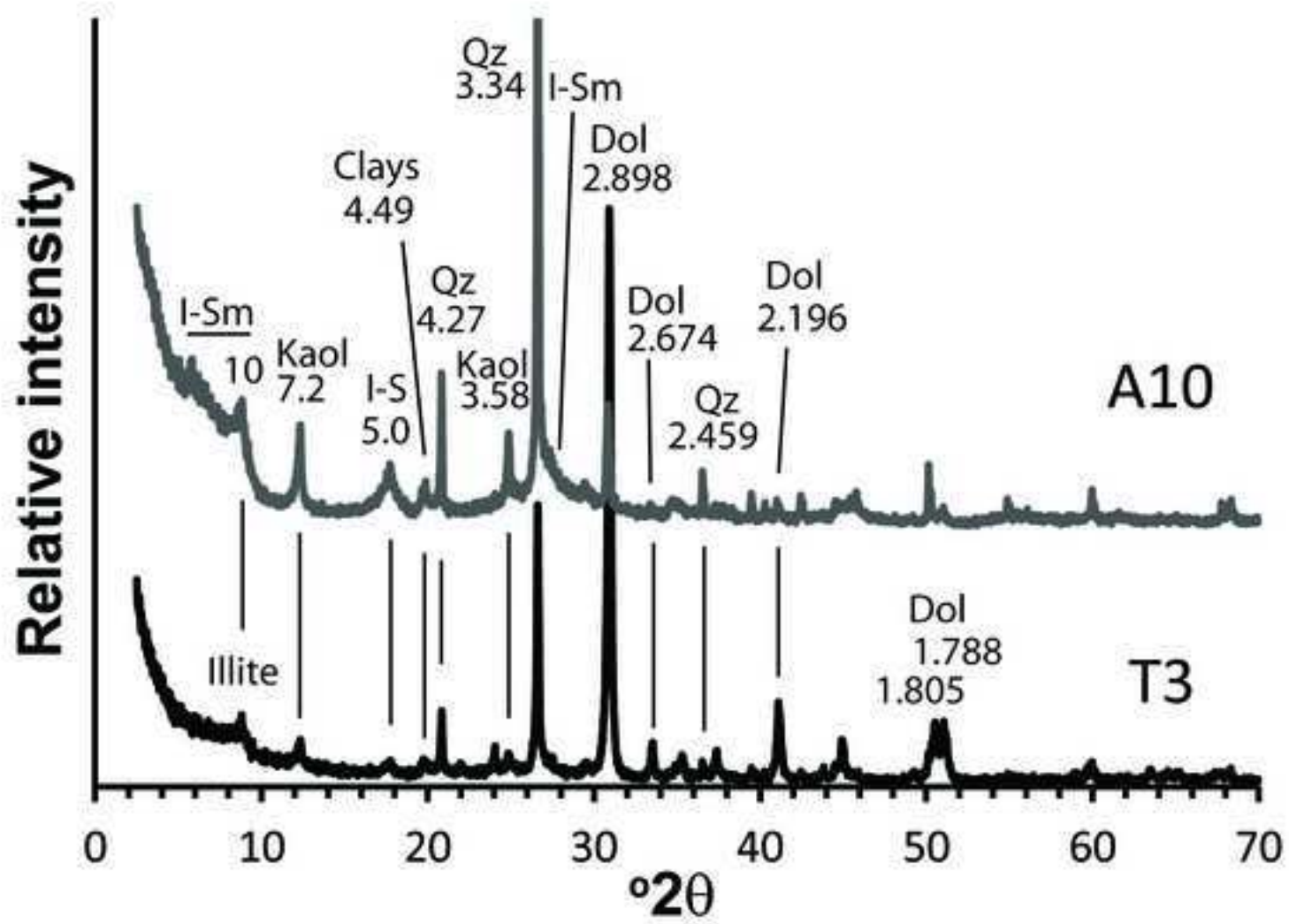
Fig. 6
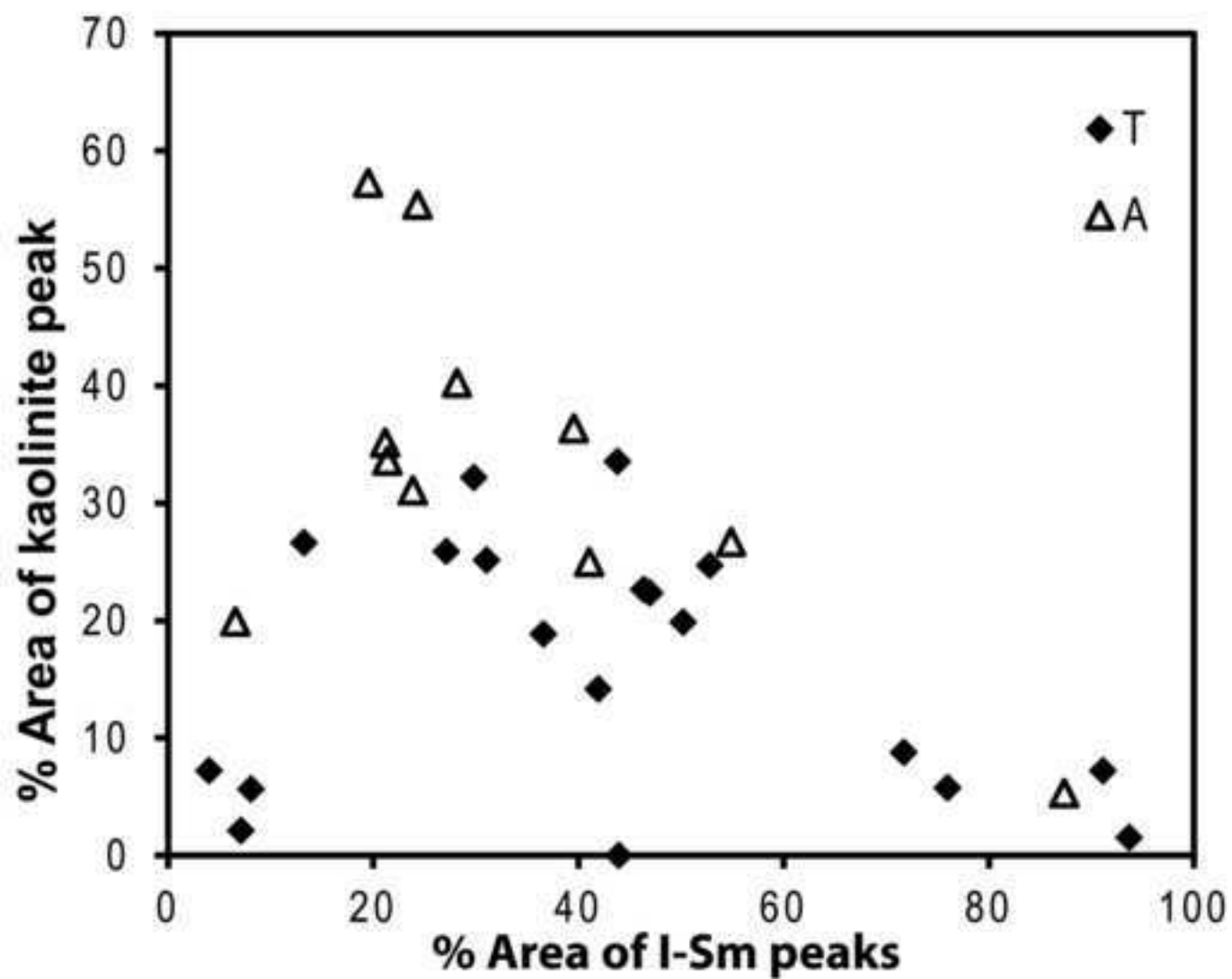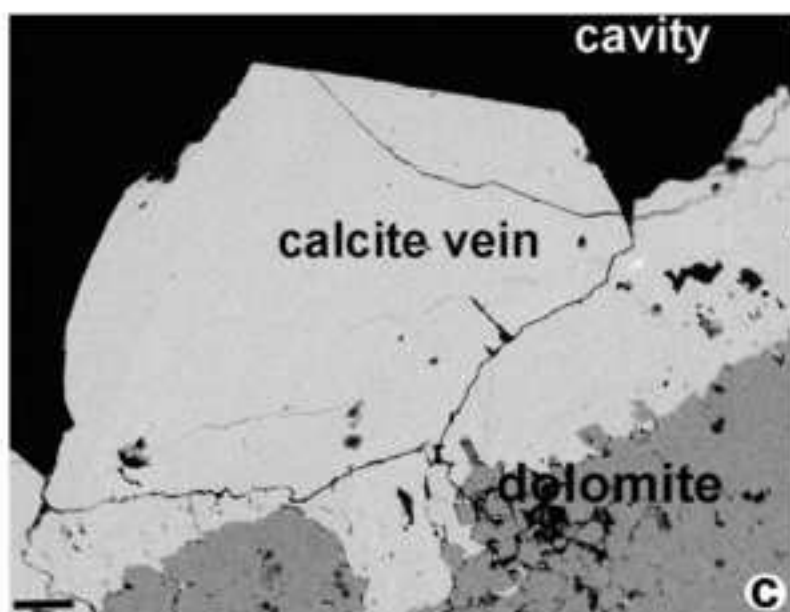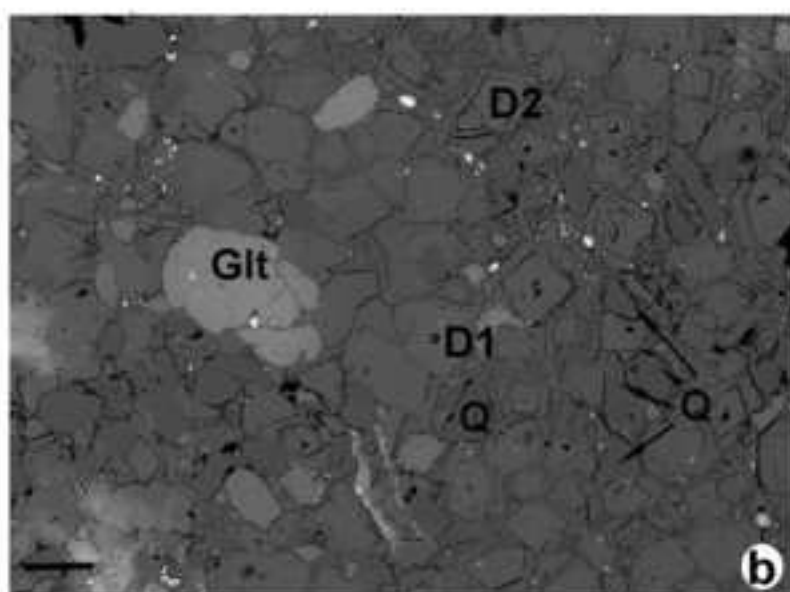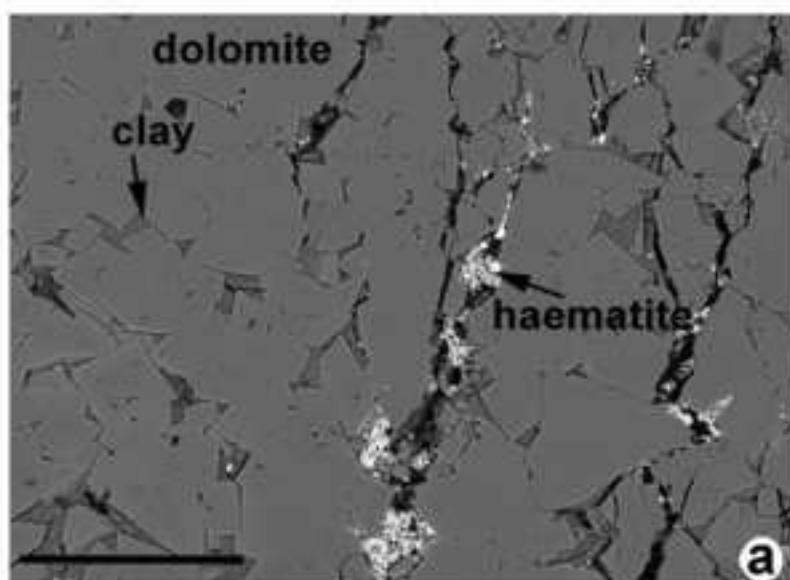
Fig. 8
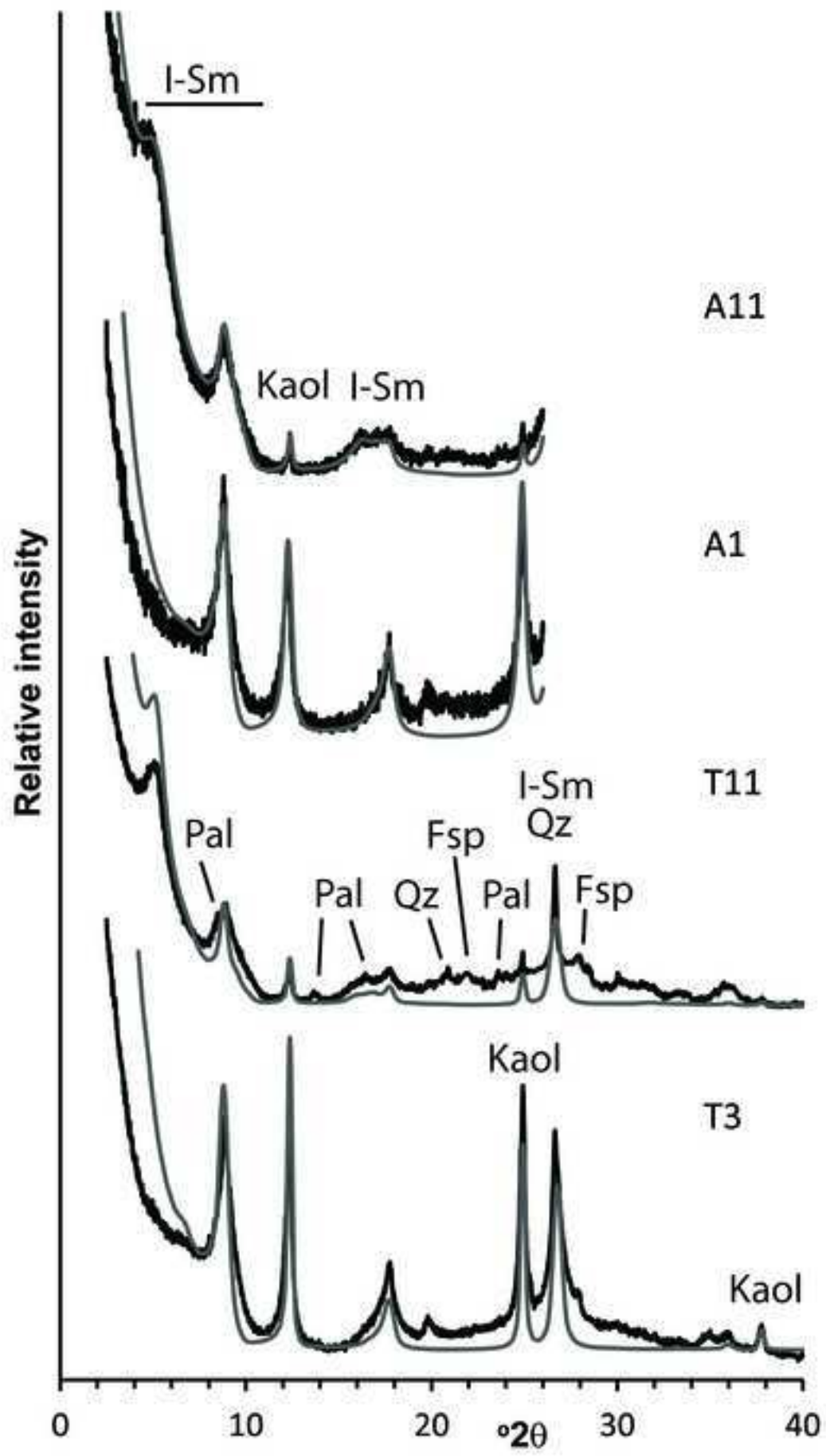
Fig. 9
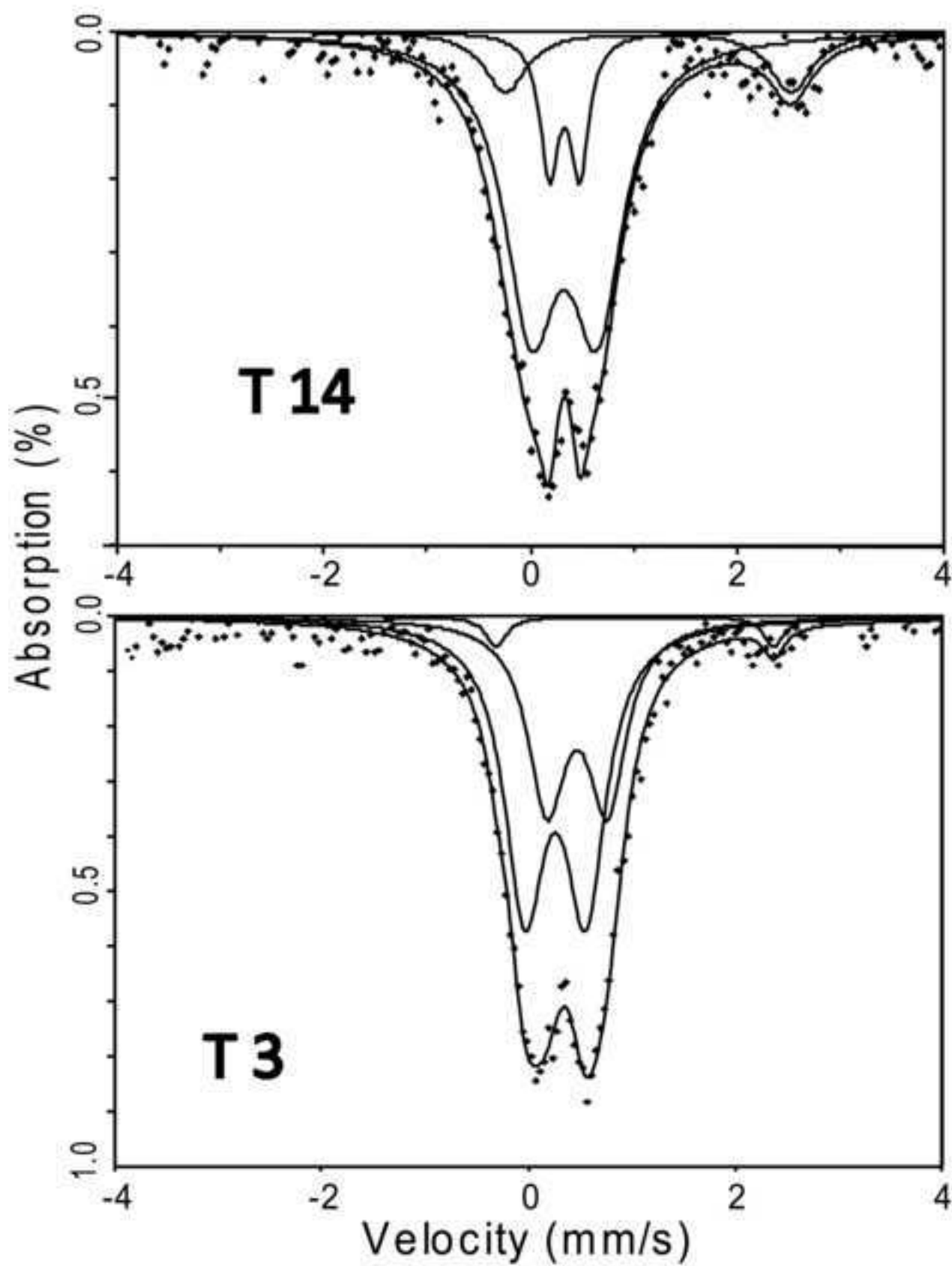
Fig. 10
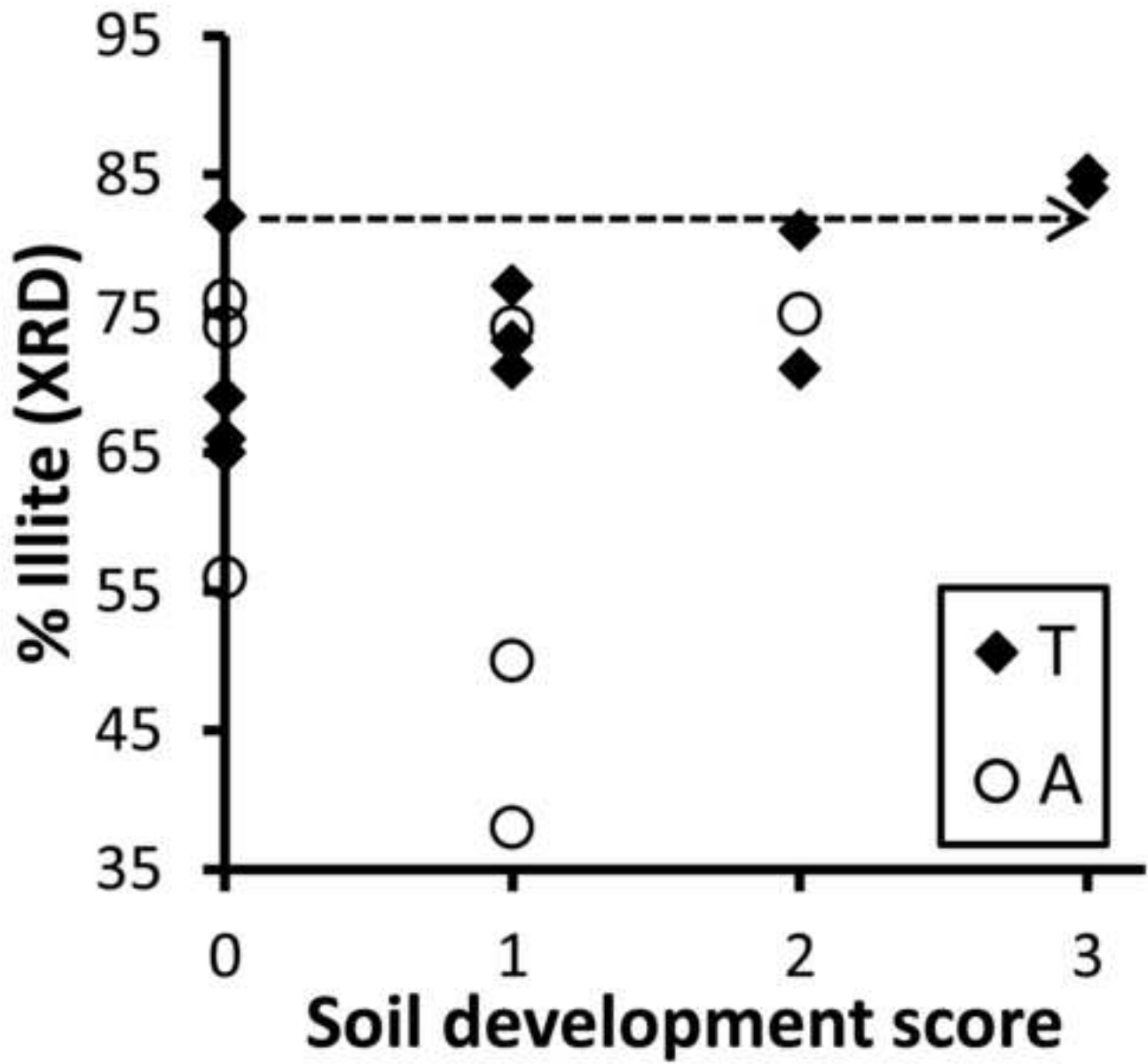
Fig. 11
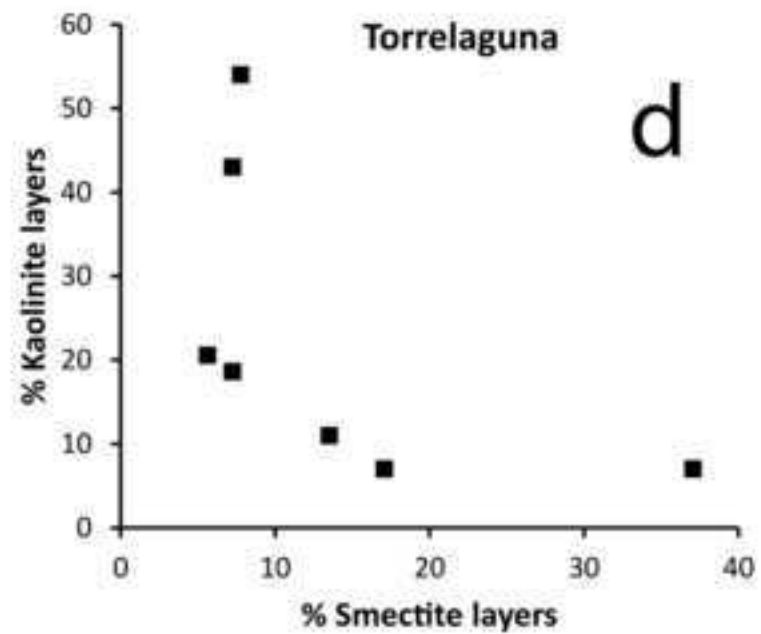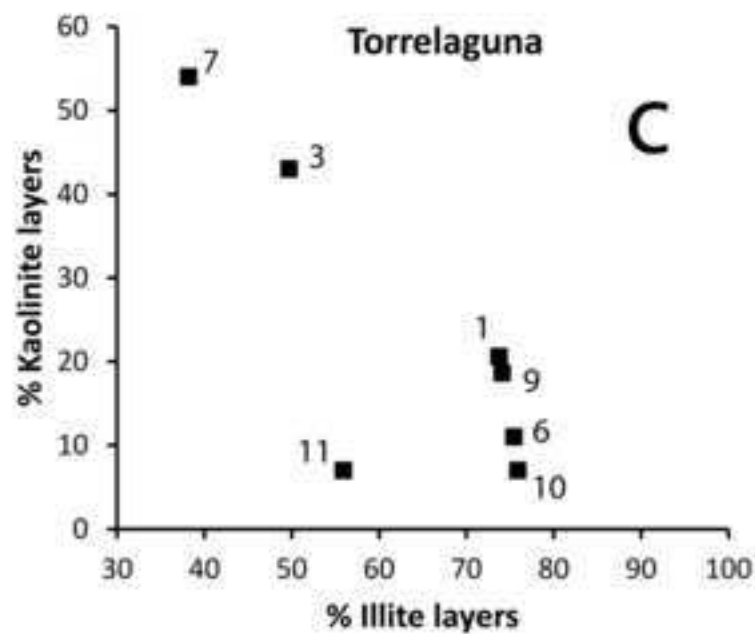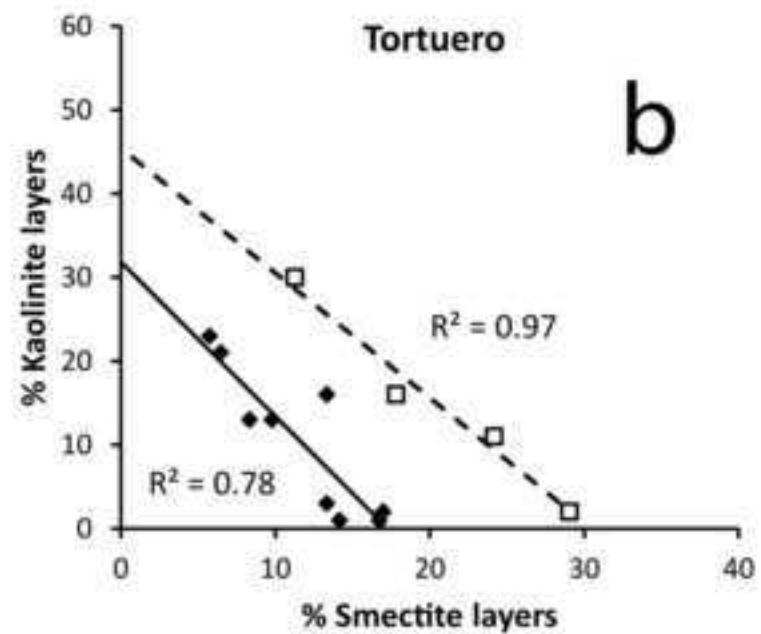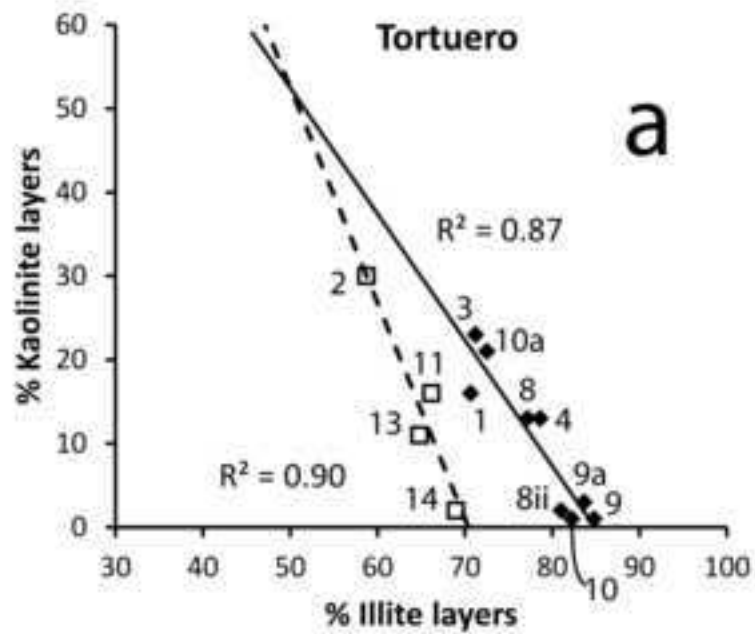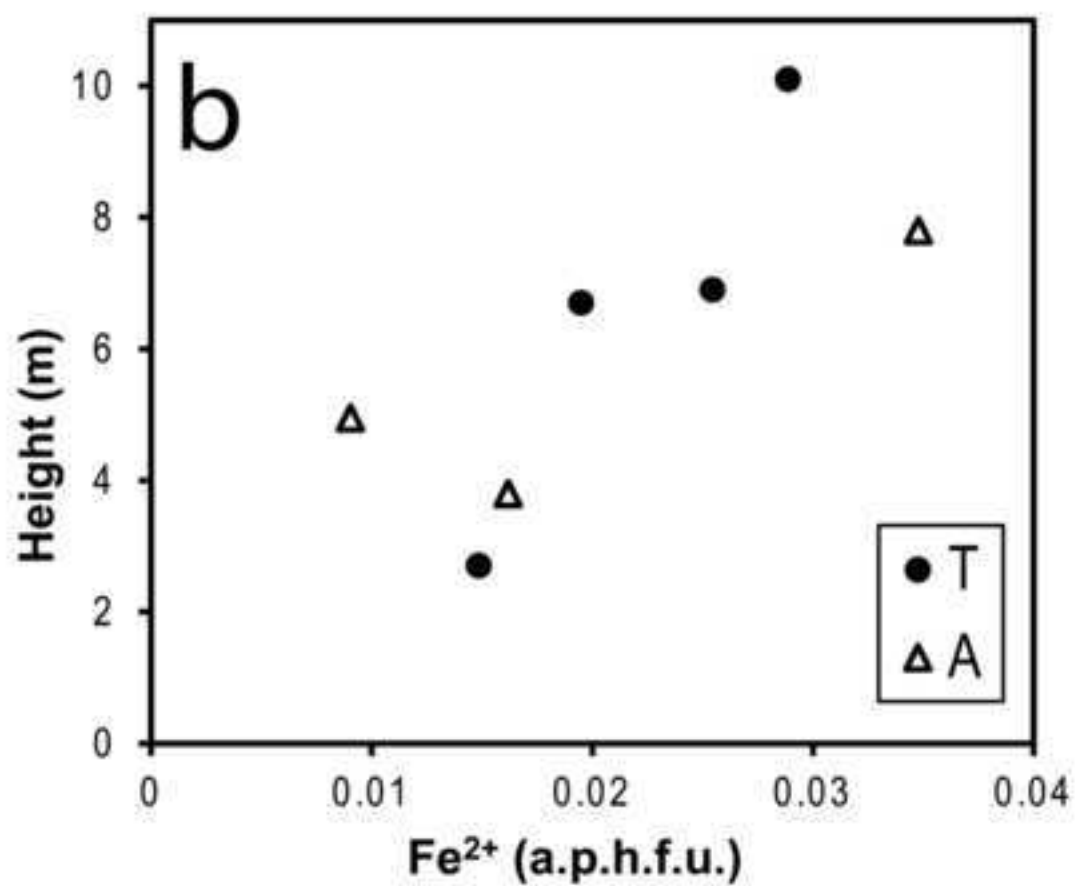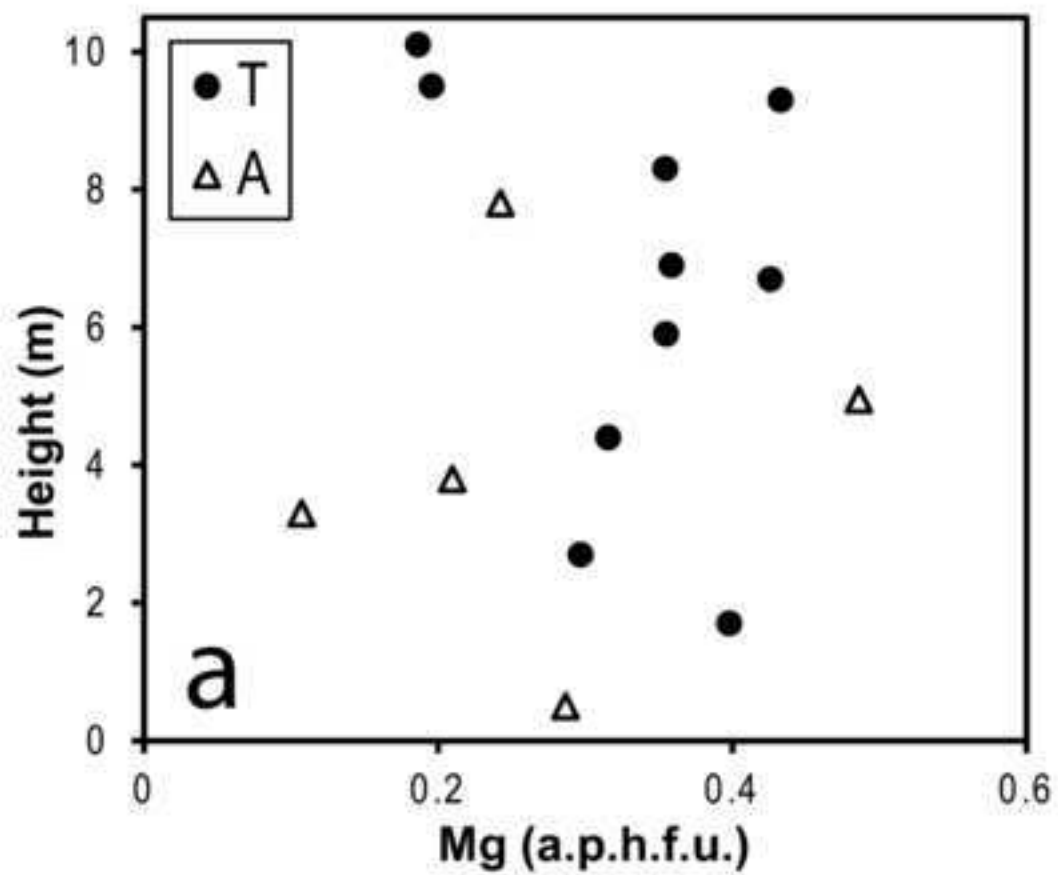
ABSTRACT

The aim of this study was to further our understanding of the pedogenic and lacustrine modification of clay minerals. Some of these modifications are of special interest because they constitute reverse weathering reactions, rare in surface environments, and because there is not yet an accurate assessment of their global relevance in mineralogical and geochemical cycles. For this study, two sections from the Central System in Spain were selected. Both are sections through the Uppper Cenomanian-Turonian mixed clastic and carbonate succession, containing both calcite and dolomite, in the Sierra de Guadarrama. Mid-Turonian sea level fall resulted in the formation of a coastal plain environment in which extensive pedogenesis occurred around saline lagoons. The mineralogical changes that have occurred as a result of sedimentation in saline lagoons and as a consequence of pedogenesis are described. Textural relationships indicate that the dolomite cement pre-dates the calcite. Silicate minerals are represented by quartz, kaolinite, illite-smectite, illite, minor plagioclase and alkali feldspar, and trace chlorite and palygorskite. There is a positive correlation between the intensity of pedogenesis and the proportion of illite in the clay assemblage in one of the sections, indicating pedogenic illitisation. In this section, the intensity of the illitisation process increases up, reaching a maximum where pedogenesis is most intense in the middle part, and then decreases as marine influence increases towards the top of the Alcorlo Formation and the overlying marine Tranquera Formation. The clay assemblages are consistent with a slow transformation process from kaolinite to illite by way of illite-smectite, taking

place under surface conditions. The illitisation process has resulted in a less Fe-rich, more Mg-, and Al-rich illite than the majority of previously documented cases in the near surface. Formation of Al-rich illite is not therefore restricted to the deep subsurface.

The mechanism for low temperature illitisation involves enhanced layer charge resulting from Mg^{2+} substitution for Al^{3+} (or Fe^{3+}) and Fe^{3+} to Fe^{2+} reduction. Mg^{2+} enrichment may have occurred principally in saline lagoons or lakes, while Fe^{3+} to Fe^{2+} reduction occurred as a result of wetting and drying in a pedogenic environment. So far as it has been possible to establish, this dual mechanism has not previously been documented. This study indicates clearly that the dolomite and calcite are authigenic cements that precipitated in a clastic sediment, probably soon after deposition. Dolomitisation and Mg enrichment of the clay may have occurred at the same time. Seawater is the most probable source of Mg.